UNIVERSITÉ DE MONTRÉAL

FIRST SIMULINK BENCHMARK FOR OFF-LINE AND REAL-TIME SIMULATION OF MORE-ELECTRIC AIRCRAFT (MEA) ELECTRICAL POWER SYSTEM

LEONARDO MONTEALEGRE LOBO

DÉPARTEMENT DE GÉNIE ÉLECTRIQUE

ÉCOLE POLYTECHNIQUE DE MONTRÉAL

MÉMOIRE PRÉSENTÉ EN VUE DE L'OBTENTION

DU DIPLÔME DE MAÎTRISE ÈS SCIENCES APPLIQUÉES

(GÉNIE ÉLECTRIQUE)

Août 2011

UNIVERSITÉ DE MONTRÉAL

ÉCOLE POLYTECHNIQUE DE MONTRÉAL

Ce mémoire intitulé:

FIRST SIMULINK BENCHMARK FOR OFF-LINE AND REAL-TIME SIMULATION OF MORE-ELECTRIC AIRCRAFT (MEA) ELECTRICAL POWER SYSTEM

présenté par : MONTEALEGRE LOBO Leonardo

en vue de l'obtention du diplôme de : Maîtrise ès sciences appliquées

a été dûment accepté par le jury d'examen constitué de :

M. KOCAR, Ilhan, Ph.D., président

M.SIROIS Frédéric, Ph.D., membre et directeur de recherche

M.MAHSEREDJIAN Jean, Ph.D., membre et codirecteur de recherche

M.DUFOUR Christian, Ph.D., membre

DEDICATION

In loving memory of my grandmother Carmen, whose flame extinguished shortly after I started this program, but her memory kept me warm during this amazing ride. Para vos abuelita!

ACKNOWLEDGEMENTS

I would like to thank my lovely Elani, for her support, her presence and her soft and calming words in the most challenging moments of this project. To my family, from whom, despite the distance, I felt the support and encouragement that allowed me to keep me going until the end. To my friends, the ones I made here and allowed me to travel through their amazing stories and the ones I left back home. The support during this process was remarkable.

I would like to thank the Instituto Costarricense de Electricidad for the chance to pursue this master's degree, one of the most rewarding experiences of my life.

I would be always grateful to Professor Frédéric Sirois for opening me the door to this wonderful institution and to Professor Jean Mahseredjian for selecting me to participate in this project. For their support, knowledge and understanding, I will be forever indebted.

Last but not least, I would also like to thank my co-workers, especially Marc-André Lemaire, for their help and support throughout the project, Mr. Claude Lavoie from Bombardier, and Mr. Luc-André Grégoire from Opal-RT for his invaluable contribution in work on the real-time simulation.

This research is supported and funded by Bombardier Aerospace, Pratt & Whitney Canada, Opal-RT Technologies and by the Consortium for Research and Innovation in Aerospace in Quebec (CRIAQ).

RÉSUMÉ

Le concept des avions plus-électrique est une nouvelle cible technologique pour les fabricants d'avions. Il concerne la réduction du poids de l'avion, de la consommation de carburant et l'amélioration de l'efficacité de l'énergie. Tous ces éléments constituent des avantages potentiels importants.

Les avions conventionnels utilisent les puissances hydraulique, mécanique, pneumatique et électrique en tant que sources d'énergie. Pour augmenter l'efficacité de ces systèmes, des études sont effectuées dans le but d'augmenter la part d'énergie électrique utilisée dans les avions pour la génération, la distribution et l'utilisation de la puissance électrique. Parallèle à l'augmentation de l'efficacité, le nombre et la qualité des études techniques relatives aux étapes de conception, design et essais de validation, doivent aussi être augmentés et/ou améliorées. Les modèles mathématiques et les outils de simulation constituent des moyens efficaces permettant de prédire le comportement du réseau électrique, corriger des erreurs de design, éliminer certaines étapes de prototypage et réduire le temps d'essai des composantes. Les outils de simulations peuvent augmenter la robustesse des systèmes tout en réduisant les essais dispendieux au sol et en vol. De plus, les outils de simulation offrent une infinité d'options pour l'étude d'un grand nombre de scénarios d'opération et pour l'optimisation. Les outils de simulation modernes deviennent de plus en plus sophistiqués et permettent, si les données sont disponibles, de créer des modèles très près de la réalité autant pour les composants que pour les systèmes. La simulation en temps réel permet de faire des essais sur des équipements réels (« hardware-in-the-loop ») pour valider des modèles et déterminer des paramètres.

Ce mémoire de maîtrise présente un premier test de simulation et d'analyse pour le réseau électrique du Global Express de Bombardier. Les simulations sont effectuées en temps différé et en temps réel. Les outils utilisés sont Simulink pour la simulation en temps différé et le simulateur OPAL-RT basé sur Simulink pour la simulation en temps réel. Cette recherche sert à définir les goulots de modélisation ainsi que les besoins au niveau des données nécessaires à la modélisation. Ce mémoire établit aussi les besoins de validation et de mesure pour la modélisation d'un avion plus électrique. La simulation en temps réel est particulièrement contraignante et ce mémoire a permis de tester une nouvelle méthode de résolution en temps réel.

ABSTRACT

Conventional aircrafts use hydraulic, mechanical, pneumatic and electrical energy sources to supply their systems. In order to increase the efficiency of such systems, it is needed to increase the penetration level of electrical systems and components in aircrafts for generating, distributing and utilizing electrical power. An important step is to develop numerical models for studies related to the conception, design and testing stages. Mathematical modeling and simulation tools constitute an efficient approach for predicting operational behaviour, correcting design errors, eliminating prototyping steps and reducing component and overall testing cycles. Simulation tools can increase system robustness while reducing expensive ground and flight tests on the actual aircraft. Moreover, simulation tools offer limitless options for studying huge numbers of operational scenarios and detecting failure conditions. Modern simulation tools for electrical circuits and systems have become very sophisticated and, if data is available, can be used to create extremely precise models for components and complete systems. Real-time simulation tools allow testing actual physical components (hardware-in-the-loop) and can be used to validate models and derive model parameters.

This research presents an initial benchmark for the simulation and analysis of the Bombardier Global Express aircraft electrical power system. Both for off-line and real-time simulations are considered. The considered tools are Simulink for off-line simulations and the Opal-RT simulator (based on Simulink) for real-time simulations. These tools allow achieving advanced models and testing the aircraft system in a high scope of scenarios. The research identifies modeling bottlenecks and data needs, establishes validation needs and proposes measurement tests for qualifying component models. It is established that the real-time simulation of the developed power system is particularly complex. An available and new real-time simulation method is tested at the end and demonstrates the need for further research.

TABLE OF CONTENTS

LIST OF TABLES

LIST OF FIGURES

LIST OF ABREVIATIONS

AC	Alternating Current
ACPC	Alternating Current Power Centre
ACSCC	Alternating Current Switching Control Centre
Ah	Ampere Hour
AM	Asynchronous Machine
APU	Auxiliary Power Unit
BATT	Battery
CAIMS	Central Aircraft Information and Maintenance System
CDU	Control Display Unit
CMU	Communications Management Unit
DC	Direct Current
DCPC	Direct Current Power Centre
DCSCC	Direct Current Switching Control Centre
ECS	Environmental Control System
EHP	Electro-hydraulic Pump
EICAS	Engine Indication and Crew Alert System
ELA	Electrical Load Analysis
EMTP-RV	Electromagnetic Transient Program, Revised Version
ESS	Essential
ETC	Emergency Tie Contactor
ETFE	Ethylene Tetrafluoroethylene
ETOPS	Extended Range Operation with Two-Engine Airplanes
EVS	Enhanced Vision System

EW	Electronic Warfare)
EXT	External
FADEC	Full Authority Digital Engine Controller
FCU	Flight Control Unit
FMS	Flight Management System
GCU	Generator Control Unit
GLC	Generator Line Contactor
ISA	International Standard Atmosphere
KEAS	Knots Equivalent Air Speed
kVA	Kilovolt-amperes
LC	Line Contactor
NiCd	Nickel Cadmium
NM	Nautical Mile
PF	Power Factor
RAT	Ram Air Turbine
SATCOM	Satellite Communications
SIGINT	Signal Intelligence
SSPC	Solid State Power Controller
TRU	Transformer Rectifier Unit
VA	Volt-amperes
VF	Variable Frequency
VFG	Variable Frequency Generator
Vrms	Volts rms
W	Watts

LIST OF ANNEXES

INTRODUCTION

The more-electric concept is a new technological target for the aerospace manufacturers which involves reduction of fuel consumption, improvement of power efficiency and the eventual possibility of a significant reduction of aircraft weight, as some of the important potential benefits [1]. Conventional aircraft construction is based on hydraulic, mechanical, pneumatic and electrical energy sources. Therefore, in order to increase the efficiency of such systems, it is necessary to increase the penetration level of electrical systems and components in aircrafts for generating, distributing and utilizing electrical power. The goal of the all-electric aircraft concept is to eliminate as many hydraulic power sources and lines as possible, so that the more electric engine can be redesigned to produce thrust and more electrical power [2].

The more-electric aircraft (MEA) concept impacts significantly on aircraft electrical power system design, due to the fact that many functions conventionally managed by hydraulic, pneumatic and mechanical power are replaced by electric systems in order to reduce size and weight, and improve fuel efficiency [2]. This may result into a significant amount of power electronic converters and motor drive systems. Electrical power system design may evolve in many directions: AC, DC, hybrid, frequency-wild, variable voltage, together with the possibility of novel connectivity topologies, resulting in very large and perhaps impractical computing times when considering modeling and simulation [3].

In contrast, the increased usage of electrical power increases the power demands on the electrical system, placing new constraints on its dynamic performances and on power quality, so that new power system architectures must be designed, extensively analyzed, tested, validated and certified before implementation in an actual aircraft. Simulation tools must be used to support the more-electric concept.

Mathematical modeling and simulation tools constitute an efficient approach for predicting operational behaviour, correcting design errors, and optimizing the fabrication process [4]. Thereby, modeling of aircraft power systems is essential to study impacts on costs and electric architecture modifications. Furthermore, continuing developments in aircraft power systems lead to studies on power distribution systems at fixed frequency [5], [6] and variable frequency [4], as well as on power distribution at high DC voltage [7]. Despite all these studies, many approximations are made, either by necessity or by lack of data. Greater efforts must be invested

to study more precisely the stability of new distribution architectures, as the presence of power electronics on aircrafts is in constant growth. Other studies on power quality, transients and faults must be added to the long list of design steps in aircrafts [8], [9].

Sophisticated modeling and simulation tools considered in this research constitute an efficient methodology for predicting operational behaviour, extracting specific requirements and developing specific techniques for applications to the more-electric aircraft technologies, so that the expected models and simulation results would help to clarify complex problems, support the decision making and the technological deployments for the strategic design process. Furthermore, simulation tools can increase in accuracy, so that modeling could be made as realistic as possible with a great level of details and complexity.

There are off-line and real-time simulation tools. In off-line simulation tools, model accuracy usually takes precedence on the computational speed of the complete simulation. Real-time simulation tools offer the computational speed advantage and allow studying a very large number of operational scenarios within reduced time. In addition, such tools can provide real-time synchronized simulations and allow interfacing with external physical devices (hardware-in-the-loop). Such interfacing can be used to validate physical controllers, improve designs and even develop models through the analysis of black-box type physical device performance waveforms.. Both off-line and real-time simulation tools are part of this research.

Socio-economical context

Currently, the specifications for the aircrafts are more or less similar depending on the category: commercial, business or utility. An aircraft with the important technological breakthrough of the more-electric concept becomes more competitive in almost all of these operational specifications. An extensive list of expected benefits could be drawn for the more-electric concept over the conventional aircraft power systems. The most noticeable ones come from an envisioned conceptual and technical simplification of the systems [5].

- Reduction of: components count, empty weight, systems and components volume, life-cycle costs, design effort, fuel consumption.
- Improvement of: operational range, systems and engine efficiency, reliability, maintainability, safety, power density, system flexibility.

Based on a literature overview, remarkable initiatives have been developed in US and Europe to design more-electric aircrafts. Airplane manufacturers, such as Airbus and Boeing, have already applied new concepts of electric actuation within their last state-of-the-art development programs for Boeing 787 [10] and Airbus A380 [11]. Many manufacturers put their hopes in the increase of electric power usage as the solution for reducing fuel consumption and emissions levels.

To accelerate the development of more-electric aircrafts, it is important to establish a tight collaboration between the participating manufacturers and the universities as it has been done during this research, which is, with the help of manufacturers, a powerful innovation path that can quickly result into practical developments and implementations.

According to available economical analysis (see [12]), global commercial aviation electrical power systems and infrastructure market is estimated to reach $24 billion by 2017. Furthermore, more-electric aircraft architectures attempt to offer lower recurring costs, require less parts, reduce fuel consumption, improve operational performance, reduce maintenance and reduce the cost of operation.

Technical context

In a technical context, modern research and advancements in aircraft systems are in the fields of flight control, power generation and power control, and engine control [6]. In addition, there are substantial benefits in weight reduction when replacing hydraulic circuits by more-electric flight controls. Other benefits are in maintenance and reliability.

To present a global picture, the conventional aircraft hydraulic systems include primary and secondary flight controls, landing gear and utility actuation. In the past, electrical machines did not provide sufficient power density to drive these loads. Recent developments in induction, switched reluctance and permanent magnet motors provide new design options. Moreover, the use of hydraulic fluid is hazardous since it could leak. By using electrically-driven pumps or even eliminating all hydraulic components, mechanical simplicity and increased reliability can be achieved.

The increased number of electrical applications in aircrafts increases the demands on the aircraft electrical power generation and distribution system. Traditional aircrafts are based on the constant frequency generator concept, which requires extra equipment to cancel speed variations

within the generator. Such equipments can be eliminated through variable frequency generators. The Bombardier's Global Express jet is already using a variable frequency system.

In a conventional aircraft, electrical power generation is done by externally engine-driven generators. The electrical machines are connected to the engine via shafts and gearboxes. The goal of the more-electric approach is to integrate them into the core of the engine.

An important aspect is power generation during emergency situations. New developments in fuel cells and fan-driven generators allow replacing the currently used ram air turbine (RAT) technology, increasing reliability, and offering supplemental power options. The feasibility of the more-electric concept relies on the development of lightweight and fault tolerant power distribution architectures. There are many design options. The primary electrical power includes generation and distribution to the main busses and primary loads. The electrical sources on an aircraft are the main generators, Auxiliary Power Unit (APU), Ram Air Turbine (RAT), battery and external power.

This system could be constant frequency AC (3Φ/115 VAC/ 400 Hz), variable frequency AC (324 Hz to 720 Hz), high-voltage DC (270 V DC or 350 V DC) and even multiphase (5Φ, 7Φ). Also, these main power levels need conditioning and conversion in order to feed different loads inside the aircraft, such as the 28 V DC avionic busses. This is referred to the secondary electrical power system. The conversion can be achieved on the basis of different converter topologies.

In the power generation and engine control aspects, the more-electric engine (MEE) plays a key role in the more-electric design of aircrafts [2]. The engine itself includes electric loads, such as electric fuel and oil pumps, active magnetic bearings and electrically actuated engine guide vanes. Complicated hydro-mechanical controls are replaced by digital electronics controls (see FADEC: full authority digital electronic engine control) [13]. The MEE incorporates smart fuel valves, fuel pumps and distributed control technologies for simplification of control system architectures. The elimination of hydraulic, mechanic and pneumatic functions in the MEE is for concentrating on the production of thrust and electrical power [13].

It is apparent that advanced aircraft power system architectures may include various levels of sophistication. Such architectures are based on bi-directional, DC/DC, AC/DC and DC/AC power converters [8]. The term Multi-converter Power Systems is used to designate such systems with solid state switching power converters [8]. In addition, it is required to study and coordinate

protection systems, so modeling and simulation is essential for the design, development and operational reliability of more-electric aircrafts.

Two types of tools can be used for the simulation and analysis of aircraft power systems: off-line and real-time. On both cases the simulation methodology encompasses electromagnetic transients. Steady-state initial conditions can be established using phasor domain analysis.

Off-line tools offer the advantages of high modeling precision since such tools do not need to compromise for synchronized real-time interfacing with external physical devices. There are no time-step and network size constraints in off-line programs. The limitation is that currently off-line simulation tools cannot be directly interfaced with external controllers.

Real-time simulators can be applied for studying a very large number of operational scenarios within reduced time and for interfacing with external physical devices. Such interfacing is essential for validating and improving controllers and validating mathematical models.

This project includes the development of specific models, such as power converters, AC and DC cables, AC and DC loads, switching controls and rotating machines. The modeling may become dependent on the simulation type and on the required precision for the studied electrical frequencies. A complete aircraft power system is developed and presented.

The development of benchmarks for aircrafts and the setup of advanced testing facilities contribute to the study of various aircraft power system architectures and testing their performance within economical, stability and reliability constraints.

This thesis is divided as follows: Chapter 1: Global Express Aircraft Electric Power System Fundamentals, Chapter 2: Global Express Aircraft Electric Power System Model, Chapter 3: Global Express Aircraft Electric Power System Simulation and Analysis and Chapter 4: Global Express Aircraft Electric Power System simulation in a Real-Time Environment.

Main Objective

The goal of the project is to develop and validate a first real-time bechmark in Matlab/Simulink [14] for the simulation, analysis and evaluation of more-electric aircrafts, electrical power system architectures based on the Bombardier's Global Express aircraft electric power system. The setup in Simulink allows both off-line and real-time simulations. Real-time simulations are performed using the Opal-RT system [15].

Specific Objectives

In order to achieve the main objective of the investigation, three specific objectives were established:

1. Develop the MATLAB/Simulink off-line model for Bombardier's Global Express aircraft electric power system.
2. Validate results using a specialized software for the simulation and analysis of transients in power systems named EMTP-RV (Electromagnetic Transient Program, Revised Version [16]), as well as real aircraft electric measurements.
3. Convert the MATLAB/Simulink off-line model for Bombardier's Global Express aircraft power system into real-time using Opal-RT environment (based on Simulink) [15].

Methodology

The research is divided into the following steps:

1. Literature Review and Industrial Meetings with Bombardier for data gathering and acquiring knowledge on the system to be simulated.
2. Model development and assemblage of complete electrical network.
3. Simulations and analysis of results and data Processing.
4. Validation with EMTP-RV and measurements.
5. Simulation in real-time of the Global Express Aircraft Electric Power System.

Literature review and industrial meetings

The literature review shows the way research programs in more-electric aircrafts have been conducted in the past 20 years, providing a fundamental starting point for the research. Topic issues as the general concept of MEA ([1], [2], and [3]), its expected benefits and objectives, in addition to simulation methodologies and strategies ([6], [17]) and complex problems related to stability assessment of power electronics were studied and analyzed during this stage.

Meetings with the industrial partners are to provide: co-supervision, data on the simulated aircraft systems, available measurements and test data, problematic operational cases and guidance on applicable standards and internal certification methods.

In the model development stage, the first task is to tackle the computational efficiency of the model. The second task addresses the precision of the model. Each time a new improvement or network component is introduced into the benchmark it is needed to validate efficiency, accuracy and stability of the model. In addition, each model is simulated as isolated from the aircraft electric power system and then incorporated in the entire power system model for increasing the accuracy of the simulations.

Once the off-line benchmark achieves the desired objectives, it is converted into real-time using the Opal-RT real-time simulator. The Opal-RT simulator is based on MATLAB/Simulink which offers an advanced open-architecture and allows reconfigurations as needed [8]. In addition, there is a Simulink interface with EMTP-RV for large scale system simulations [15].

Validation and improvement of the real-time Global Express aircraft power system model

Each new improvement is tested sequentially in order to compare the performance of the model with and without the improvement, allowing an immediate feedback and the correction of possible problems or errors. The obtained model is implemented into the real-time platform of Opal-RT Technologies Inc. and some case studies are run in this simulator.

CHAPITRE 1 GLOBAL EXPRESS FUNDAMENTALS

This chapter specifies the electrical characteristics for the Global Express Aircraft Electrical Power System. It attempts to summarize the main lines found in technical manuals related to aircraft electrical architectures, specially the so called “Aircraft Type Course Technical Training Guide: ATA 100 Breakdown” [18].

1.1 Global Express Description

The Global Express is a luxury business jet aircraft for medium and long range mission and multi-role applications such as flight inspection, search and rescue, SIGINT (Signal Intelligence), EW (Electronic Warfare) and 30 passenger transporters. The aircraft is powered by BMW/Rolls Royce engine BR710 and it is designed to meet the intent of the Extended Range Operation with Two-Engine Airplanes (ETOPS) requirements, with 180 minutes diversion time. In addition, the aircraft is designed to be self-sufficient and have the capability to operate without limitation or restriction at a 13000 ft elevation airport, as well as safely cruise at 51000 ft [19].

The aircraft has a 41000 ft minimum initial cruise altitude at ISA + 10°C and a 51000 ft maximum operating altitude. It is capable of operating from a 6000 ft runway at ISA sea level. The rate of climb for a heavy aircraft (91000 lbs) is 3650 ft/min. at sea level and 600 ft/min. at 41000 ft (M 0.8). The rate of climb for a light aircraft (50000 lbs) is 7300 ft/min. at sea level and 2400 ft/min. at 41000 ft (M 0.8). The aircraft maximum range is 6500 NM (Nautical Mile) and it cruises between 41000 ft and 51000 ft for approximately 14 flight hours [19].

1.2 Electrical Power System Characteristics

The electrical system is separated into AC and DC system as shown in Figure 1.1. The AC system is a variable frequency type system, powered by four engine-driven variable frequency generators (VFGs). An auxiliary generator, located on the Auxiliary Power Unit, operates at a fixed frequency. In the event of an emergency, a Ram Air Turbine Generator is provided for Essential Bus feed. The generator outputs are supplied to the AC Power Centre (ACPC), which in turn distributes the power to the aircraft subsystems.

The DC system power supplies consist of four Transformer Rectifier Units (TRUs) for normal power distribution and two NiCad batteries (a nickel-cadmium battery which is a type of

rechargeable battery using nickel oxide hydroxide and metallic cadmium as electrodes [19]). The batteries are used for initial system power-up but are then put in the standby mode for emergency power requirements. On the other hand, the TRUs receive power from the AC system, transforms and rectifies that power into DC power, which is supplied to the DC Power Centre (DCPC). The DCPC in turn distributes the power to the aircraft subsystems.

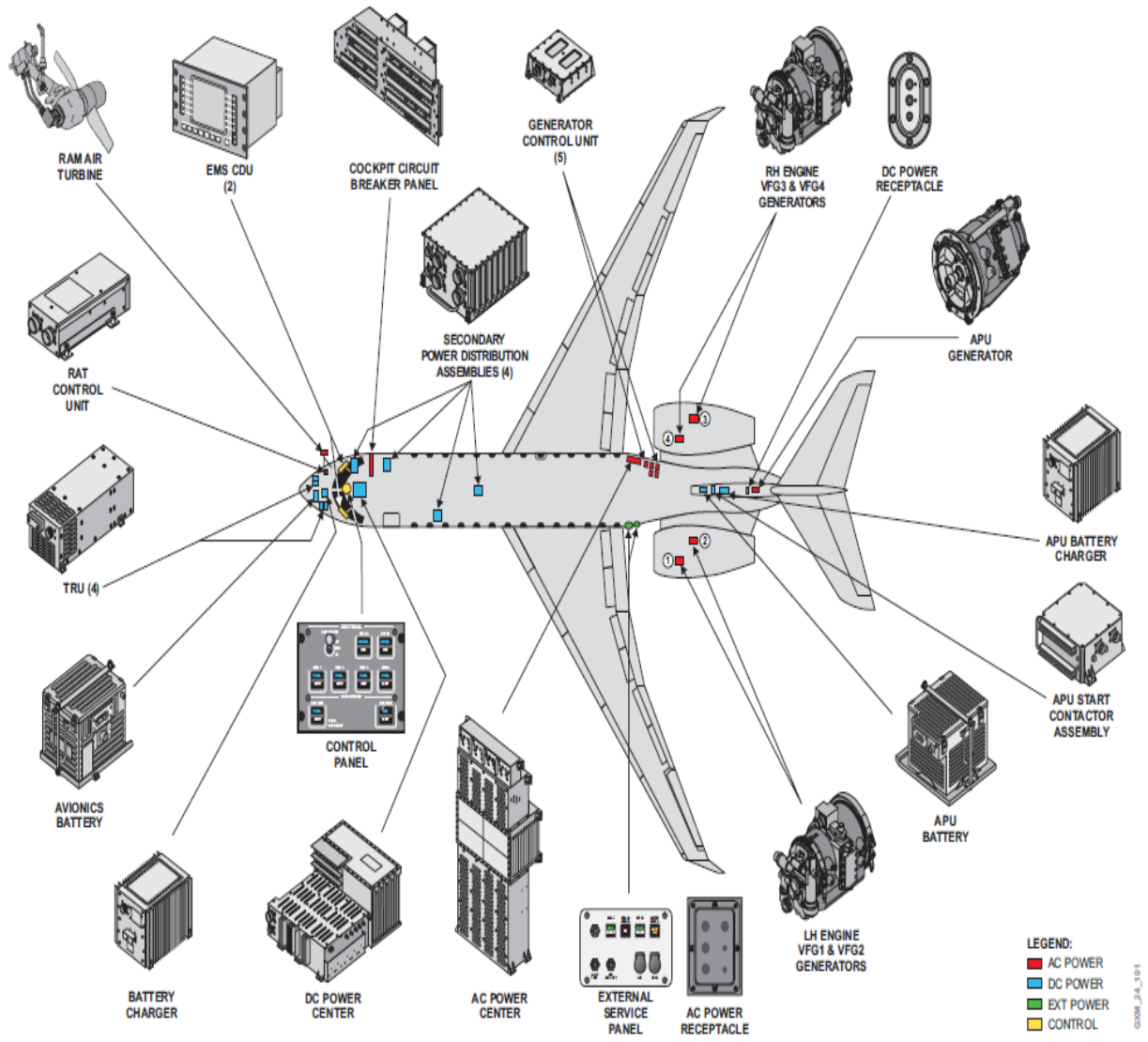

Figure 1.1. Electrical power system [18]

1.2.1 Primary AC Generation System

The AC system Variable Frequency Generators (VFGs) are rated at 115/200 VAC 3 phase 324-596 Hz. They have a load limit of 40 kVA continuous, 60 kVA for 5 minutes and 80 kVA for 5 seconds. VFG 1 and VFG 2 are located on the left engine. VFG 1 is mounted on the forward side of the engine accessory gearbox while VFG 2 is mounted to the aft side. VFG 3 and VFG 4 are located on the right engine. VFG 3 is mounted on the aft side of the accessory gearbox while VFG 4 is mounted on the forward side. Figure 1.2 illustrates what is indicated above.

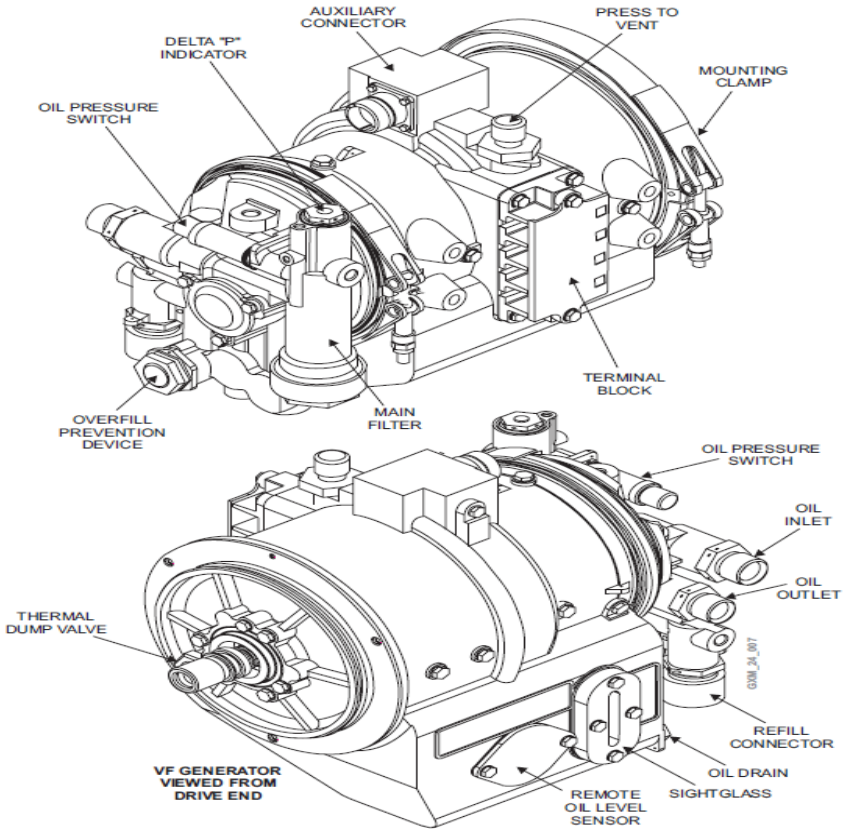

Figure 1.2. Variable Frequency Generator [18]

The variable frequency generator (two per engine) is made up of three component machines connected in cascade as shown in Figure 1.3. These component machines consist of Pilot Exciter, Main Exciter, and Main Alternator. The Pilot Exciter (PE) is a permanent magnet generator, with the rotor constructed with cobalt magnets. The output from the PE is supplied to the GCU, which uses this power for its internal circuitry, as well as rectify the power to supply the Main Exciter of the generator. The output of the Main Exciter (ME) is fed to shaft mounted diodes that are

configured for three-phase full wave rectification. The DC output supplies the rotating field of the Main Alternator.

The Main Alternator output is supplied to the Generator Line Contactor and Transfer Contactors. Each phase of the output is monitored by three toroidal current transformer assemblies for GCU fault protection interface.

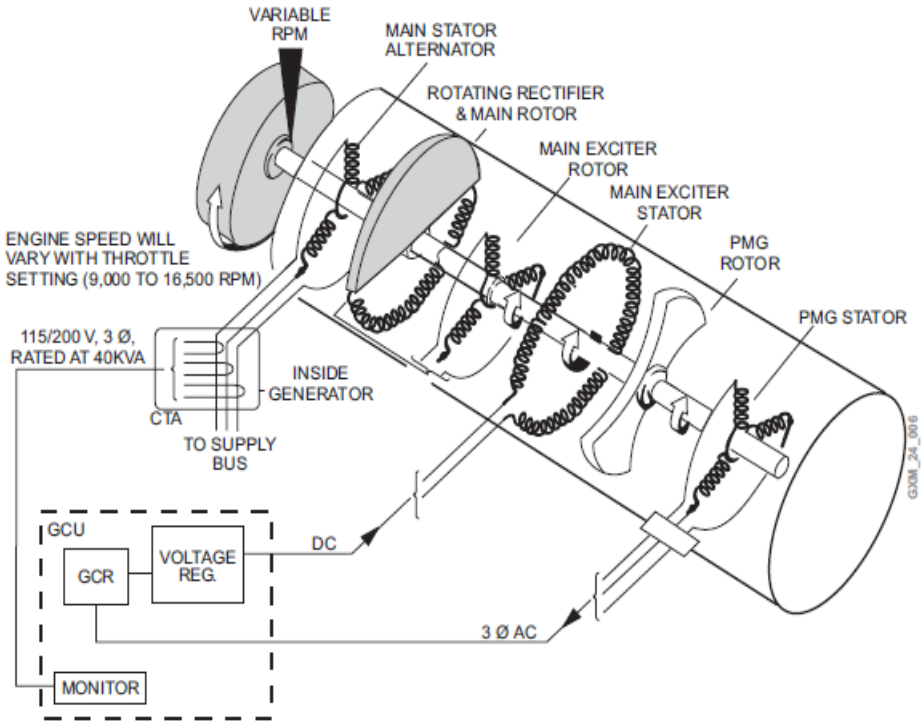

Figure 1.3. Variable Frequency Generator Block Diagram [18]

Regarding the main terminal block, it has four stud connections designated: T1, T2, T3, G. The feeders to the AC Power Centre (ACPC) are connected here. The neutral is connected because it is required for the 115V single phase electrical loads. The studs are covered with a removable cover. Since the generators rotate in different directions depending on their position, the phase output differs. Phase sequence of generator 1 & 4 is A, B, C at T1, T2, T3. Phase sequence of Generator 2 & 3 is C, B, A at T1, T2, & T3 phase sequence is corrected by switching A and C phases of Generators 2 and 3 at the AC Power Centre (ACPC).

Each generator supplies its own AC bus via a generator line contactor (GLC). All four GLCs are located in the AC Power Centre (ACPC) primary power subassembly. The GLC has two positions, Generator & Transfer, as shown in Figure 1.4. The Generator position allows the

generator to supply its own AC bus. The Transfer position allows an alternate power source (other VFG, APU or External) to feed the AC bus. The GLC is controlled by the Generator Control Unit (GCU).

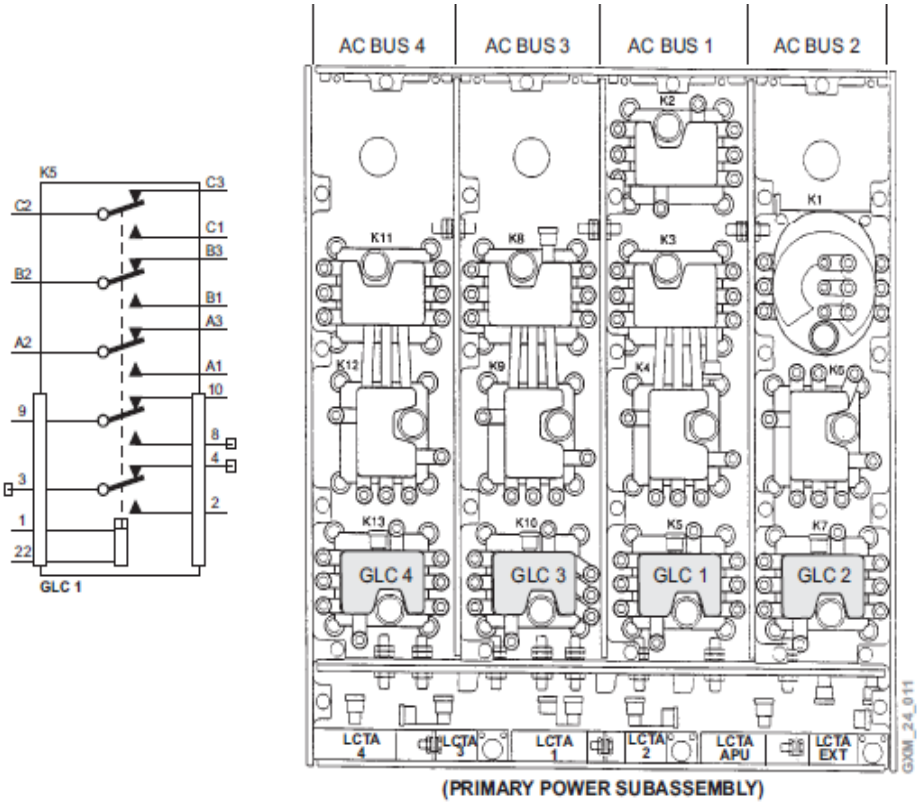

Figure 1.4. Generator Line Contactors [18]

On the other hand, each generator interfaces with its respective Generator Control Unit (GCU). The GCU performs the following functions:

- Monitors generator operating parameters
- Controls generator field excitation
- Interfaces with AC Power Centre (ACPC) via analog signals and RS 422 data bus
- Supplies information to EICAS system via ARINC 429 data bus to the Data Acquisition Units
- Interfaces with CAIMS

1.2.2 Auxiliary AC Power

Auxiliary AC power is provided by the APU Generator which produces 3-phase 115 VAC. It is rated at 40 kVA continuous duty during flight conditions, and 45 kVA during ground operations. The APU generating system is very similar to the Primary AC generation system, therefore, only the differences are discussed. The APU generator is constructed similar to the engine variable frequency generators and produces power in an identical manner. The generator is located on the APU gearbox, which is located in the aircraft tail cone as shown in Figure 1.5.

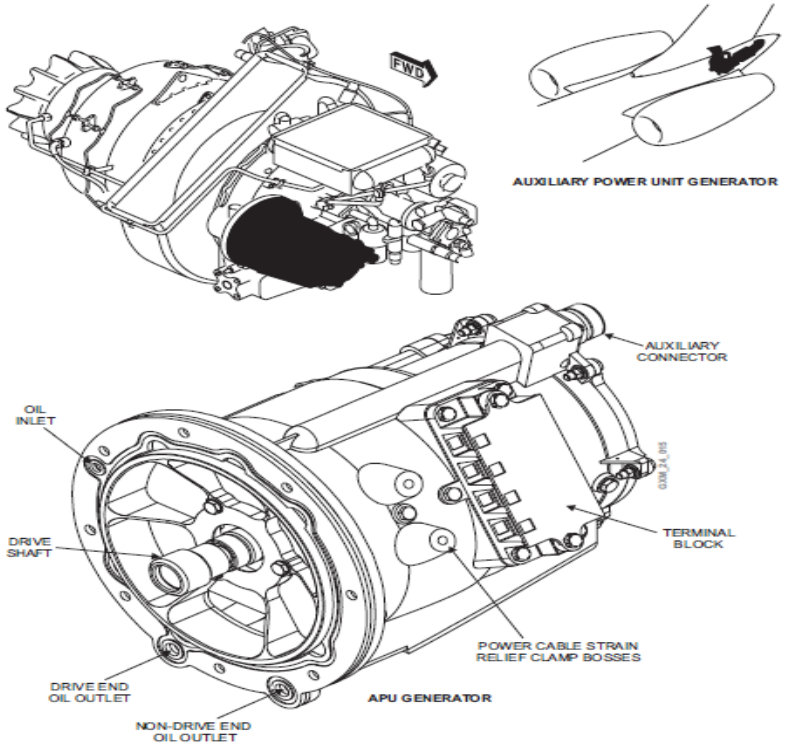

Figure 1.5. Auxiliary Power Unit (APU) Generator [18]

A Pin programming informs the GCU installed in the APU position of the following additional information interface, and operating parameters listed in Table 1.1:

Table 1.1. Operating parameters for APU control unit [18]

Parameter	Logic
Underfrequency	< 380 Hz for > 1 sec.
Overfrequency	> 430 Hz
Overcurrent	Any phase > 195 A
Load Prediction	Load parameters supplied to APU FADEC for load prediction purpose.

Finally, WOW Input is received by the GCU to change its load acceptance rate from 40 kVA to 45 kVA when on the ground. The GCU also gives load parameters to the APU Full Authority Digital Engine Control (FADEC) for fuel adjustments, depending on generator load.

Concerning the operation, the APU Generator excitation and control is performed by the GCU. Once the APU is started and RPM is above 95%, the GCU energizes its internal Generator Control Relay (GCR) circuit which gives the generator its excitation voltage. Once generator voltage is established and within operating parameters, the GCU energizes the APU/EP line contactor and informs the ACPC Primary Logic Cards that the generator is available (see Table 1.2). The Primary Logic Cards return a signal to the APU GCU if its distribution logic requires the APU generator. The APU generator does not supply the aircraft if more than one VFG is on-line. Any two VFGs power all four buses. Power from the APU/EPLC is distributed to the AC buses via the Generator Transfer Contactors (GTC) which are controlled by the ACPC Primary Logic Cards.

Table 1.2. Auxiliary AC Power management according different conditions [18]

Condition	**AC Bus 1**	**AC Bus 2**	**AC BUs 3**	**AC Bus 4**
APU Only (On Ground)	APU GEN	APU GEN	APU GEN	APU GEN
APU Only (Airborne)	APU GEN	SHED	SHED	APU GEN
GEN 1 & APU	GEN 1	APU GEN	APU GEN	GEN 1
GEN 2 & APU	GEN 2	GEN 2	APU GEN	APU GEN
GEN 3 & APU	APU GEN	APU GEN	GEN 3	GEN 3
GEN 4 & APU	GEN 4	APU GEN	APU GEN	GEN 4

The Secondary Logic Cards control the secondary distribution to allow a limited load to be applied to the APU generator under certain conditions. For example, with APU GEN alone, and the aircraft on the ground, only one electrical hydraulic pump can be powered at one time.

1.2.3 AC Electrical Power Distribution

The AC Electrical power distribution is contained in two areas, the AC Power Centre (ACPC), located in the baggage compartment, and the Cockpit Circuit Breaker Panel (CCBP), located behind the copilot’s seat (see Figure1.6). The ACPC contains the four primary AC buses and the required contactors, Solid State Power Controllers (SSPC) and Circuit Breakers to distribute the power from the four VFGs, the APU GEN and External Power. The Cockpit Circuit Breaker Panel (CCBP) contains four AC buses (AC Bus 1A, AC Bus 2A, & AC Bus 3A and the AC ESS

Bus), thermal circuit breakers and relays to control AC Power distribution to the forward areas of the aircraft. There are never two power sources feeding an AC bus at the same time. Therefore, bus faults are not transferred from one bus to the other.

Meanwhile, the Ram Air Turbine (RAT) Generator only powers the AC Essential Bus. Thereby, remote control of all power distribution, with the exception of remote thermal circuit breakers, is performed via the cockpit EMS CDUs, and the Primary & Secondary Logic Cards.

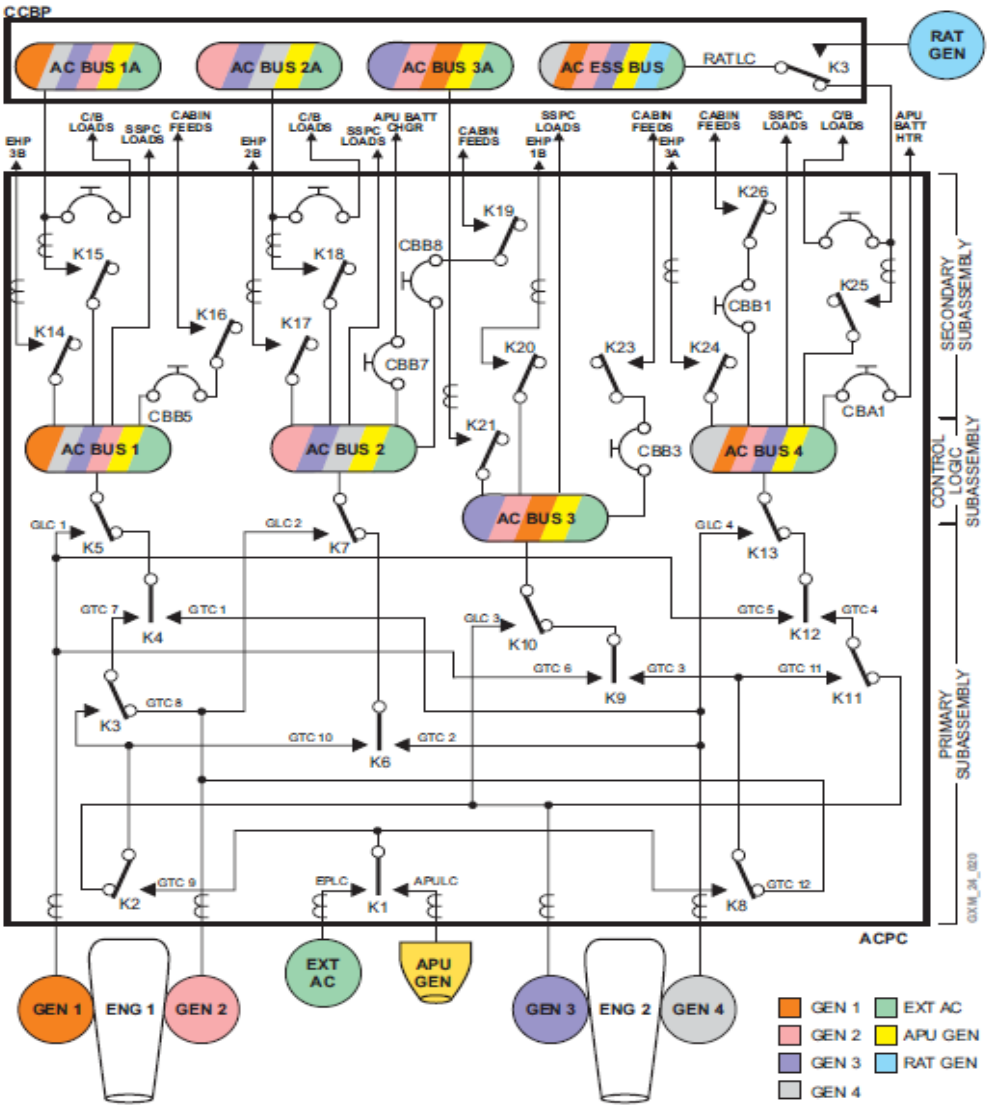

Figure 1.6.AC Electrical Power Distribution [18]

1.2.3.1 AC Electrical Power Distribution

An ACPC functional block is presented in Figure 1.7 and it is made up of three sections starting from bottom to top:

- Primary Power Subassembly
- Control and Logic Subassembly
- Secondary Power Subassembly

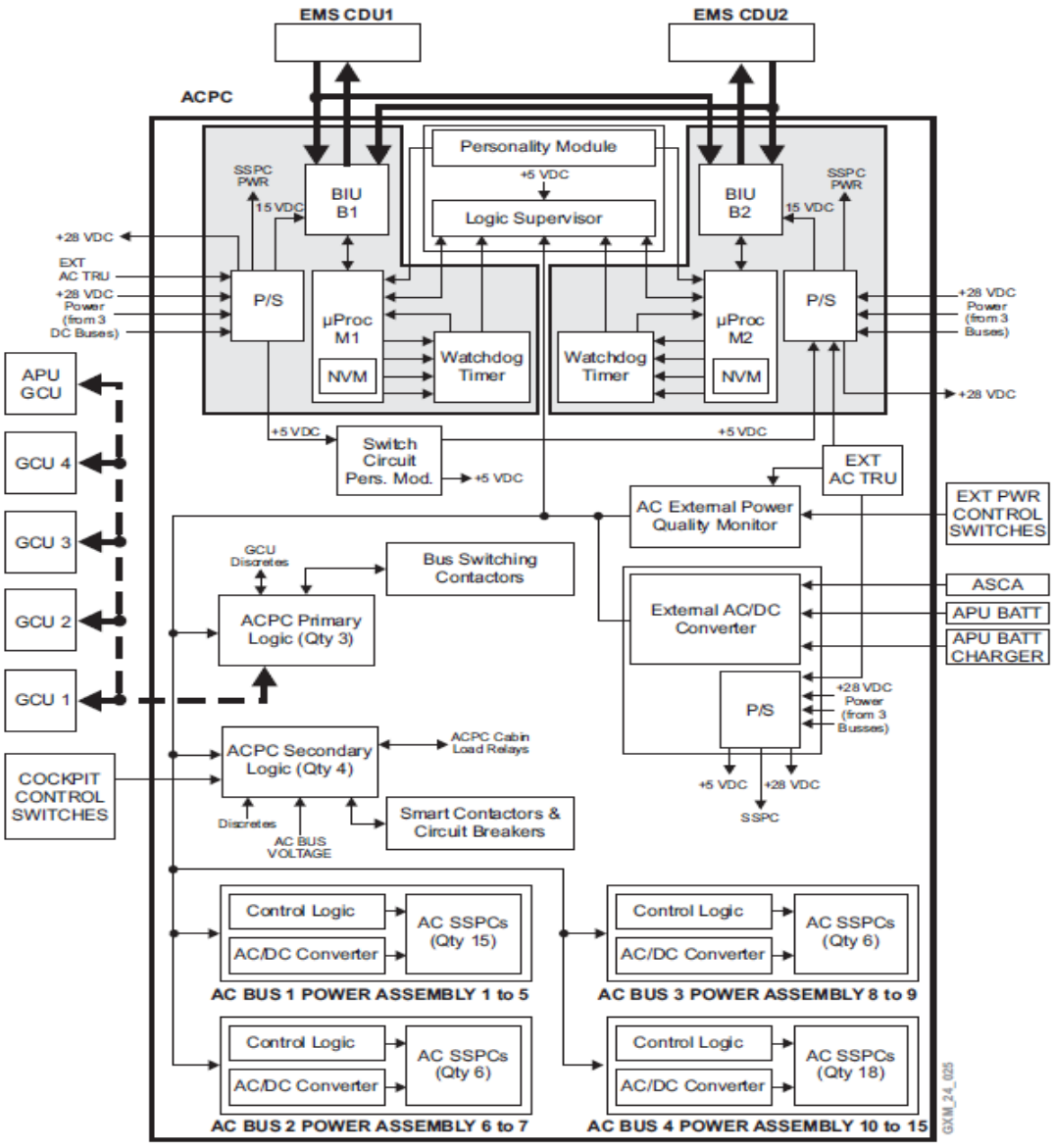

Figure 1.7. ACPC functional block [18]

1.2.3.2 Cockpit Circuit Breaker Panel (CCBP)

Located on the bulkhead behind the co-pilot's seat (see Figure 1.8 for a CCBP's electrical schematic), the Cockpit Circuit Breaker Panel (CCBP) contains:

- Thermal Breakers
- AC Bus 3A Shed relay
- Essential TRU Transfer Contactor (ETTC)
- RAT Line Contactor

The thermal circuit breakers provide distribution and protection of AC power to loads in the forward area of the aircraft. The AC Bus 3A Shed Relay (K1) is controlled by the DCPC when in the ground service mode. Thus, the Essential TRU Transfer Contactor (K2 or ETTC), is a single-pole, double-throw relay that controls the source of power to ESS TRU 1, either AC Bus 1 or AC ESS. Besides, K2 is controlled by the DCPC.

Finally, the Rat Line Contactor (K3) is a single-pole double-throw relay, controlled by the RAT Generator Control Unit and reset by the overhead control panel RAT Push Button Annunciator. It controls the source of power fed to the AC Essential Bus, either from AC Bus 4 or the RAT Generator.

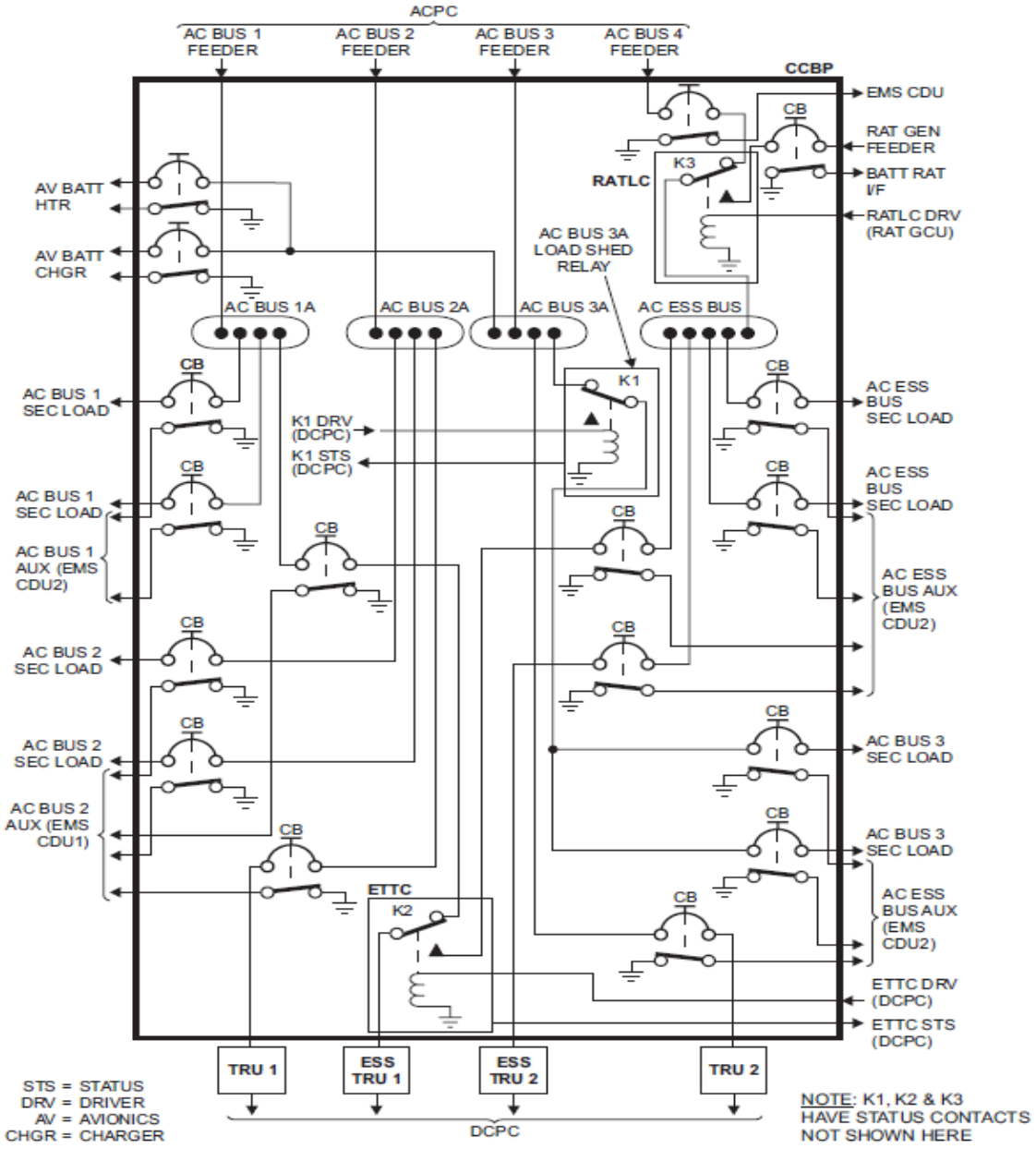

Figure 1.8. Cockpit Circuit Breaker Panel (CCBP) Electrical Schematic [18]

In relation to the Cockpit Circuit Breaker Panel (CCBP) Distribution, the CCBP buses receive power from the ACPC Primary AC Buses. Each bus is fed from only one ACPC bus. If the ACPC bus becomes unpowered, then the CCBP bus is also unpowered, with the exception of the AC Essential Bus, which can also be powered from the RAT generator. Distribution from the ACPC to the CCBP is controlled by the Secondary Logic Cards.

Power sources from the ACPC to the CCBP are listed Table 1.3:

Table 1.3. Power sources from the ACPC to the CCBP configuration [18]

CCBP	ACPC feed & Contactor
AC Bus 1A	AC Bus 1 via contactor K15
AC Bus 2A	AC Bus 2 via contactor K18
AC Bus 3A	AC Bus 3 via contactor K21
AC Essential Bus	AC Bus 4 via contactor K25 & RAT Generator Line Contactor K3. When the RAT contactor is energized power is routed directly from the RAT generator disconnecting the ACPC feed.

It is noteworthy that power sources are never paralleled on a bus. Each bus is normally supplied from its VFG via a Generator Line Contactor (GLC). One generator can power two buses, if required, via its GLC and the Generator Transfer Contactors (GTCs). Buses are physically and electrically separated from each other so that a fault on one does not affect the others. If a bus fault occurs, the GCU disconnects the generator from its bus by de-energizing its GLC but maintaining generator excitation so that the generator is available to power other ACPC Primary AC Buses.

Moreover, switching operations limit power interruptions to 50 milliseconds or less. The ACPC Secondary Power Logic Cards control and protect the AC distribution feeders, routed to the circuit breaker panel and the four electro-hydraulic pump feeders. A Variable Frequency Generator (VFG) powers only two AC Buses. If only one VFG is available, AC BUS 1 & 4 have priority (AC Bus 2 & 3 are load shed). Hence, if AC bus 1 or 4 loses its generator, the generator in the same position on the opposite engine powers it. If that one is not available, the other generator on the opposite engine powers it. If that is also unavailable, the next choice would be the other generator on its own engine, followed by the APU generator or external power.

The APU generator on its own supplies all the AC Buses when on the ground, however, some subsystem feeds are automatically load shed (i.e. Hydraulic pumps only operate one at a time). When airborne, the APU generator only supplies two AC Buses and two hydraulic pumps.

Regarding Bus Fault Protection, the GCU monitors generator loads for current draw. If an overcurrent occurs, the GCU de-energizes generator line contactor for that bus to the off position and informs the ACPC. The ACPC then configures the generator transfer contactors to isolate the bus. Table 1.4 summarizes what is intended to describe above.

Table 1.4. Bus power source logic [18]

Power Source (s) Available	AC BUS 1 PWR Source	AC BUS 2 PWR Source	AC BUS 3 PWR Source	AC BUS 4 PWR Source
VFG 1, 2, 3, & 4	VFG 1	VFG 2	VFG 3	VFG 4
VFG 1, 2, & 3	VFG 1	VFG 2	VFG 3	VFG 1
VFG 1, 2, & 4	VFG 1	VFG 2	VFG 2	VFG 4
VFG 1, 3, & 4	VFG 1	VFG 3	VFG 3	VFG 4
VGF 2, 3, & 4	VFG 4	VFG 2	VFG 3	VFG 4
VFG 1 & 2	VFG 1	VFG 2	VFG 2	VFG 1
VFG 1 & 3	VFG 1	VFG 3	VFG 3	VFG 1
VFG 1 & 4	VFG 1	VFG 4	VFG 1	VFG 4
VFG 2 & 3	VFG 3	VFG 2	VFG 3	VFG 2
VFG 2 & 4	VFG 4	VFG 2	VFG 2	VFG 4
VFG 3 & 4	VFG 4	VFG 3	VFG 3	VFG 4
VFG 1	VFG1	SHED	SHED	VFG 1
VFG 2	VFG 2	SHED	SHED	VFG 2
VFG 3	VFG 3	SHED	SHED	VFG 3
VFG 4	VFG 4	SHED	SHED	VFG4
VFG 1 & APU	VFG 1	APU	APU	VFG 1
VFG 2 & APU	VFG 2	VFG 2	APU	APU
VFG 3 & APU	APU	APU	VFG 3	VFG 3
VFG 4 & APU	VFG 4	APU	APU	VFG 4
APU GRD*	APU	APU	APU	APU
APU FLT	APU	SHED	SHED	APU
VFG 1 & EXT	VFG 1	EXT	EXT	VFG 1
VFG 2 & EXT	VFG 2	VFG 2	EXT	EXT
VFG 3 & EXT	EXT	EXT	VFG 3	VFG 3
VFG 4 & EXT	VFG 4	EXT	EXT	VFG 4
EXT**	EXT	EXT	EXT	EXT

* Some loads are shed with only APU power feeding, for example only one AC Hydraulic Pump can function at a time.

** External AC can be provided with aircraft on jacks due to airborne logic requiring Weight off wheel and 90 KIAS (Knots Indicated Airspeed).

1.2.3.3 EMS Control Display Unit

There are two identical Electrical Management System (EMS) Control Display Units (CDU) conforming part of the electrical distribution system. One CDU is located on each pilot's side panel. The CDUs provide the operator with remote control of certain circuit breakers, distribution contactors and switches, and the test facility for some circuits. They operate in two modes of operation: Normal & Maintenance mode.

1.2.4 External AC System

The External AC system has two modes of operation (see Figure 1.9), i.e. Normal mode and Service mode. Normal Mode allows all AC Buses to be powered by external AC while Service mode allows external AC to power all four ACPC AC Buses (1, 2, 3, & 4), although, their subsystem feeds are limited, with the exception of ACPC AC Bus 3, powering the Cockpit Circuit Breaker Panel (CCBP) AC Bus 3. There is one control switch for each mode of operation. It is to notice that Normal mode of operation has the priority over the Ground Service mode.

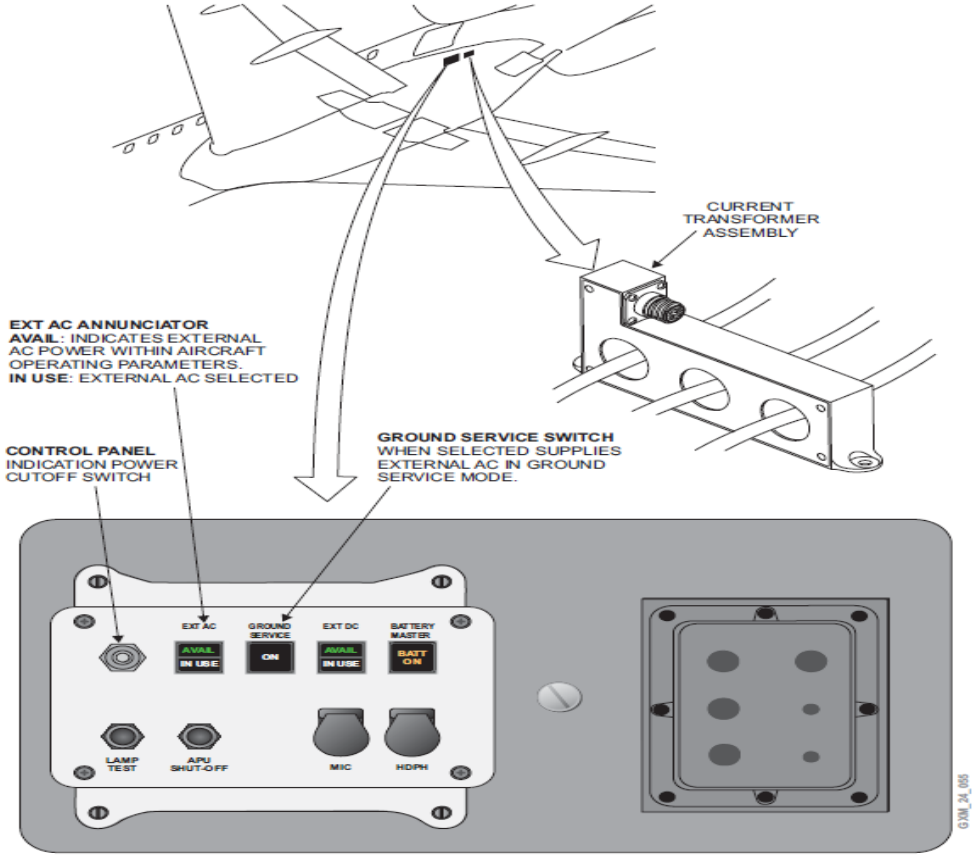

Figure 1.9. AC External Power [18]

1.2.5 Emergency AC Power Generation System

The Emergency AC Power Generation System (see Figure 1.10) is provided by a Ram Air Turbine (RAT) driven generator which is normally stowed. The RAT is rated at 9 kVA, 115/200 VAC, 3-phase, over the frequency range of 324 to 475 Hz. Deployment is automatic whenever the aircraft is airborne and a total loss of primary and auxiliary AC power occurs or loss of both

engines.. Automatic deployment can be time-delayed (14 seconds) depending on conditions during loss of power. The RAT is operational throughout the flight envelope and provides AC power to the AC Essential Bus within 6 seconds of deployment.

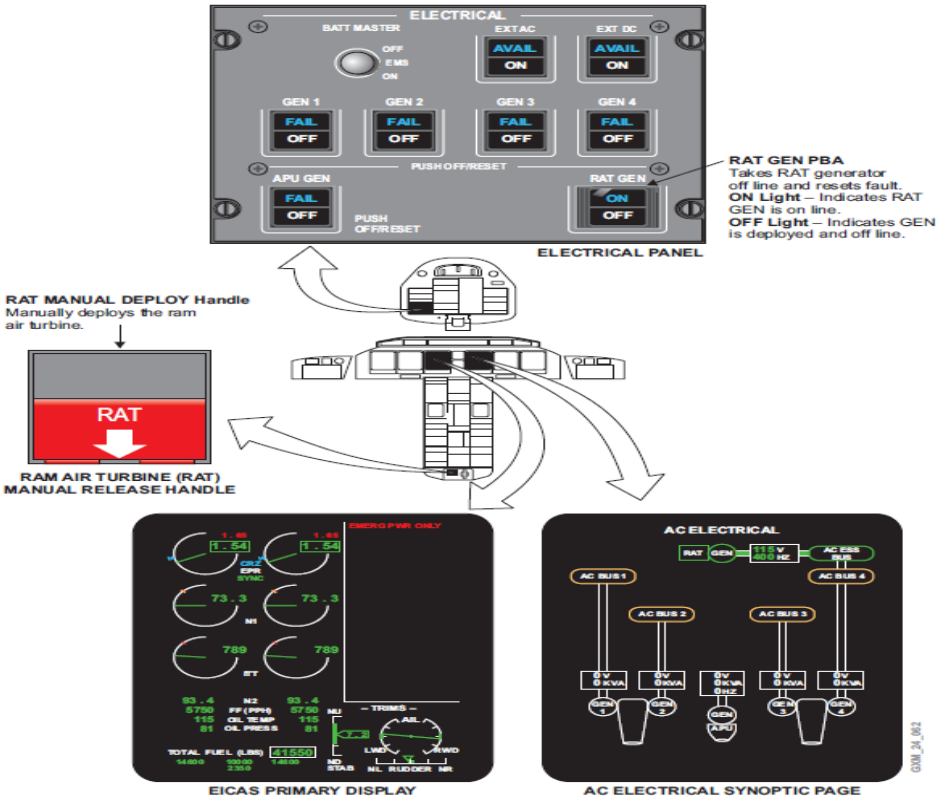

Figure 1.10. AC Emergency Electrical System Power Control and Monitoring [18]

1.2.6 DC Electrical System

The DC supply is subdivided into two systems: Static Conversion and Battery. The static conversion system is supplied by four Transformer Rectifier Units (TRUs), each TRU produces 28 VDC rated at 150 A. Meanwhile, the DC power is distributed through the DC Power Centre (DCPC) and Secondary Power Distribution Assemblies (SPDAs), while Battery backup power provides a power interrupt free system during TRU contactor switching.

Two NiCad batteries supply their respective Battery Direct bus through fast-acting, solid-state power controllers (SSPCs). The APU battery is a 21-cell nickel cadmium battery with a nominal output of 25.2 VDC, rated at 42 ampere-hours and is located in the aft equipment bay. The Avionics battery is a 20-cell nickel cadmium battery with a nominal output of 24 VDC, rated at

25 ampere-hours and located in the nose avionics compartment. Both batteries are held on charge by their associated battery chargers whenever primary, auxiliary or external AC power is available.

Regarding the DC power distribution, this is done by four TRUs supplying power to the DCPC. The DCPC is also fed by two NiCad batteries. TRU output is supplied to four primary DC buses called DC Bus # 1, DC Bus # 2, DC Essential Bus and the Battery Bus. Hence, the Battery Bus supplies the Emergency DC Bus. Also located in the DCPC is the Avionics Battery Direct Bus, which is connected directly to the Avionics battery output, and also powers the DC Emergency Bus if required.

A schematic and physical distribution of the DC power system is presented in Figure 1.11:

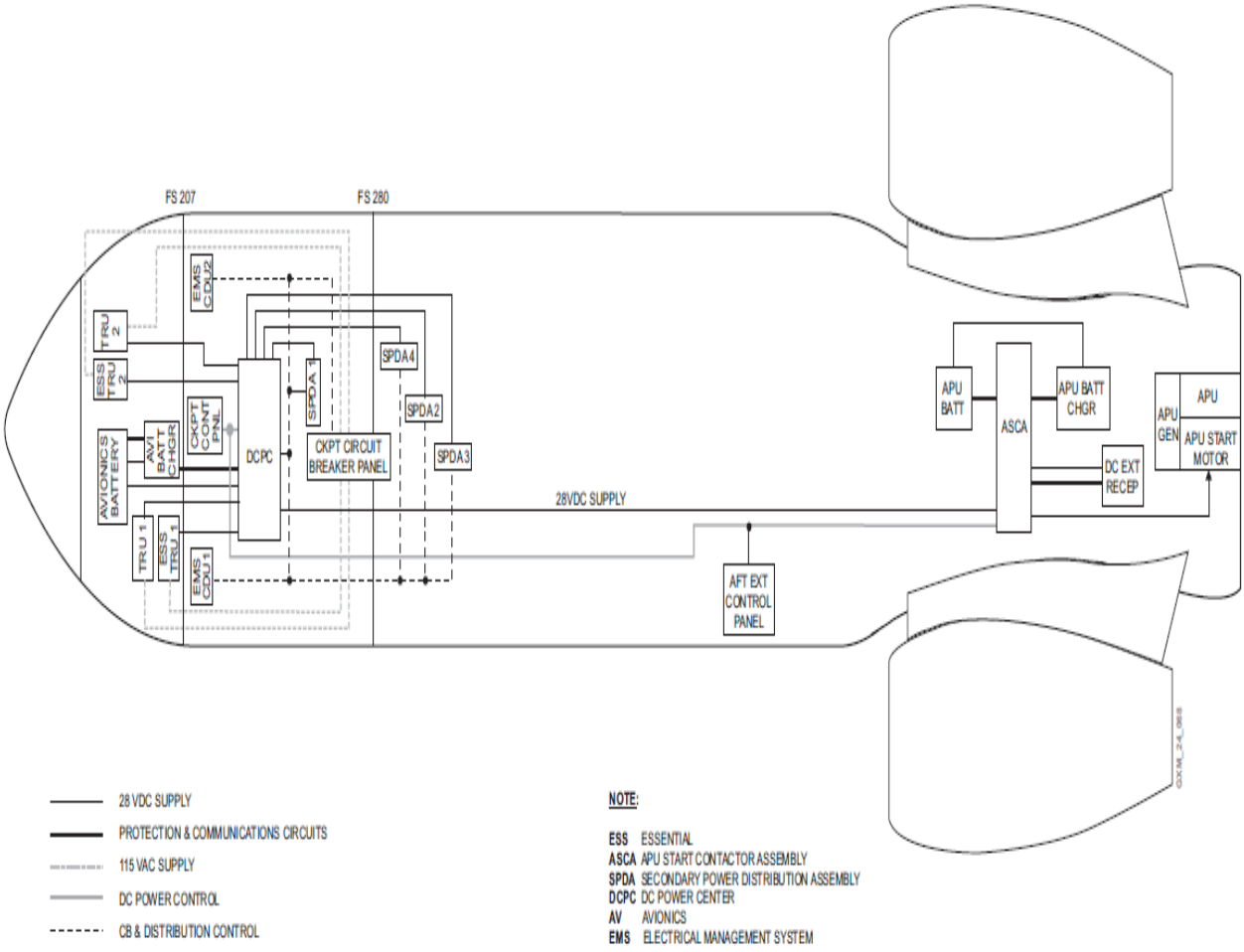

Figure 1.11. DC Electrical Power Generation and Distribution System [18]

1.2.6.1 Primary DC System

Primary DC Power, shown in Figure 1.12, is supplied by four Transformer Rectifier Units (TRU), each TRU is powered by a Cockpit Circuit Breaker Panel AC Bus as described in Table 1.5:

Table 1.5. TRU feeding configuration [18]

TRU	AC BUS FEED
TRU 1	AC Bus 2A
ESS TRU 1	AC Bus 1A
ESS TRU 1 Alternate Power Source*	AC ESS Bus (via ETTC)
ESS TRU 2	AC ESS BUS
TRU 2	AC Bus 3A

*Only when RAT deployed and essential TRU 2 has failed.

Power from the four TRUs is routed to the DCPC where it is distributed to DC Bus 1, DC Bus 2, DC Essential Bus and Battery Bus. System control is automatic but distribution or power feed control logic can be altered with the use of the EMS CDUs.

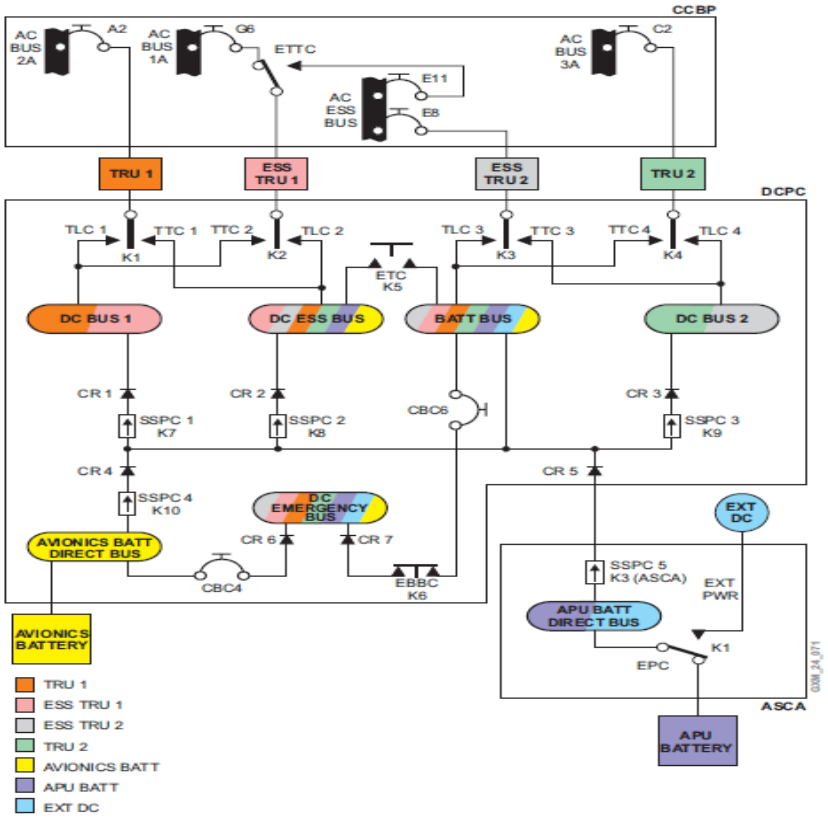

Figure 1.12. DC Electrical Power [18]

1.2.7 Battery System

The Global Express is equipped with two batteries, the APU battery and the Avionics battery, each battery is provided with a dedicated charger to charge and maintain it at the proper level during flight. Battery power is used for start-up power requirements and during emergency DC requirements.

Avionics Battery is rated at 24 VDC, 20 cell of 25 Ah. Avionics battery power is fed to the Avionics Battery Direct Bus continuously. The Avionics Battery Direct Bus supplies the DC Emergency Bus when no TRUs are on line and supplies the DCPC BATT BUS via SSPC 4 (K10) when the Battery Master switch is selected ON with no TRUs on line. Meanwhile, APU Battery is rated at 25.2 VDC, 21 cells 42 Ah. APU battery power is fed to the APU Battery Direct Bus continuously via the DC External Contactor (K1). APU Battery Direct Bus power supplies the APU Starter and via SSPC 5 (K3) supplies the DC Power Centre BATT BUS.

The Avionics Battery and the APU Battery are always supplying power to their direct buses as long as their feed receptacle is connected to the battery. The Avionics Battery Direct Bus supplies the DC Emergency Bus as long as no TRUs are supplying the BATT Bus. When TRU power is available on the BATT Bus, the TRU power is supplied to the Emergency Bus.

1.2.8 External DC System

The External DC system is designed to replace the APU Battery power feed to the APU Battery Direct Bus (see Figure 1.13). Once selected, the APU battery is isolated from the APU Battery Direct bus.

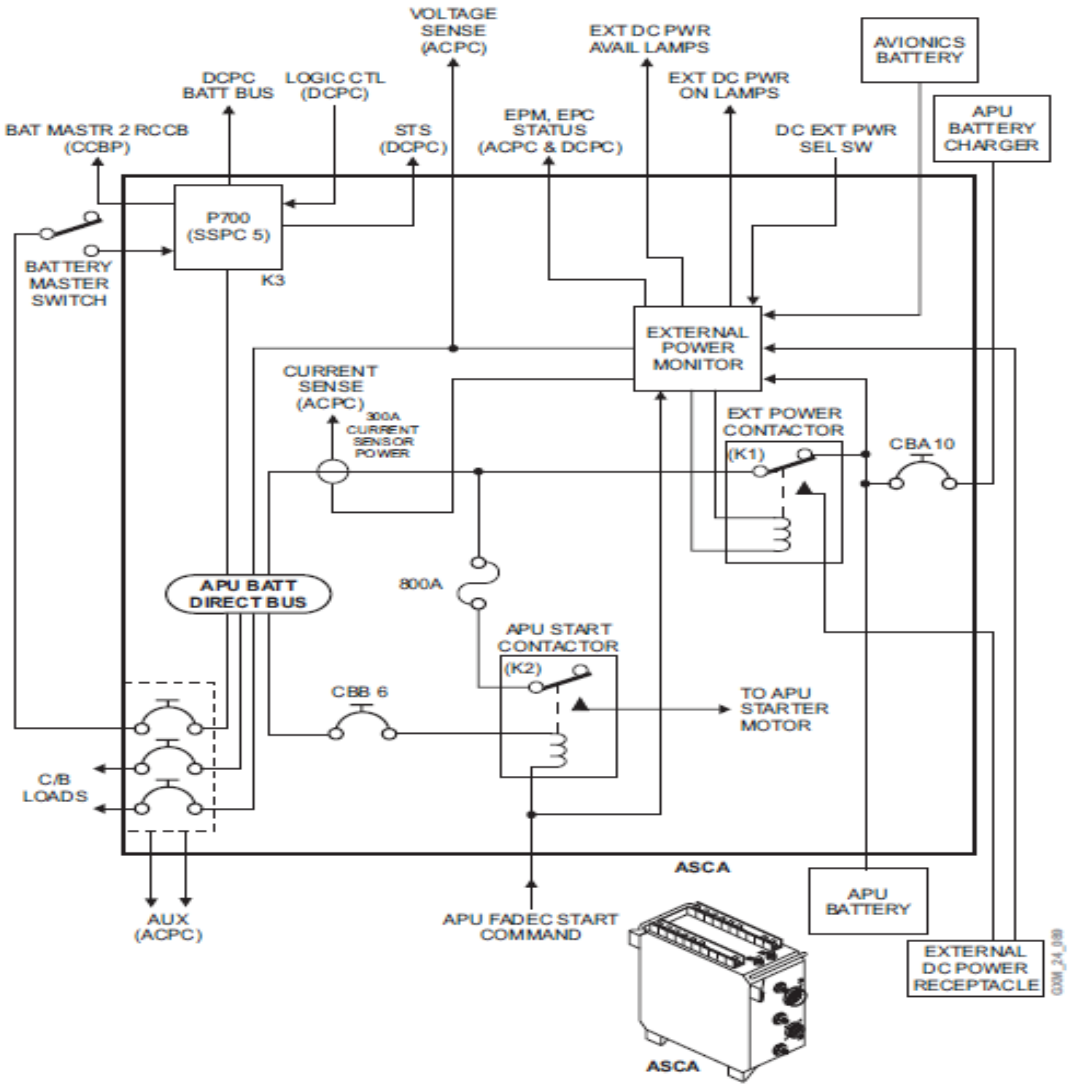

Figure 1.13. External DC Power Schematic [18]

Finally, a complete overview of the Global Express electric system is presented in Figure 1.14. The AC and DC load of Global Express are analyzed in the next chapter.

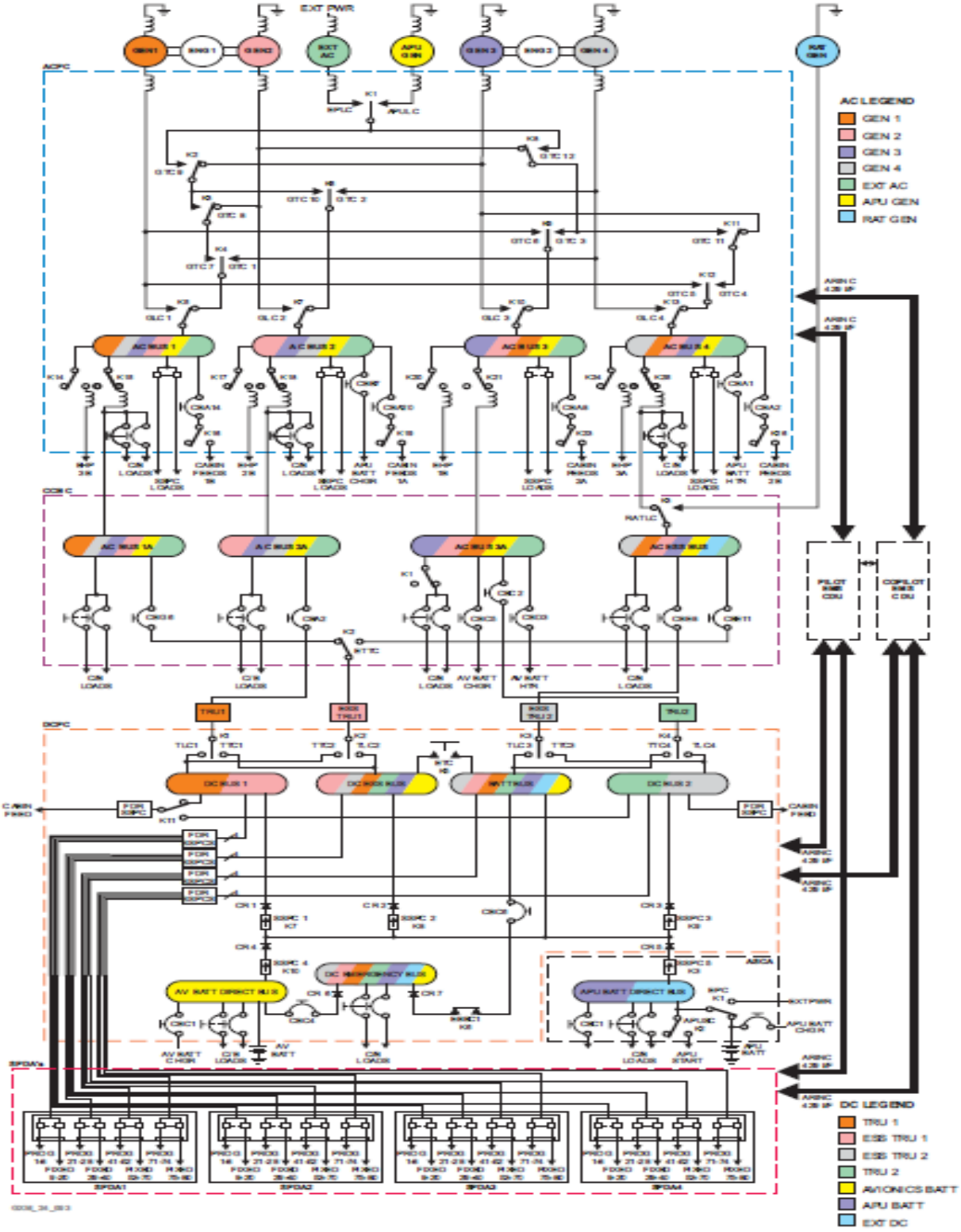

Figure 1.14. Electrical System Schematic [18]

CHAPITRE 2 GLOBAL EXPRESS AIRCRAFT ELECTRIC POWER SYSTEM MODEL

The objective of this chapter is to explain the behaviour of generators, TRUs, AC and DC loads, AC and DC cables, switching controls and other electric elements inside the aircraft modeled during this research.

The main analysis presented in this chapter is based on the baseline Global Express and meets the intent of MIL-E-7016F [20]. This military standard called "Analysis of Electric Load and Power Source Capacity", addresses the methods and analysis of electric loads and source capacity on military aircrafts and commercial aircrafts as well.

2.1 Operating Conditions

The operating conditions are as listed below with the applicable frequency. The actual frequency ranges for these conditions may vary according to RAE-700-103 [19].

Table 2.1. Operating Conditions [19]

Reference	Description	Frequency [Hz]
G1	Ground Maintenance	400
G2	Loading and Preparation	400
G3	Start and Warm-up	324
G4	Taxi	380
G5	Take-off	580
G6	Climb	540
G7	Cruise	500
G8	Descent	400
G9	Landing	430
G10	Emergency	400

The ground maintenance (G1) operating condition exists when electric components are being repaired, checked or tested, and electric power is supplied by an external power source. All AC and DC busses are powered. Loading and preparation (G2) is a condition between securing and starting. Operations performed during this period may consist of fuelling, lighting, heating, cooking, etc. During this period, power is supplied by the auxiliary power unit, battery or external source to specific service loads.

Start and warm up (G3) is the condition from preparation for starting to taxiing. All busses are available. Meanwhile, Taxi (G4) is from the aircraft's first movement under its own power to the start of the takeoff run. It also includes from completion of landing rollout to engine shutdown. All busses are powered in normal electrical configuration. Takeoff (G5) is a condition commencing with the pilot pushing the throttle for takeoff until beginning of climb. All busses are powered in normal electrical configuration.

Climb (G6) is the condition beginning with the climb and ending with the aircraft in the levelled-off attitude and set for cruising operation. All busses are powered in normal electrical configuration.

Cruise (G7) is the condition during which the aircraft is in flight level. All busses are powered in normal electrical configuration.

Descent (G8) is the condition commencing with descent run and entering into the base leg. All busses are powered in normal electrical configuration.

Landing (G9) begins with the landing approach and completes at rollout. All busses are powered in normal electrical configuration.

Finally Emergency (G10) is any period of flight during which the normal sources of power are inoperative. During such periods, all loads essential to aircraft safety of flight (under any flight condition) are transferred to an emergency generator driven by a ram air turbine. In this condition, only the Air Driven Generator (ADG), DC ESS and Battery Busses are powered from that emergency generator.

2.2 AC Electrical System

Figure 2.1 shows the schematic for the Global Express electric power system. There are four main AC busses, normally supplied from four 40 kVA frequency variable generators. The busses are titled AC Bus 1, AC Bus 2, AC Bus 3 and AC Bus 4. There is also an AC ESS BUS which has the essential loads connected to it. Normally the AC ESS Bus is supplied via AC Bus 4, but under the emergency operational mode when the RAT is deployed, power is sourced by the RAT generator [18].

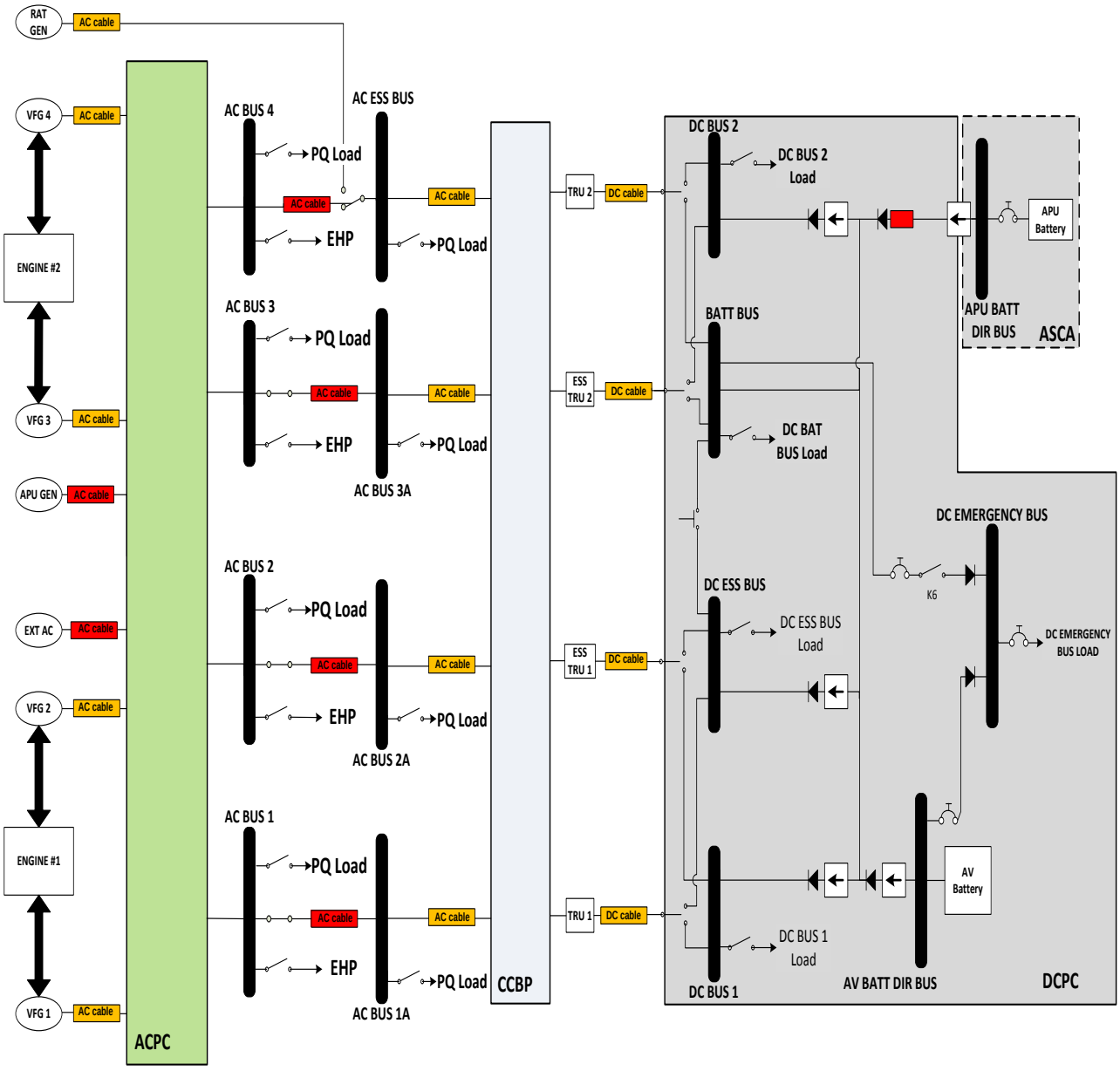

Figure 2.1. One-line diagram of aircraft electric power system

The busses are of various priority levels, which are as follows in order of increasing priority: AC Bus 2 and AC Bus 3 (equal priority), AC Bus 1 and AC Bus 4 (equal priority), and AC ESS Bus.

A fifth generator rated at 45 kVA (ground operation) driven by the APU (Auxiliary Power Unit) is also available; however, this generator is primarily intended for ground use. In addition, a sixth generator rated at 9 kVA, 400 Hz, 0.75 to unity power factor continuously, is driven by a

RAT (Ram Air Turbine) and provides power for emergency use [19]. The RAT also drives a hydraulic pump located at the AC BUS 4 for this operational condition. The RAT is automatically deployed upon loss of all other aircraft AC power supplies. The RAT is subject to de-rating as air speed decreases, and therefore limitations on loading may apply at low airspeeds. If all AC loads are off-loaded then the aircraft systems would rely on battery power. At 145 KEAS (Knots Equivalent Air Speed) the RAT generator is off-loaded in order to ensure that hydraulic power can be supplied to the flight control surfaces. During flap and slat actuation (approximately 6.6 kVA peak), the DCPC (Direct Current Power Centre) ensures that ESS TRU 1 and ESS TRU 2 outputs are disconnected, so that the short term loading on the RAT generator does not cause the RAT to stall.

2.2.1 Variable Frequency Generators Model

As mentioned in Chapter 1, VFGs are rated to 115/200 VAC, 3-phase, 324-596 Hz, 40 kVA. For the purpose of this research, VFGs are modeled using ideal voltage sources, so that Three-Phase Programmable Voltage Sources are used instead, located in the Electrical Sources of the SimPowerSystems (SPS) Library [14]. These blocks generate a three-phase sinusoidal voltage with time-varying parameters. The time variation for the amplitude, phase, or frequency of the fundamental component of the source, can be programmed. In addition, two harmonics can be programmed and superimposed on the fundamental signal. For this research, Table 2.2 shows the parameters that were employed for the sources, as well as their values during simulation:

Table 2.2. Parameters for Three-Phase Programmable Voltage Sources

Parameter Description	Value
Positive Sequence Voltage Amplitude in Vrms phase-to-phase	200
Positive Sequence Voltage Phase in degrees	0
Positive Sequence Voltage Frequency in Hertz	324 - 580

Figure 2.2 shows Three-Phase Programmable Voltage Sources as VFGs within the aircraft electric power system model. The implications of not modeling of VFGs as electrical machines are explained in Chapter 3, section 3.3.

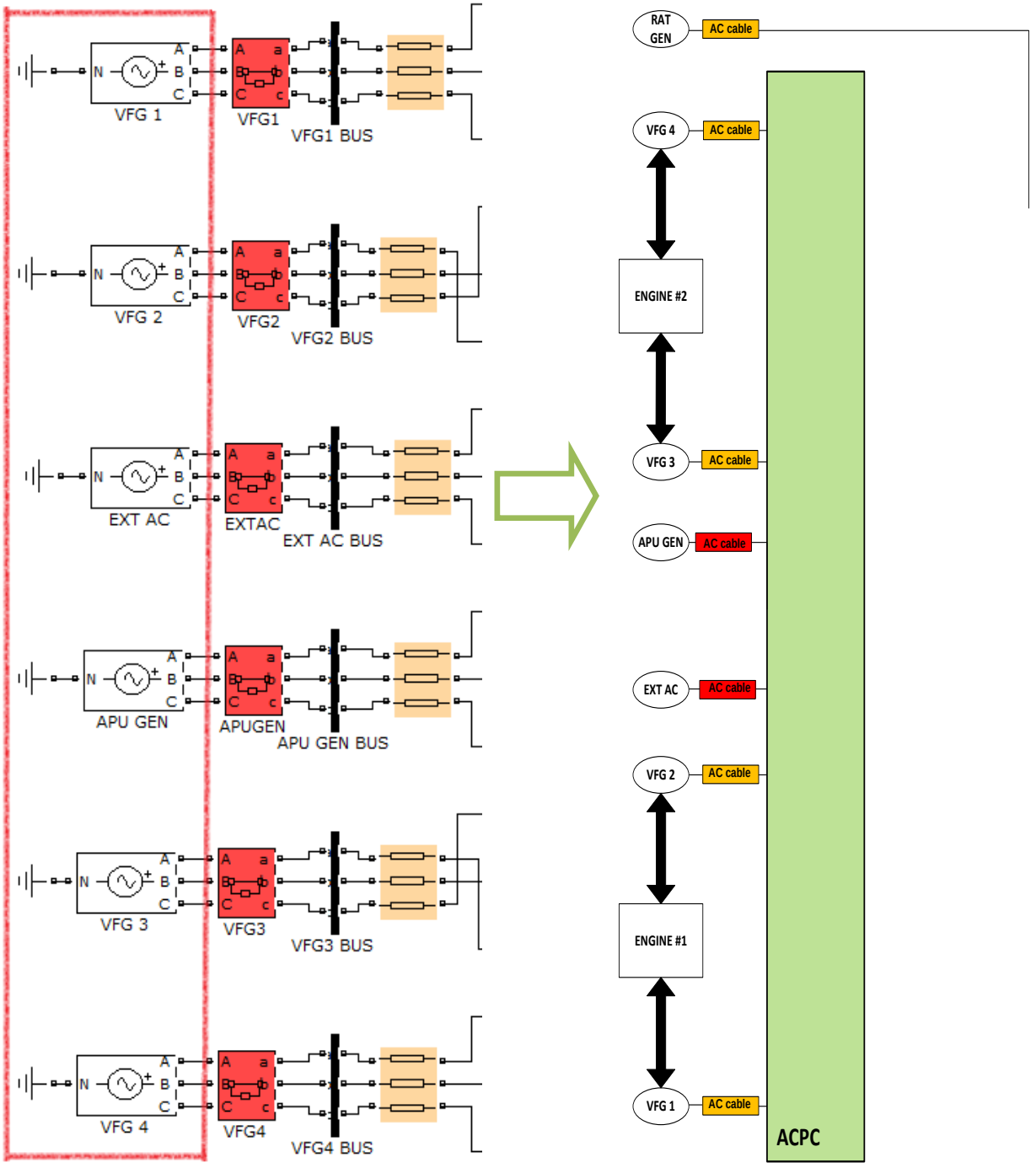

Figure 2.2. VGF's block implemented in Simulink and its location in actual aircraft electric power system

2.2.2 AC Power Centre (ACPC)

The AC system architecture is shown by Figure 2.3. A means of connecting External AC power is also provided.

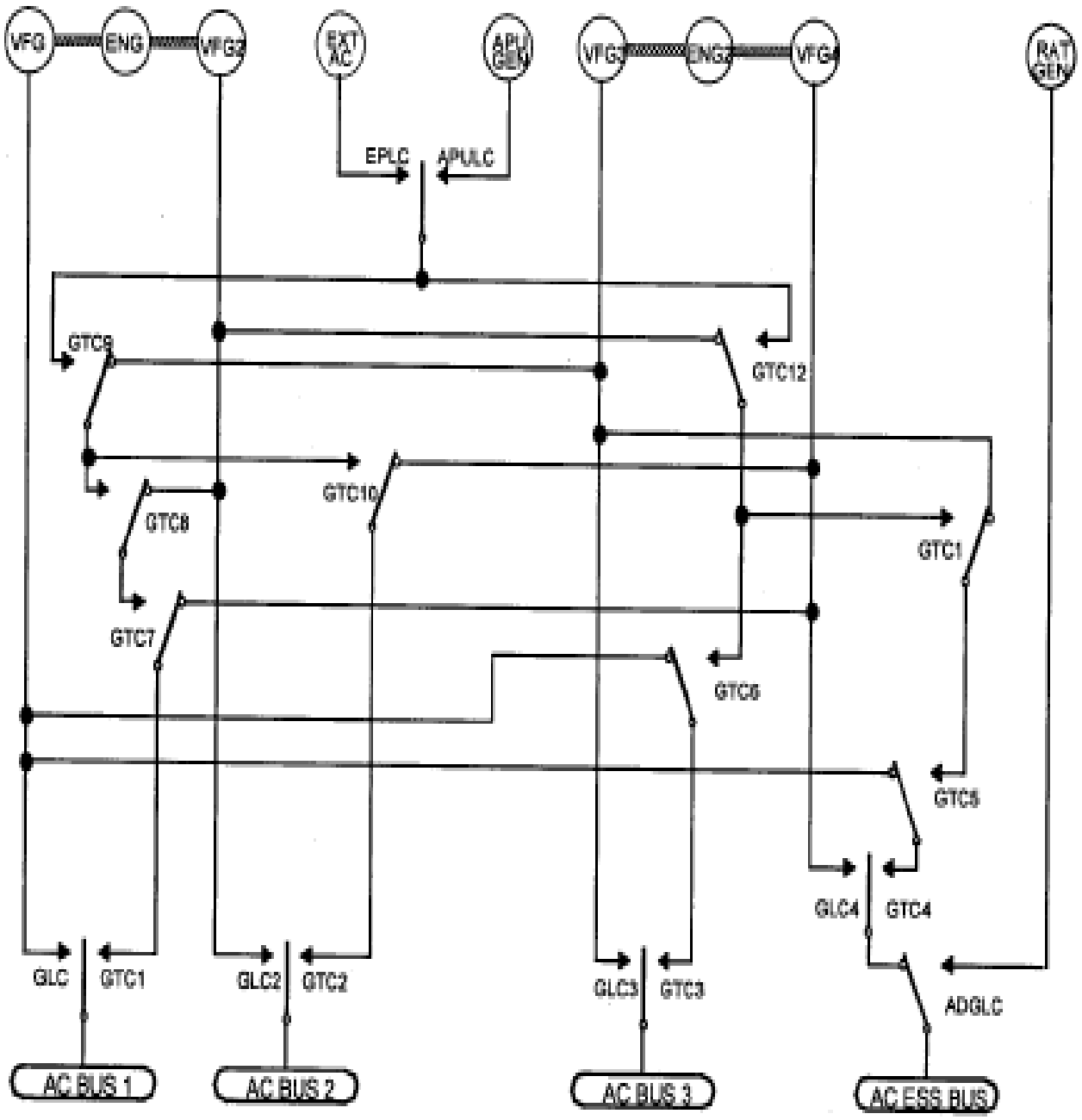

Figure 2.3. ACPC Electrical System schematic [19]

Table 2.3 gives the AC contactor logic with APU available

Table 2.3. AC system contactor operation logic with APU available [19]

POWER SOURCE STATUS	BUS POWER SOURCE				
	AC BUS 1	AC BUS 2	AC BUS 3	AC BUS 4	AC ESS BUS
NORMAL	VFG 1	VFG 2	VFG 3	VFG 4	VFG 4
VFG 4 FAIL /OFF	VFG 1	VFG 2	VFG 3	VFG 1	VFG 1
VFG 3 FAIL /OFF	VFG 1	VFG 2	VFG 2	VFG 4	VFG 4
VFG 3 & 4 FAIL /OFF	VFG 1	VFG 2	VFG 2	VFG 1	VFG 1
VFG 2 FAIL /OFF	VFG 1	VFG 3	VFG 3	VFG 4	VFG 4
VFG 2 & 4 FAIL /OFF	VFG 1	VFG 3	VFG 3	VFG 1	VFG 1
VFG 2 & 3 FAIL /OFF	VFG 1	VFG 4	VFG 1	VFG 4	VFG 4
VFG 2 & 3 & 4 FAIL /OFF	VFG 1	APU	APU	VFG 1	VFG 1
VFG 1 FAIL /OFF	VFG 4	VFG 2	VFG 3	VFG 4	VFG 4
VFG 1 & 4 FAIL /OFF	VFG 3	VFG 2	VFG 3	VFG 2	VFG 2
VFG 1 & 3 FAIL /OFF	VFG 4	VFG 2	VFG 2	VFG 4	VFG 4
VFG 1 & 3 & 4 FAIL /OFF	VFG 2	VFG2	APU	APU	APU
VFG 1 & 2 FAIL /OFF	VFG 4	VFG 3	VFG 3	VFG 4	VFG 4
VFG 1 & 2 & 4 FAIL /OFF	APU	APU	VFG 3	VFG 3	VFG 3
VFG 1 & 2 & 3 FAIL /OFF	VFG 4	APU	APU	VFG 4	VFG 4
ALL VFG FAIL/OUT	APU	LOST	LOST	APU	APU
APU GEN & ALL VFG FAIL/OUT	LOST	LOST	LOST	LOST	RAT
EXTERNAL POWER	EXT	EXT	EXT	EXT	EXT
ALL VFG FAIL/OFF	APU	APU	APU	APU	APU

An implementation of the ACPC within the Simulink environment is shown in Figure 2.4.

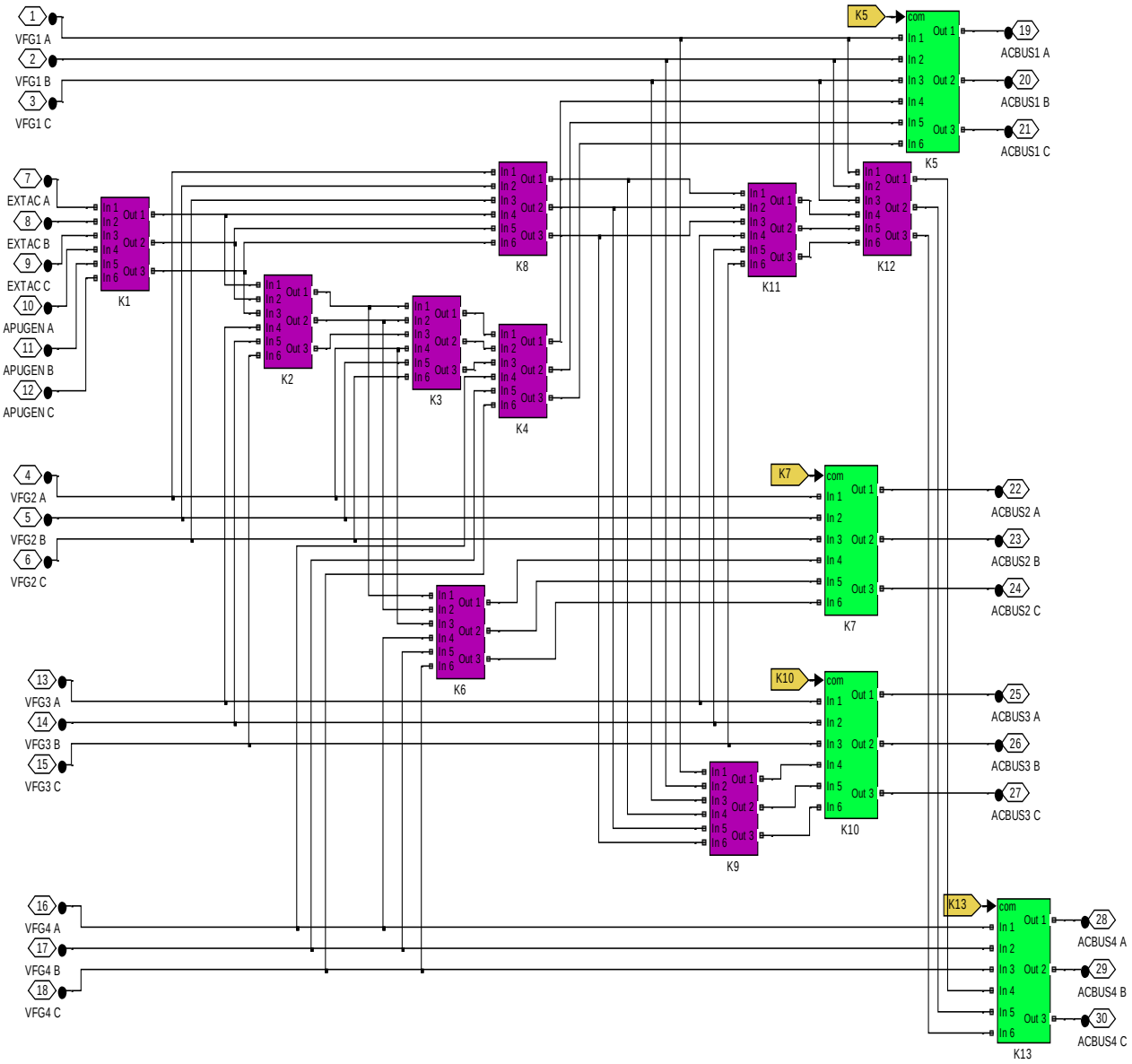

Figure 2.4.ACPC implementation in Simulink

Each switch has a 50 ms time delay which is in fact the maximum switching operation time for power interruptions. Figure 2.5 shows the implementation of the maximum switching time in Simulink. As soon as a VFG failure occurs at a specific time, the switches related to the event operate 50 ms after the failure. This value can be easily changed, since the time delay could be less than 50 ms, depending on the characteristics of the switch.

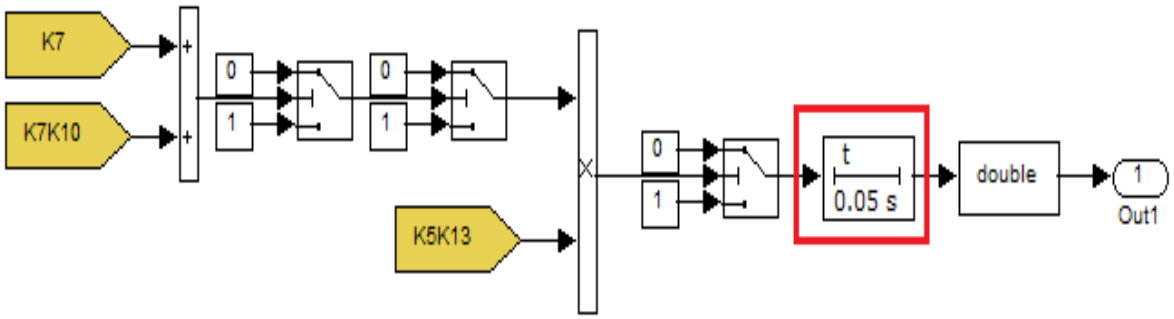

Figure 2.5. Maximum switching time implemented in Simulink

It is worth noting that generators rotate in opposite directions depending on their location, as explained in Chapter 1, section 1.2.1. Phase sequence of generator 1 and 4 is A, B, C. Phase sequence of generator 2 and 3 is C, B, A. To that effect, phase sequence is corrected by switching A and C phases of generators 2 and 3 in the ACPC. This is implemented in the aircraft electric power system modeled in Simulink, as shown in Figure 2.6. Implications of not modeling this phase sequence are explained in Chapter 3.

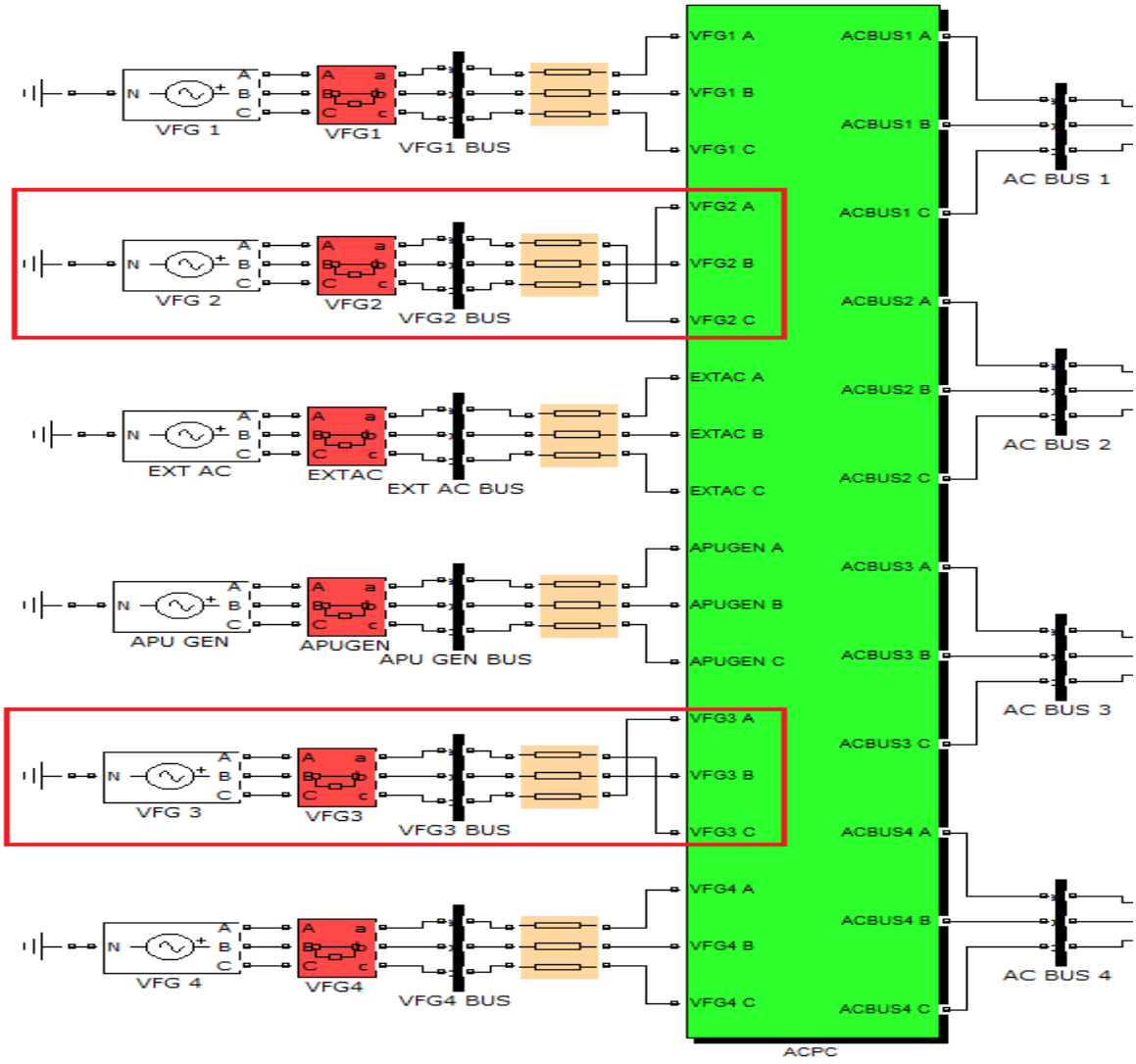

Figure 2.6. Phase sequence of Generator 2 and 3 implemented in Simulink

Logical controls must be validated within the detailed aircraft electric power system model. In this work the switches are modeled using three-phase breakers [14] and a delay is included for position changes, as mentioned before. When a SPDT (Single-Pole, Double-Throw) switch needs to go from one contact to another, the opening stage is instantaneous and there is a delay before closing on the second contact. On the Global Express, there are two types of contactors: Standard SPDTs used for architecture reconfiguration, and Solid State Power Controllers (SSPC). The SSPCs are faster than SPDT and are used to supply emergency DC power to buses that are not fed by their usual power supply. More sophisticated switch models must be used to investigate arcing problems causing a switch to stick during operation. The large number of switches can create simulation performance constraints for repetitive operation cases.

2.2.3 AC Switching Control Centre (ACSCC)

The AC Switching Control Centre (ACSCC) is responsible for sending binary signals to the external switching time control for the ACPC switches, in order to change ON/OFF state positions. It is created and implemented in Simulink for the purpose of this research, so that a more realistic and sophisticated power system model is accomplished.

The current implementation of reconfiguration switching controls is based on truth tables representing Global Express reconfiguration logic [18]. The switch states vary depending on a game of events regarding loss of VFGs and TRUs, so that the AC system architecture alternates to provide electrical power to every bus, as indicated in Table 2.3. The amount of logical controls is vast and implementing all of them is not the goal of this research. Only basic architecture reconfiguration according to VFG and TRU status is implemented in the power system presented here. Figure 2.7 shows a flowchart of the ACSSC logic switching signal command.

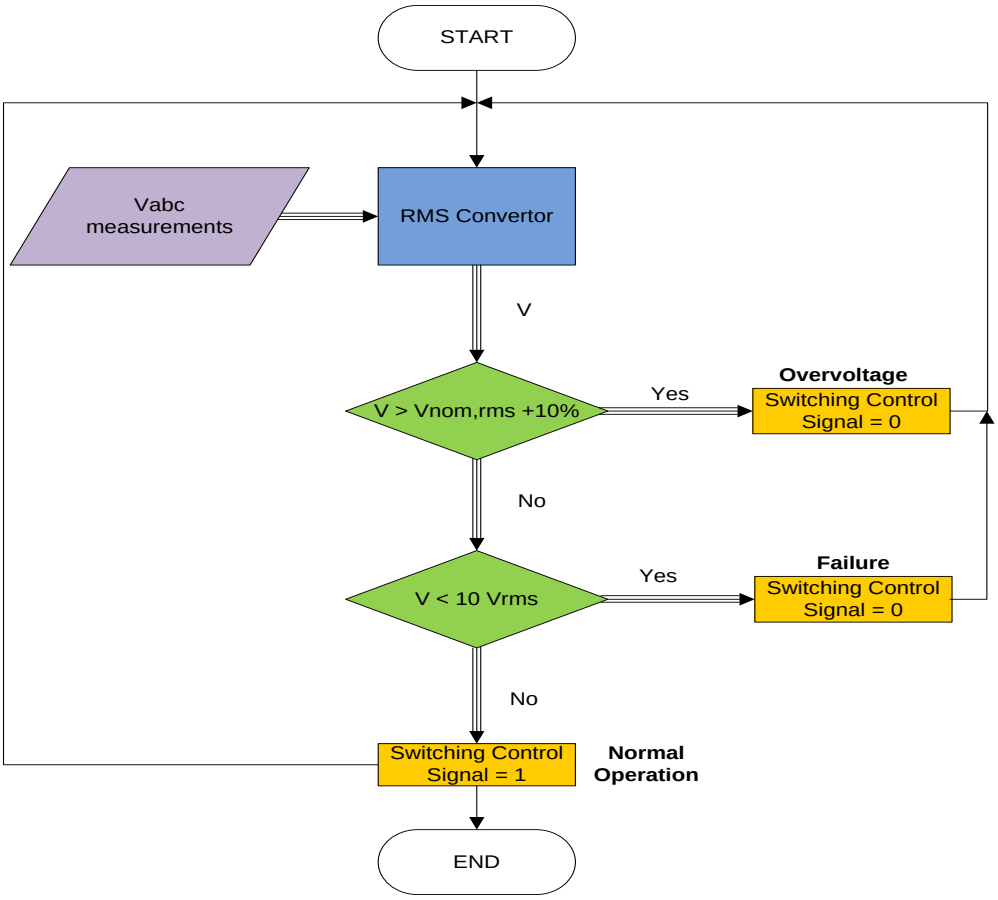

Figure 2.7. Flowchart of the ACSSC logic switching signal command

For the functionality of the ACSSC, a subsystem named "Measurements" is created for the purpose of capturing phase-to-ground voltage and current measurements for every source of energy (VFGs, APU, EXT AC and RAT GEN), AC busses, AC loads and DC loads as shown in Figure 2.8 and Figure 2.9. It calculates EHP active and reactive power and captures the rotor speed, and electromagnetic and mechanical torque signal from the ASM model. Every signal within the "Measurements" subsystem is sent to the workspace for further treatment. The "Measurements" subsystem divides data to workspace in sources, bus 1 (AC Bus 1), bus 2 (AC Bus 2), bus 3 (AC Bus 3), bus 4 (AC Bus 4), ehp (EHP) and dc (DC Bus1, DC ESS Bus, DC Emergency Bus, DC APU Battery, Avionic Battery, and Battery Bus).

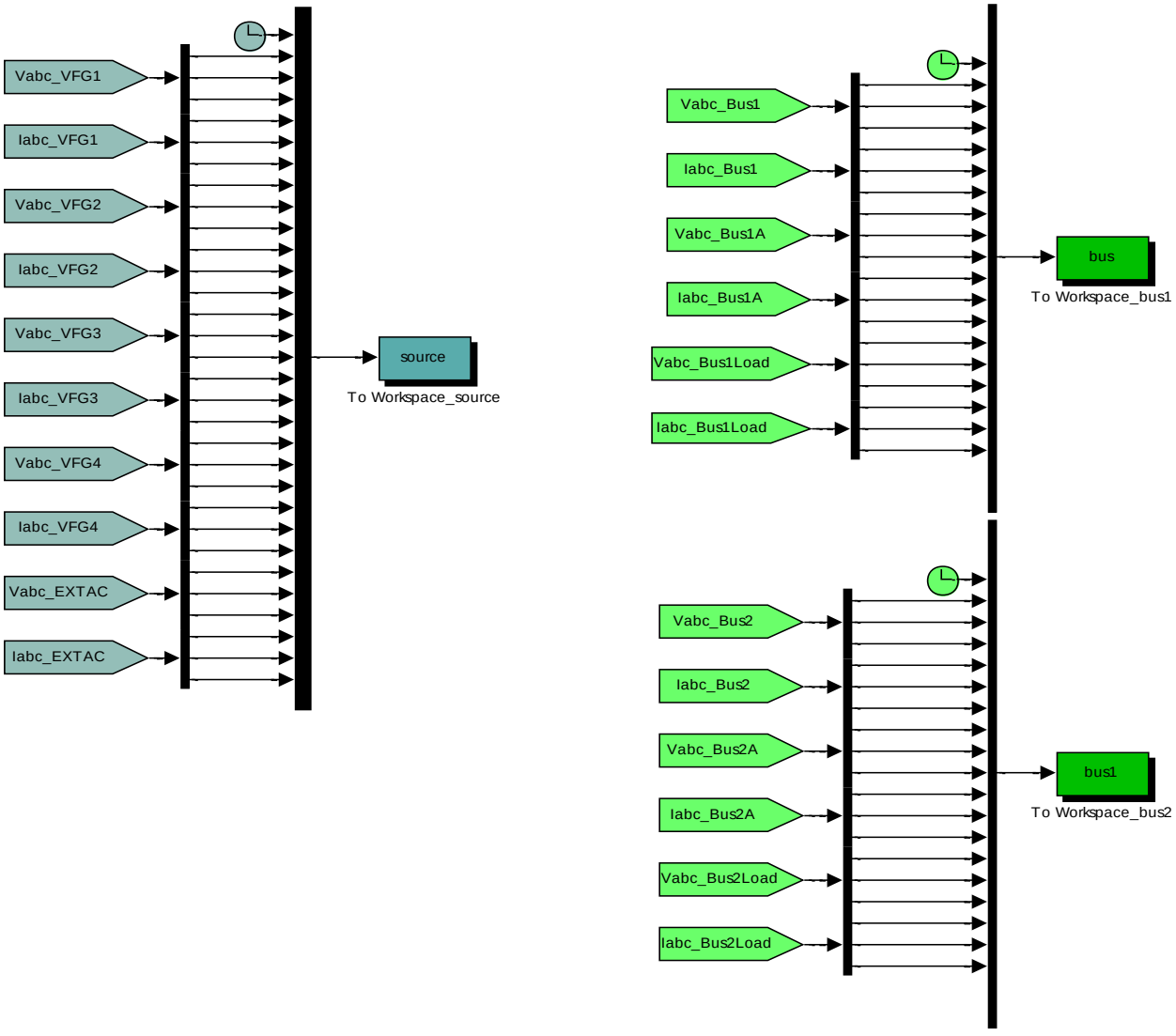

Figure 2.8. "Measurements" subsystem architecture of signal processing (first part)

ACSCC takes phase-to-ground voltage data from "Measurements" and then separates voltage data for each phase, so that VA, VB and VC are separately converted in RMS values by the Discrete RMS Value block from SPS library, which computes the true RMS value (including fundamental, harmonic, and DC components) of input voltage signal. The RMS value is calculated over a running window of one cycle of the specified frequency.

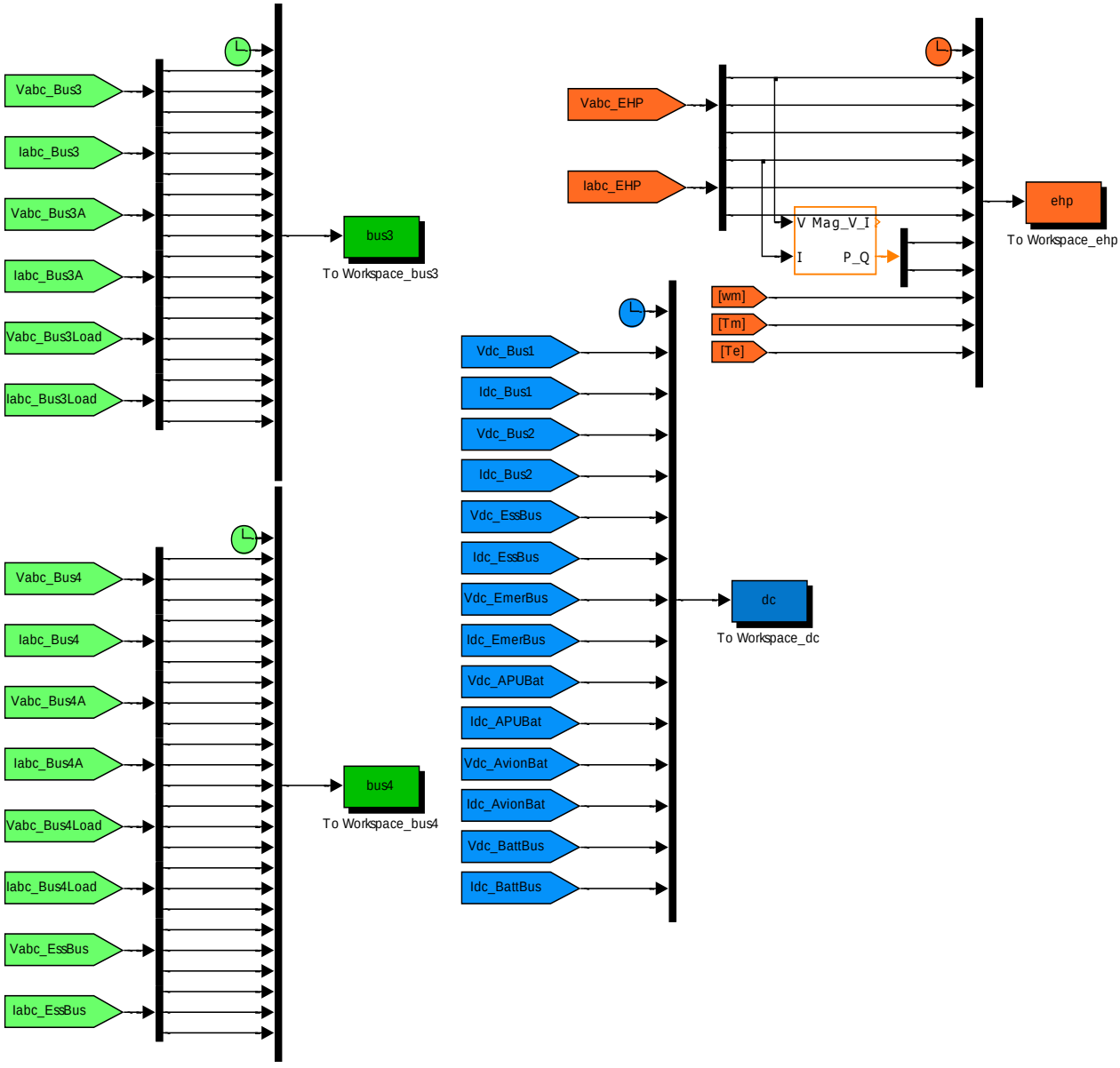

Figure 2.9. "Measurements" subsystem architecture of signal processing (second part)

Once a voltage signal is converted into RMS, each phase value passes through a dead zone block. It outputs zero then the input is within the dead zone (starting at 126.5 Vphase, RMS which is the RMS nominal voltage plus 10%). If the input signal exceeds 126.5V RMS, an

overvoltage occurs and a zero signal is sent to the ACPC, for network reconfiguration in accordance with Table 2.3. If the input signal is outside the dead zone, that is less than 10 VRMS, a failure occurs and a zero signal is again sent to ACPC, for automatic network reconfiguration. The logic command is able to detect any loss of any phase of VFGs by summing each output (after dead zone) and adding a switch block at the end of the sum. If the sum is greater than or equal to two (indicating the loss of two phases), logic command interprets it as a failure, so that ACPC automatically reconfigures the aircraft electric power system. Otherwise, if the sum is less than two (indicating the loss of just one phase), logic command does not interpret this as a failure, therefore no automatic reconfiguration is performed. Finally if the input signal is within 10 V RMS and 126.5 V RMS, the electric power system is operating under normal voltage conditions and no reconfiguration is needed. In addition when an RMS voltage measurement is within the dead zone, the ACSCC sends a one signal, indicating normal operation.

Figure 2.10 shows the first part of the ACSCC. This part is in charge of detecting any single loss of VFGs and then sending binary signals to the external switching time control for the ACPC switches K5, K7, K10 and K13, according to VFGs' failures.

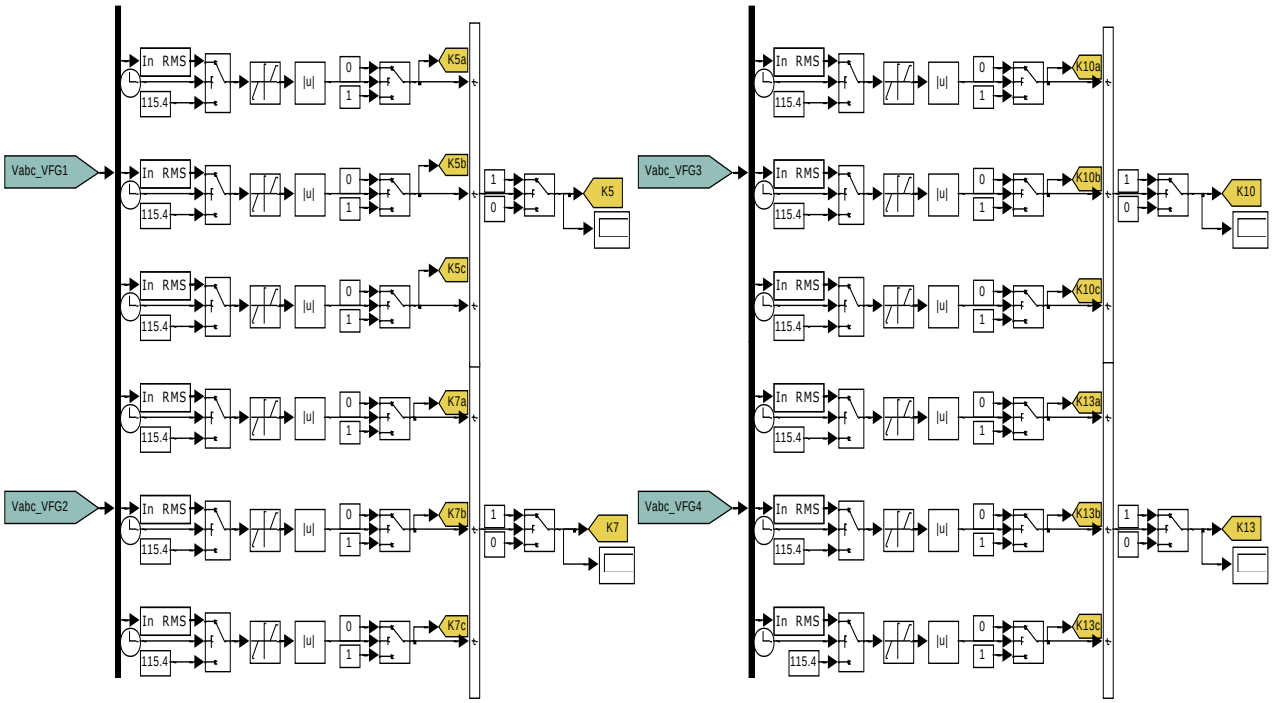

Figure 2.10. Schematic of the ACSCC implemented in Simulink (first part)

A second part is show in Figure 2.11. This part detects when two or more VFG fail and then sends binary signals to the external switching time control for the ACPC switches (K2, K3, K4, K6, K8, K9, K11, K12), according to VFGs' failures. As shown in Figure 2.9, on the left side, a logic command is presented when two VFGs fail, meanwhile at the center, the logic command is for the case of three VFGs failing. Finally, on the right side, when there is a global failure, the RAT supply is activated.

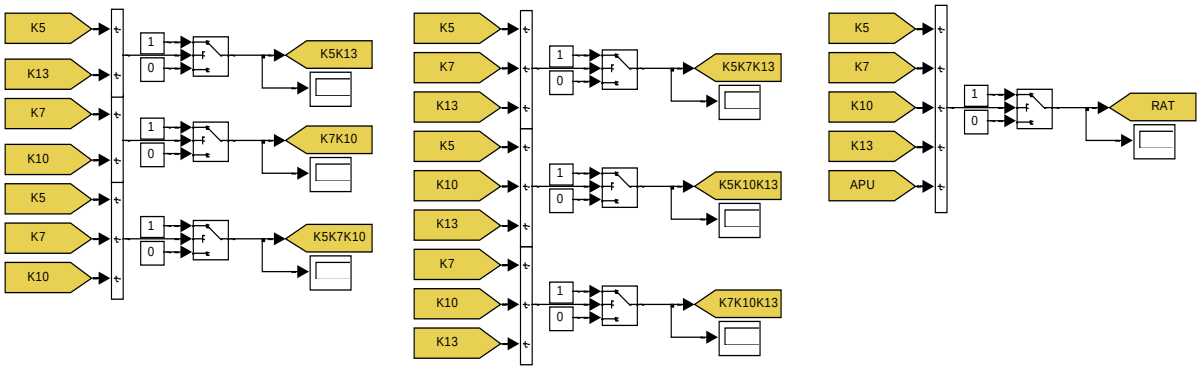

Figure 2.11. Schematic of the ACSCC implemented in Simulink (second part)

2.2.4 AC Cables

A block was created, edited and scripted in Simulink to generate AC cable impedance parameters based on [21], which presents impedance data compiled by the authors for use in designing and testing aircraft electrical systems, employing three-phase and 400 Hz auxiliary power. Figure 2.12 shows a cross-section of a nickel coated copper cable used inside the aircraft for linking AC BUS 1 and AC BUS 1A. A is for the conductor material (nickel coated copper), B is for the primary insulation (radiation cross linked, modified, flexible ETFE), and C for the jacket (radiation cross linked, modified, flexible ETFE). The maximum continuous conductor temperature rating is 200°C and the voltage rating is 600 Vrms.

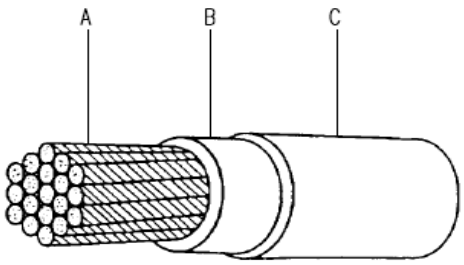

Figure 2.12. Cross-section of a nickel coated copper cable linking AC BUS 1 to AC BUS 1A [19]

It also presents, tabulated impedance data for a number of typical configurations using multiple wire feeders in 0.5 inch flat spacing and laced three-phase groups. In addition, the authors in [21] calculate positive sequence data directly from the geometry of the wire configurations, while zero sequence data is dependent upon the particular ground return circuit employed and modified by an empirically determined skin correction term. The latter correction must be carefully reviewed with respect to the current practices in aircraft design, but this is out of the scope of the current project. Figure 2.13 presents the implementation of the AC cables in Simulink.

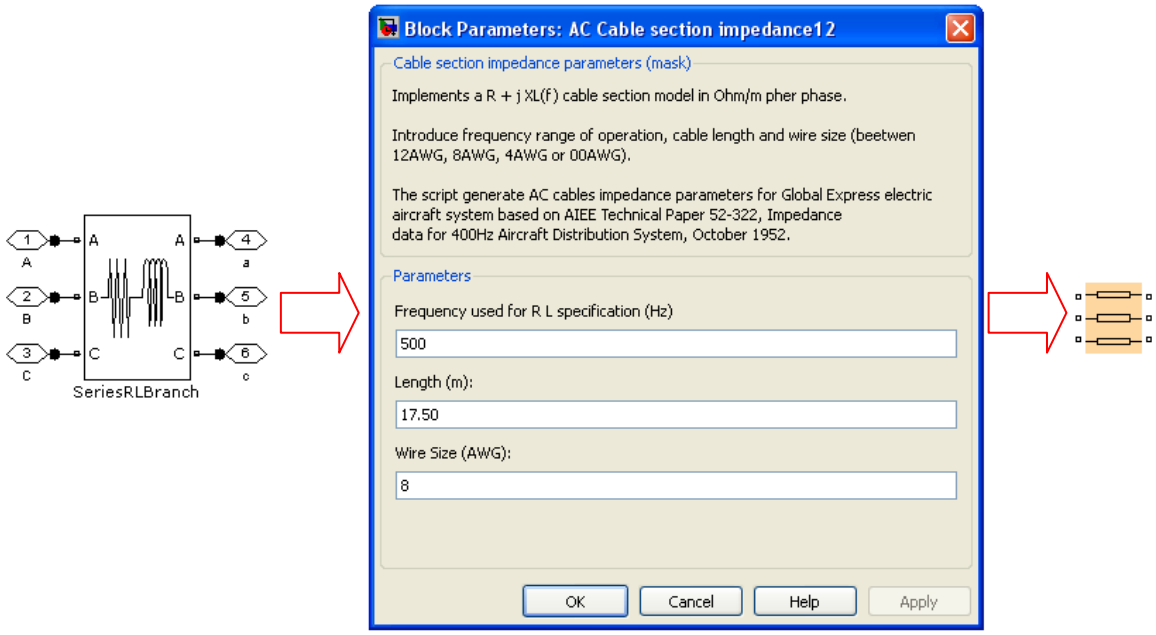

Figure 2.13. AC Cable Block implementation in Simulink

The Authors in [21] explain that the fact of working "only with laced three-phase groups and three-phase groups in 0.5 inch flat-spacing", is because "these configurations are considered the

most likely to be used in present designs" [21]. They also indicate the following statements in order to clarify the use of the tabulated data:

1. The positive sequence impedance data are all calculated values based on AN-J-C-48a wire specifications and on the 400 Hz resistance information in "General Electric Data Folder #63004", from General Electric Company. Hence, " the data is not affected by the type of body structure or whether or not the wires are run in non-magnetic conduit" [21].
2. The zero sequence data is assembled by "calculating the theoretical impedance assuming an infinite perfect skin return circuit and then applying empirical corrections terms to account for the actual skin structure" [21] for a fixed frequency of 400 Hz.
3. The zero sequence reactance is read directly from the curves for the proper size, elevation and group separation. Hence, "the zero-sequence resistance is obtained by adding the value ROC from the table in each figure to the value of RS from the RS curve for the proper group separation" [21].
4. All resistances are calculated at 20°C.

Returning to the AC cable model block, implemented in Simulink, both zero and positive (negative sequence impedance is assumed to be equal to the positive sequence impedance) are presented in Table 2.4.

Table 2.4. Positive and Negative Sequence Impedance for 400 Hz at 20°C [21]

AWG Size	**Positive and Negative sequence Impedances for 400 Hz at 20°C (Ohms/1000 ft)**	
	Max 150°C (tin plating)	**Max 200°C (silver plating)**
20	10.18+j0.304	9.47+j0.304
18	6.42+j0.289	5.96+j0.289
16	4.95+j0.278	4.66+j0.278
14	3.15+j0.264	2.97+j0.264
12	2.08+j0.247	1.96+j0.247
10	1.30+j0.228	1.23+j0.228
8	0.722+j0.226	0.678+j0.226
6	0.458+j0.221	0.431+j0.221
4	0.288+j0.212	0.272+j0.212
2	0.188+j0.206	0.175+j0.206
0	0.119+j0.04	0.111+j0.204

Due to the fact that the impedances presented in Table 2.4 were calculated for 400 Hz, so that an extrapolation was performed in order to get impedance values for the entire range of operation frequencies. As it remains at low frequencies, this cable model should work properly for steady-state simulations, but it only fits a given operational frequency. When there is a frequency content that is different from the base frequency in time, the model must be revised, as its frequency behaviour depends on how Simulink converts the inductance value. For the resistance, there may be a slight correction, but it is not critical here. The impedance could be calculated very easily by finite elements, if there were access to an actual section of the cable. However, this is beyond the scope of the project.

Meanwhile, zero sequence impedance is given by:

$$Z_0 = R_0 + j \cdot X_0 \tag{2.1}$$

where R_0 is the zero sequence resistance. The calculated value of zero sequence resistance assuming a perfect ground plane ("skin" in Figure 2.13) is found by finding the parallel resistance of the conductor configuration above the skin [21].

$$R_0 = R_S + R_{0C} \tag{2.2}$$

The value of the skin correction term R_S and the related zero sequence inductance X_0 is found by interpolating the lower curves of Figure 2.14 for h equal to 10.16 cm.

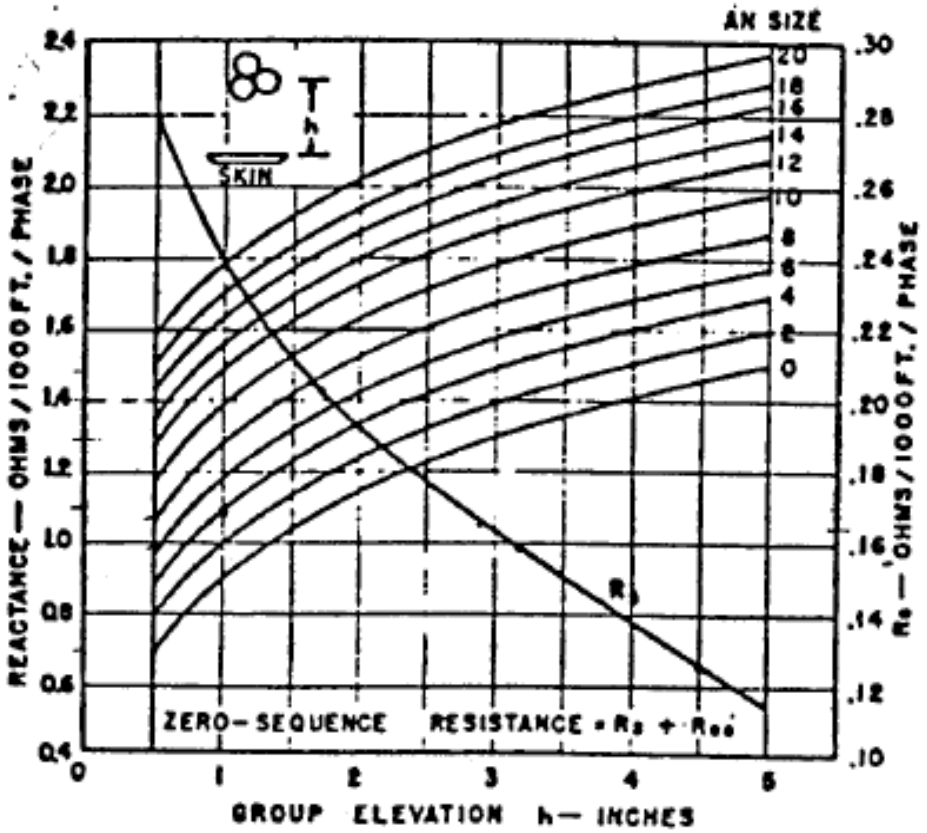

Figure 2.14. Zero sequence Impedance for one laced group at 400 Hz [21].

Furthermore, the zero sequence resistance R_{OC} is given in Table 2.5.

Table 2.5. Zero Sequence Resistance assuming a perfect ground plane at 20°C and 400 Hz [21]

AWG Size	**R_{0C} at 20°C and 400 Hz (Ohms/1000 ft)**	
	Max 150°C (tin plating)	**Max 200°C (silver plating)**
20	10.18	9.47
18	6.42	5.96
16	4.95	4.66
14	3.15	2.97
12	2.08	1.96
10	1.30	1.23
8	0.722	0.678
6	0.458	0.431
4	0.288	0.272
2	0.188	0.175
0	0.119	0.111

A sequence impedance matrix is formed by wire sizes from 12 AWG to 00 AWG (an extrapolation is performed in order to find values after 0 AWG wire size). Phase domain cable impedance parameters are found using the Clarke transformation matrix T:

$$[Z_{ABC}(\text{wire size})] = [T] \cdot [Z_{012}(\text{wire size})] \cdot [T]^{-1} \tag{2.3}$$

The result of (2.3) gives a matrix where $Z_{ABC}[1,1] = Z_A$, $Z_{ABC}[2,2] = Z_B$, $Z_{ABC}[3,3] = Z_C$. Finally, a decoupled-RL model depending on the frequency, length and wire size (AWG) is fully implemented. Figure 2.14 shows the initialization commands for the AC cable block in Simulink, where f is the frequency of operation and $Size$ is the wire size in AWG. All values are taken from Table 2.4, Table 2.5 and Figure 2.15. These values result when using equations (2.1), (2.2) and (2.3).

```
if Size == 12      %% AWG Size
    R  =  0.0067;  %% 3-phase resistance [Ohm/length]
    XL =  (3.888888889e-04)/(2*pi*f);  %% 3-phase inductance [Ohm/length]
else
    if Size == 8       %% AWG Size
        R  = 0.0025;  %% 3-phase resistance [Ohm/length]
        XL = (3.518518519e-04)/(2*pi*f);  %% 3-phase inductance [Ohm/length]
    else
        if Size == 4       %% AWG Size
            R  = 0.0011;  %% 3-phase resistance [Ohm/length]
            XL = (0.0003)/(2*pi*f);  %% 3-phase inductance [Ohm/length]
        else
            if Size == 00          %% AWG Size
                R  = 0.4018*1e-03; %% 3-phase resistance [Ohm/length]
                XL = (0.2457*1e-03)/(2*pi*f);  %% 3-phase inductance [Ohm/length]
            end
        end
    end
end
```

Figure 2.15. Initialization commands for the AC cable block

The cable lengths presented in Table 2.6 are derived approximately using the aircraft geometry, where the longest cable is approximately 20.63 m. Capacitive effects are ignored.

Table 2.6. AC Cable length estimation

				Estimation			Real
Idem	**Power**	**From**	**To**	**Straight (m)**	**Reserve (%)**	**Length (m)**	**Length (m)**
1	AC - 3Φ	VFG1	ACPC	4.50	75%	7.88	
2	AC - 3Φ	VFG2	ACPC	4.50	75%	7.88	
3	AC - 3Φ	EXTAC	ACPC	2.50	75%	4.38	4.8768
3	AC - 3Φ	EXTAC	ACPC	2.50	75%	4.38	6.096
3	AC - 3Φ	EXTAC	ACPC	2.50	75%	4.38	4.191
4	AC - 3Φ	APU GEN	ACPC	7.00	50%	10.50	
5	AC - 3Φ	VFG3	ACPC	4.00	75%	7.00	
6	AC - 3Φ	VFG4	ACPC	3.00	75%	5.25	
7	AC - 3Φ	RAT GEN	ACPC	16.50	25%	20.63	
8	AC - 3Φ	ACPC	CCBP	14.00	25%	17.50	17.653
9	AC - 3Φ	ACPC	CCBP	14.00	25%	17.50	17.7292
10	AC - 3Φ	ACPC	CCBP	14.00	25%	17.50	18.415
11	AC - 3Φ	ACPC	CCBP	14.00	25%	17.50	17.5768
12	AC - 3Φ	CCBP	ESS TRU1	3.50	75%	6.13	
13	AC - 3Φ	CCBP	TRU1	3.50	75%	6.13	
14	AC - 3Φ	CCBP	TRU2	3.50	75%	6.13	
15	AC - 3Φ	CCBP	CCBP	1.00	25%	1.25	
16	AC - 3Φ	CCBP	ESS TRU2	3.50	75%	6.13	

The reserve percentage varies from 25% to 75%. The 75% is added for short lengths (0-5m) if they travel in a non-straight path. The 50% is for medium lengths (5 -10m) if non-straight path is taken. Finally, the 25% is for long lengths (>10m).

Table 2.7 summarizes AC impedance values obtained with the AC block calculations. No frequency dependency of resistance is taken into account due to a lack of information in the aircraft design process. The values presented in Table 2.7 are in fact the self impedance values for different wire sizes and frequency of operation, since the mutual values are to small and can be neglected.

Table 2.7. Self impedance values for AC Cables in the aircraft electric power system

	Cable's Self impedances (Ohm/m)						
AWG	**Zcable @324Hz**	**Zcable @380Hz**	**Zcable @400Hz**	**Zcable @430Hz**	**Zcable @500Hz**	**Zcable @540Hz**	**Zcable @580Hz**
12	0.0067 + j0.00216	0.0067 + j0.00253	0.0067 + j0.00267	0.0067 + j0.0028	0.0067 + j0.00333	0.0067 + j0.0036	0.0067 + j0.00387
8	0.0025 + j0.0019	0.0025 + j0.0022	0.0025 + j0.0024	0.0025 + j0.0025	0.0025 + j0.0029	0.0025 + j0.0032	0.0025 + j0.0034
4	0.0011 + j0.0017	0.0011 + j0.0020	0.0011 + j0.0021	0.0011 + j0.0023	0.0011 + j0.0026	0.0011 + j0.0028	0.0011 + j0.0031
00	0.0004 + j0.0013	0.0004 + j0.0016	0.0004 + j0.0016	0.0004 + j0.0018	0.0004 + j0.0020	0.0004 + j0.0022	0.0004 + j0.0024

It is worth noting that more sophisticated models must be developed to account for higher frequency transients. It might be also necessary to account for temperature and altitude effects using dynamic functions.

2.2.5 AC Loads

Both passive and dynamic AC loads are considered in the modeled Global Express aircraft electric power system. Passive loads are modeled as constant impedance unbalanced loads using the nominal active and reactive power data provided by Bombardier [19] and listed in the Annexe I.

Figure 2.16 shows the location of the AC loads, within the dotted red lines, modeling using Simulink.

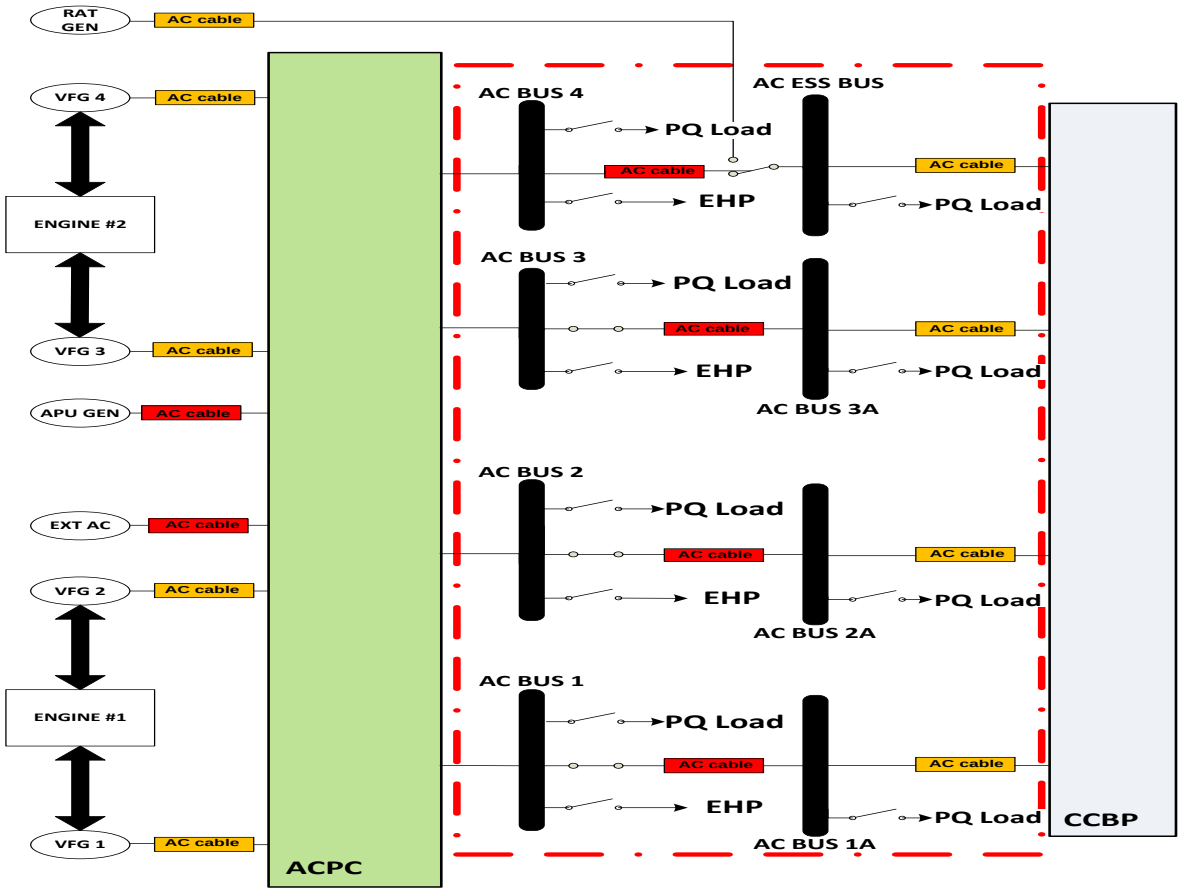

Figure 2.16. Location of the AC loads in the Global Express one-line diagram

In order to simulate real ac load distribution, an AC unbalanced load model block was implemented in Simulink (see Figure 2.17) and based on the parallel RLC load block, which

implements a linear load as a parallel combination of RLC elements [14]. At the specified frequency, the load exhibits constant impedance. The active and reactive powers absorbed by the load are proportional to the square of the applied voltage.

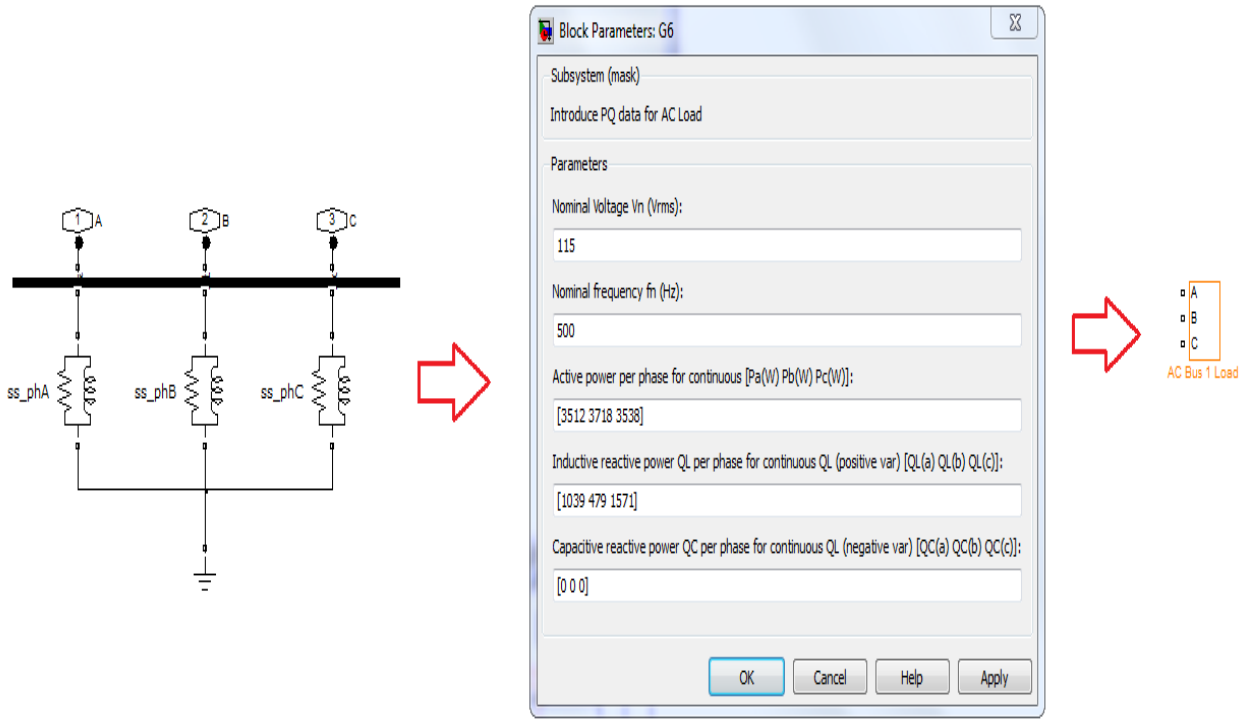

Figure 2.17. AC Unbalanced Load implementation in Simulink

2.2.5.1 Electric Hydraulic Pump (EHP)

Some significant hydraulic loads (like the Electrical Hydraulic Pump, EHP) are simulated using 20 kVA three-phase asynchronous machines (ASM) with torque control. The EHPs for electro-hydro mechanical actuation are connected to the 115/200 V, variable frequency main AC bus, and they are designed for 400 Hz operation even if it is supposed to work for all range of operating frequencies. In addition, the motors are loaded with variable load torque [19] based on rotor speed. Machine parameters are determined using frequency dependent steady-state input active and reactive powers, transient inrush current and stator resistance, all provided by the manufacturer. Despite the information provided by Bombardier, some assumptions found in [22] are used, in order to obtain a model for the EHP. The rest of the parameters are calculated as from this hypothesis.

The assumptions are listed in Table 2.8. Once the model is elaborated considering these assumptions, a little variation in the mutual inductance from the model in Simulink is performed, in order to reach the same behaviour shown in EMTP-RV.

Table 2.8. Assumption during EHP's modeling

Parameter	Value
Frequency of operation	400 Hz
Voltage of operation	115 VAC
Stator Resistance per phase	0.077 Ω
Nominal slip [22]	3%
Relationship between Stator and Rotor Resistance [22]	$X_r = \frac{7}{3} X_s$
Start-up current	280 A

Figure 2.18 presents the EHP model implemented in Simulink, using the Asynchronous Machine [14].

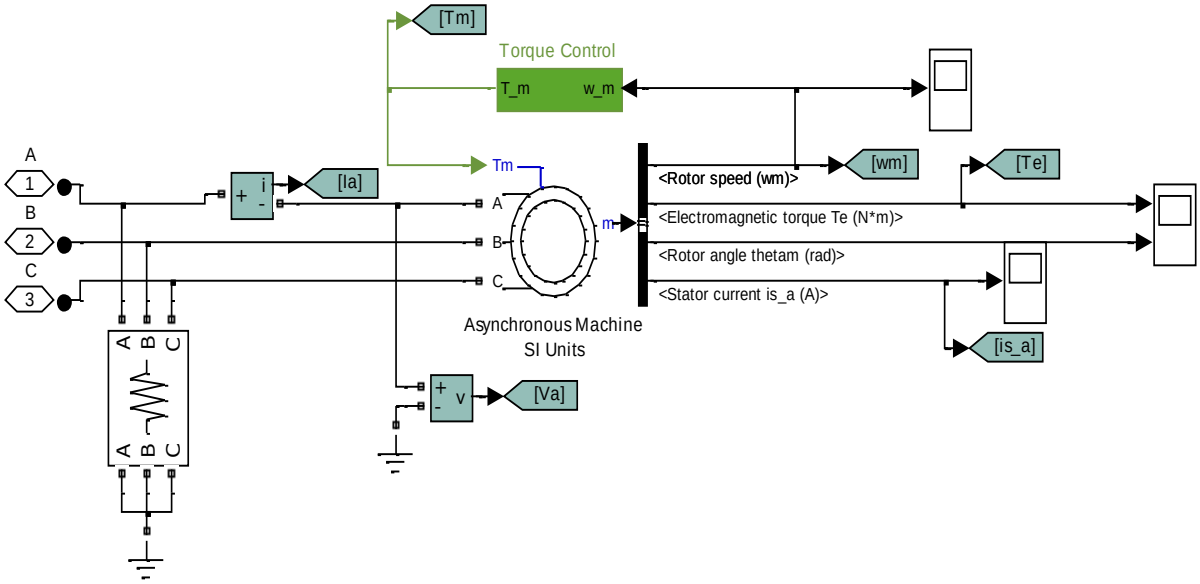

Figure 2.18. EHP implementation in Simulink

It is worth noting that in the model, a small parasitic resistive load is added in the model, connected at the machine terminals, in order to avoid numerical oscillations [14]. In order to validate the EHP model in Simulink with real measurements and the EHP model implemented in EMTP-RV, Table 2.9 shows the parameters employed, as well as their values during simulation.

Table 2.9. Parameters for Asynchronous Machine block

	Resistance		Inductance		Mutual Inductance	Inertia	Friction	Number
Value	Stator Rs (Ohm)	Rotor R'r (Ohm)	Stator Lls (H)	Rotor Ll'r (H)	Lm (H)	J(kg.m^2)	factor F(N.m.s)	of Poles
Simulink	0.1488	0.029131	0.0000904	0.000136	0.002921	0,000575	0	4
EMTP-RV	0.1488	0.029131	0.0000904	0.000136	0.004494	0,000575	0	4

In addition, the variable frequency steady-state performance should be revised as well as the machine model equations, in order to account for changes in parameters.

The definition of all loads is not currently available. Moreover, the information provided is limited and does not allow characterizing the transient performance. It should become a mandatory requirement that component manufacturers provide specific measurements and data for characterizing more precisely aircraft's loads for both steady-state and transient performances. Load certification is an important issue for MEA designs. Standards must be defined for load integration according to the performance requirements of aircraft manufacturers. This idea is similar to a grid code practice used in power systems. Such standards must also define the type of studies that should be performed when integrating loads in the aircraft electric power system.

2.2.6 Transformer Rectifier Unit (TRU)

The DC supply is subdivided into two systems: Static Conversion and Battery. The static conversion system is supplied by four Transformer Rectifier Units (TRUs). Each TRU produces unregulated 28 VDC and is rated at 150 A [3]. Furthermore, a battery system is used to maintain the DC system voltage constant under transient conditions, to supply power for short term heavy loads and under emergency conditions.

For this reason, TRUs are essential parts for the power distribution systems, in order to supply power to all kinds of DC loads from a variable frequency AC bus. Such systems are required to have low volume, high reliability, ability to carry overcurrent and present low current harmonics [23].

The conventional TRU system uses mainly passive rectifiers as shown in Figure 2.19, because its operating frequency causes the power density to be quite high. It consists of diodes and some filtering components, and hence is very robust, although passive converter systems with approximately sinusoidal input currents like the 12-pulse rectifier, are typically used in mid- and

high-power applications [23]. Such passive systems do not require control electronics and are therefore characterized by a very low realization effort and high reliability.

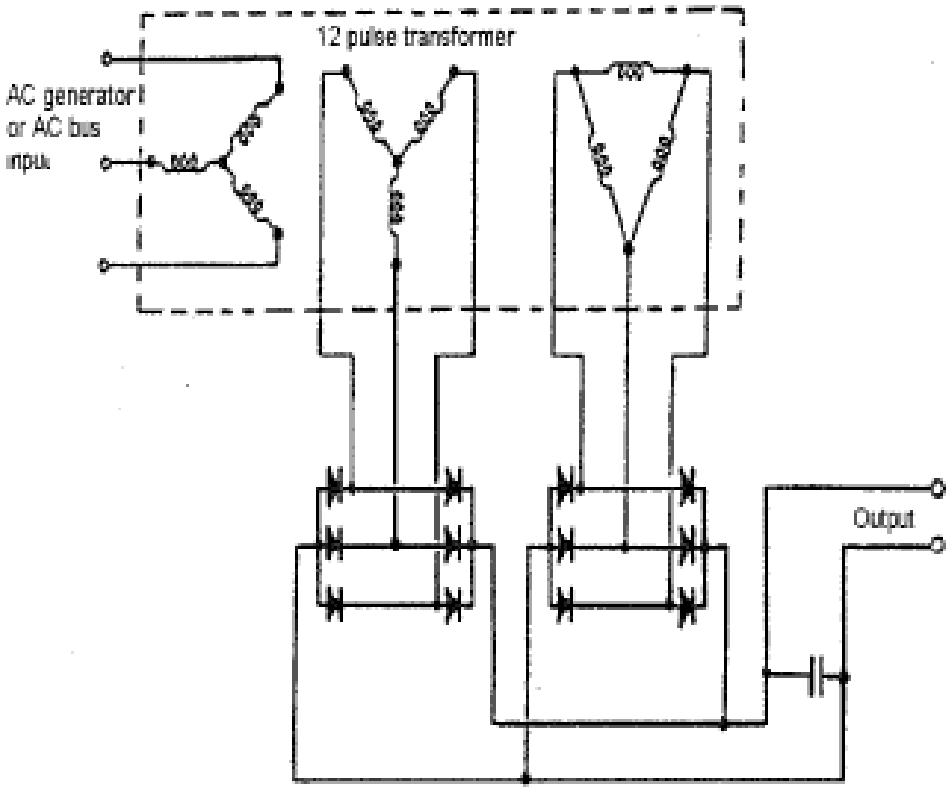

Figure 2.19. Schematic diagram of a typical TRU [23]

Figure 2.20 shows the location of the four TRUs linking AC and DC part of the electric power system, within the dotted red lines, modeling using Simulink.

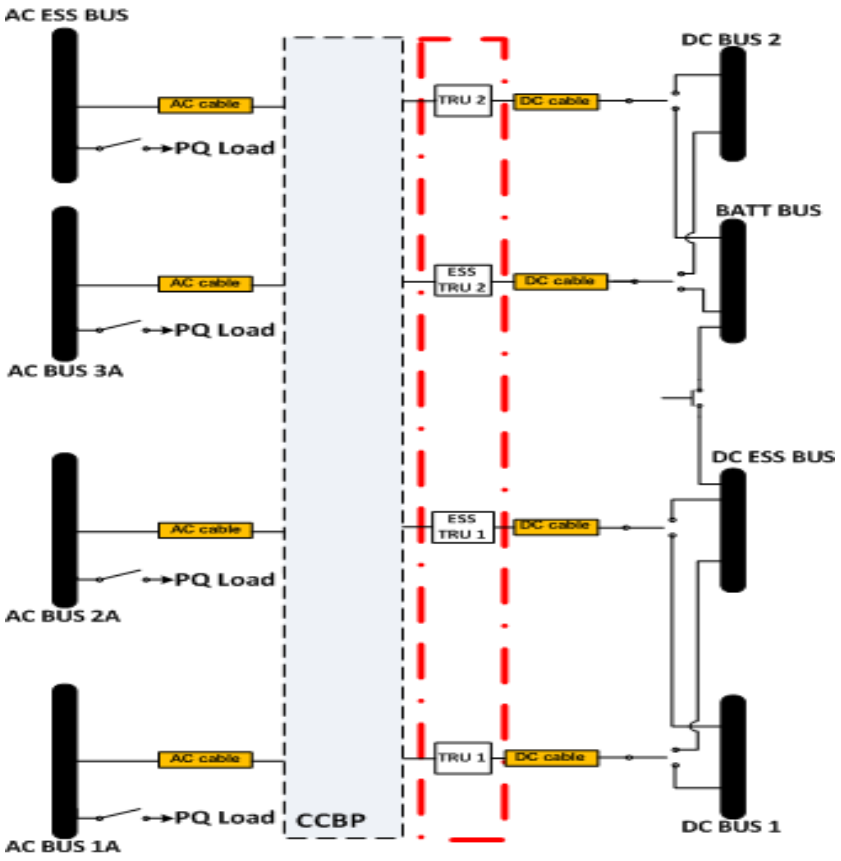

Figure 2.20. Location of the TRUs within the Global Express one-line diagram

A simplified model similar to [24] was created in Simulink. In order to eliminate the low-frequency output current harmonics of the generator and to convert 3-phase 115 VAC to 28 VDC, the TRU is designed with a passive 24-pulse converter. However, a 12-pulse power converter [24], [25] is used in this study. For further power quality studies, the actual 24-pulse converter should be modeled in order to get more accurate results. The TRU provides inherent high power factor and low harmonic distortion.

Power diodes are used in the TRU to eliminate switching and achieve significant reduction in losses and, hence, improved efficiency and power quality. The rectifier part of the TRU is implemented using the Universal Bridge block, which is a universal three-phase power converter that consists of up to six power switches connected in a bridge configuration [14]. The Universal Bridge block allows simulation of converters using naturally commutated (or line-commutated) power electronic devices. In addition, RC snubber circuits are connected in parallel with each switch device. Table 2.10 shows the universal bridge parameters.

Table 2.10. Parameters of the Universal Bridge

Parameter Description	Value
Number of bridge arms	3
Snubber resistance R_S (Ohm)	1830
Snubber capacitance C_S (F)	5.47e-08
Power Electronic device	Diodes
R_{on} (Ohm)	1e-03
L_{on} (H)	0
Forward voltage Vf (V)	0.8

The D/Y transformer in the aircraft power system provides the necessary phase shift of 30° for the 12-pulse operation feeding into the main 28 VDC bus. It is implemented using the Three-Phase Transformer (Two Windings) block, which consist of a three-phase transformer made from three single-phase transformers. The model takes into account the winding resistances and the leakage inductances, as well as the magnetizing characteristics of the core [14]. Table 2.11 shows the main transformer parameters used, as well as their values during simulation.

Table 2.11. Parameters for Three-Phase Transformer (Two Windings) Block

Parameter Description	Value
Nominal power Pn(VA)	5500
Winding 1 Vph-ph (Vrms)	200
Winding 1 Resistance R1 (pu)	0.004
Winding 1 Inductance L1 (pu)	0.02
Winding 2 Vph-ph (Vrms)	24.45
Winding 2 Resistance R2 (pu)	0.004
Winding 2 Inductance L2 (pu)	0.02
Magnetization Resistance Rm (pu)	200
Magnetization Inductance Lm (pu)	200

In addition, a 200 μH inductor and 5000 μF capacitor are connected at the output of the power converter to smooth out the DC voltage.

The TRU model implemented in Simulink is presented in Figure 2.21. The parameters of the input and output filters are those provided by the manufacturer, while typical values are used for other parameters. To develop a model as accurate as possible, the power system military standard MIL-STD-704f [26] is used in order to meet basic steady-state and transient output requirements. A generic magnetization curve is used to obtain a more realistic behaviour of the TRU. Transformers output characteristics are set using TRU steady-state output requirements (28 VDC

with a 12-pulse ripple). Interphase inductance parameters are determined using transient characteristics found in [26] regarding envelope of normal voltage transients for 28 volts DC system [26]. The performance of the TRU model is presented in the next chapter.

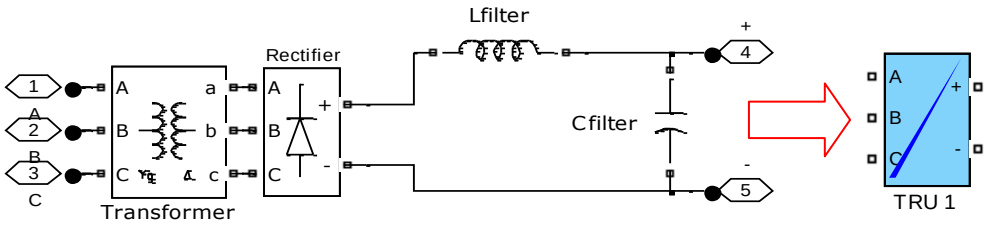

Figure 2.21. TRU model in Simulink

2.3 DC Electrical System

2.3.1 DC Cables

Regarding the modeling of DC cables, a block was created, edited and scripted in Simulink to generate DC cable resistance parameters for Global Express aircraft electrical system based on [21] and manufacturer datasheets. Inductive effects are taken into account as there are calculated directly from the analytical equations assuming that the DC cables are coaxial. It is important to consider them in order to account for transient behaviour.

Figure 2.22 shows a cross-section of a tin coated copper cable used inside the aircraft for linking ESS TRU and DC ESS BUS. A is for the conductor material (tin coated copper), B is for the primary insulation (radiation cross linked, extruded, modified, ETFE), and C for the jacket (radiation cross linked, extruded, modified, ETFE).

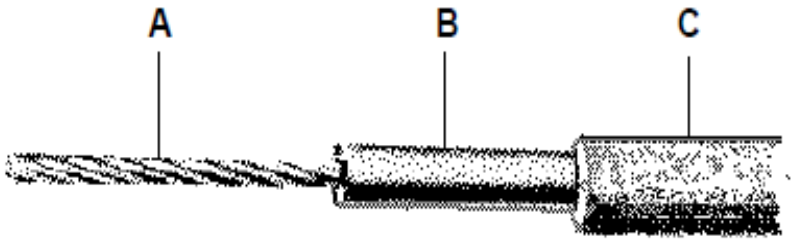

Figure 2.22. Cross-section of a tin coated copper cable used for linking ESS TRU and DC ESS BUS [19]

Meanwhile, Figure 2.23 shows the DC cable user interface developed in Simulink.

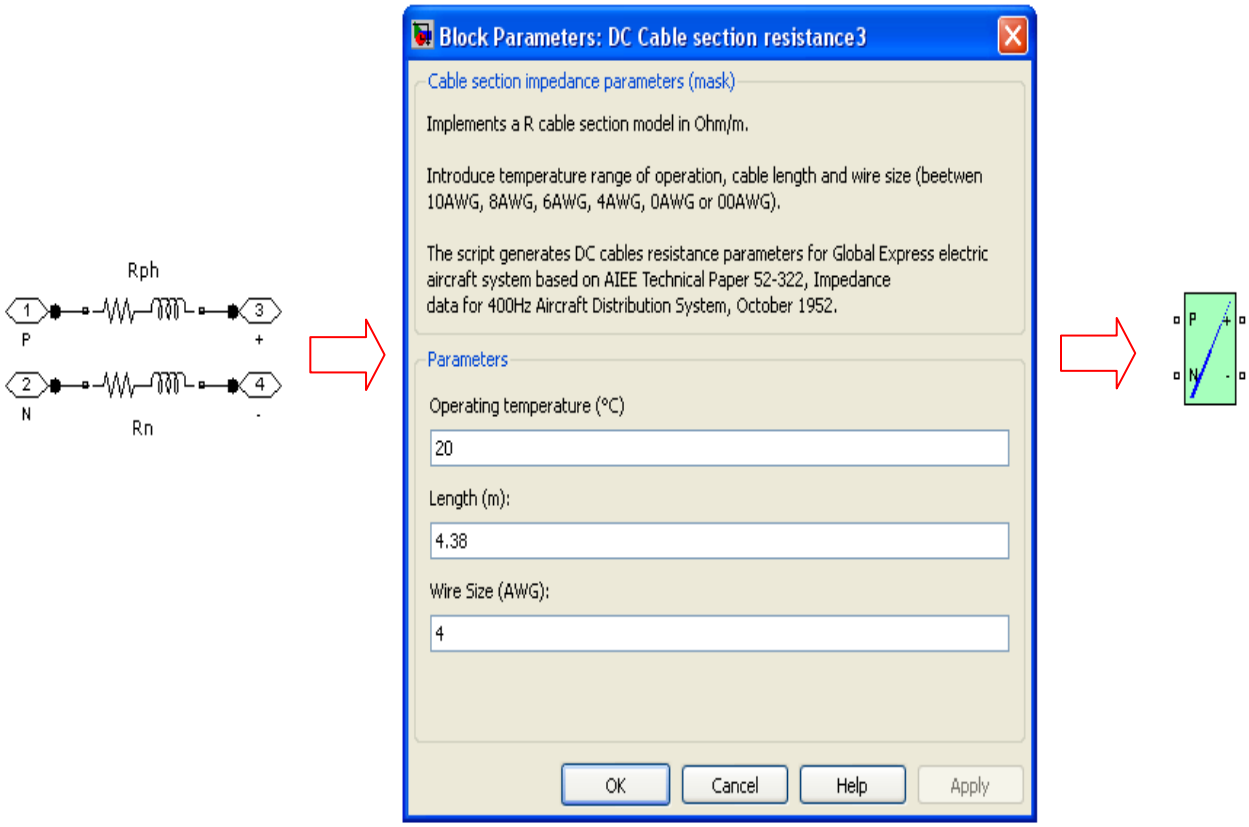

Figure 2.23. DC Cable Block implemented in Simulink

Table 2.12 shows manufacturer resistance DC values for 20°C for different wire sizes presented in the aircraft. Inductive effects are included assuming a coaxial cable.

Table 2.12. DC resistance and inductance values for the aircraft power system [21]

AWG	R@20°C (Ohm/m)	L (µH/m)
10	0.004068241	0.2937
8	0.002299869	0.4166
6	0.001459974	0.4209
4	0.000902231	0.4210
0	0.000370735	0.3362
00	0.000291995	0.3516

The DC resistance values are given in Ohm/m and should vary with temperature as follows [21].

$$R_{DC,cable} = R_{20°C} \cdot \left[1 + \rho_{Cu}\left(T_{op} - 20°C\right)\right] \quad (2.2)$$

where, ρ_{Cu} is the copper resistivity, T_{op} is the temperature of operation, $R_{DC,cable}$ is the resistance value in Table 2.12. A resistive model depending on the temperature of operation, length and wire size (AWG) is fully implemented. The temperature parameter is static.

In addition, the DC inductance values are given in μH/m and they are calculated as follows [21]:

$$\mathrm{L_{DC,cable}} = 0.4593 \cdot \ln\left(\frac{\mathrm{D}}{\mathrm{d}}\right) \tag{2.2}$$

where, D is the outer conductor and d is inner conductor. The constant value is related to the permeability. Finally, an impedance model depending on the temperature of operation, length, wire size (AWG) and the geometry of the conductor is fully implemented. The temperature parameter is static.

The cable lengths presented in Table 2.13 are derived approximately using the aircraft geometry, where the longest cable is approximately 24 m. In addition, the AC cable length reserve percentage criteria was also used for the DC cable length.

Table 2.13. DC Cable length estimation

				Estimation			**Real**
Idem	**Power**	**From**	**To**	**Straight (m)**	**Reserve (%)**	**Length (m)**	**Length (m)**
17	DC	TRU1	DCPC	2.50	75%	4.38	
18	DC	ESS TRU1	DCPC	2.50	75%	4.38	
19	DC	ESS TRU2	DCPC	2.50	75%	4.38	
20	DC	TRU2	DCPC	2.50	75%	4.38	
25	DC	ASCA	DCPC	19.20	25%	24.00	24.64
32	DC	AV BATT	DCPC	2.50	75%	4.38	
21a	DC	DCPC	SPDA#	1.00	75%	1.75	
21b	DC	DCPC	SPDA#	4.50	75%	7.88	7.9248
21c	DC	DCPC	SPDA#	6.50	50%	9.75	9.144
21d	DC	DCPC	SPDA#	2.00	75%	3.50	3.2512

Figure 2.24 presents the initialization commands for the DC cable block in Simulink, where T is the temperature of operation and *Size* is the wire size in AWG. According to the wire size selected by the user and the temperature of operation, the script calculates R, which is the resistance per length for the DC cables. After that, the model multiplies this value by the length introduced by the user and distributes this value to both resistance presented in the Simulink model.

```
if Size == 10   %% AWG Size
    R  = 0.004068241 * (1 + 0.00393 * (T-20));                    %% [Ohm/m]
    H  = 4.593 * log (0.113/0.106);                               %% [µH/m]
else
    if Size == 8   %% AWG Size
        R  = 0.002276903 * (1 + 0.00393 * (T-20));                %% [Ohm/m]
        H  = 4.593 * log (0.173/0.158);                           %% [µH/m]
    else
        if Size == 6   %% AWG Size
            R  = 0.001430446 * (1 + 0.00393 * (T-20));            %% [Ohm/m]
            H  = 4.593 * log (0.212/0.198);                       %% [µH/m]
        else
            if Size == 4   %% AWG Size
                R  = 0.000902231 * (1 + 0.00393 * (T-20));        %% [Ohm/m]
                H  = 4.593 * log (0.274/0.250);                   %% [µH/m]
            else
                if Size == 0  %% AWG Size
                    R  = 0.000370735 * (1 + 0.00393 * (T-20));    %% [Ohm/m]
                    H  = 4.593 * log (0.425/0.395);               %% [µH/m]
                else
                    if Size == 00  %% AWG Size
                        R  = 0.000291995 * (1 + 0.00393 * (T-20)); %% [Ohm/m]
                        H  = 4.593 * log (0.475/0.440);           %% [µH/m]
                    end
                end
            end
        end
    end
end
```

Figure 2.24. Initialization commands for the DC cable block

As for AC cables, more sophisticated cable models must be developed to account for higher frequency transients. It may be also needed to account for temperature and altitude effects using dynamic functions.

2.3.2 DC Loads

The DC loads are distributed throughout the aircraft and used for various purposes, including heating services, actuation, subsystem controllers and Avionic systems [18]. The large amount of different types of loads increases the load model development and validation efforts. There are three levels of DC power sources operating at different voltage levels: TRUs at 28 VDC and NiCad batteries at 24 VDC and 25.2 VDC. In the proposed aircraft electric power system model, DC loads were assumed to be constant impedance loads, drawing a specific current at 28 VDC, as mentioned in Electrical Load Analysis (ELA) [19] provided by Bombardier for certification purposes and listed in the Annexe. NiCad batteries are modeled using simple ideal DC sources. Improved battery models including charge and discharge curves and respective chargers must be modeled in further studies of the complete electric power system model.

Even if DC loads are simulated as resistances, efforts are required in order to meet their real DC load behaviour, and therefore take into account variable input voltages and temperature effects. They can affect both steady-state and transient load behaviour. In addition, more accurate models must be developed in order to demonstrate the limited use of ELA in certification processes. In fact, traditional ELA does not give detailed information about load behaviour. Manufacturers should provide required information to ease aircraft certification process while preventing over-design erroneous evaluations of transients.

2.3.3 DC Switching Control Centre (DCSCC)

The DC Switching Control Centre (DCSCC) is responsible for sending binary signals to the external switching time control for the SSPC blocks, in order to change ON/OFF state positions. While breakers need 50 ms to switch, SSPCs can switch within 2 ms. Hence, DCSCC commands the closure of the SSPC needed for supplying battery power to a specific bus. Once AC system reconfiguration is over, SSPCs switch off and disconnect the battery from the bus. It was created and implemented in Simulink for the purpose of this research, so that a more realist and sophisticated operating electric power system model can be obtained.

The current implementation of the reconfiguration switching controls is based on truth tables representing Global Express reconfiguration logic [18]. The switch states vary depending on a game of events regarding loss of VFGs and TRUs, so that DC loads can be supplied while AC system architecture changes to provide electrical power to every bus. Figure 2.25 shows the DCSCC subsystem implementation in Simulink.

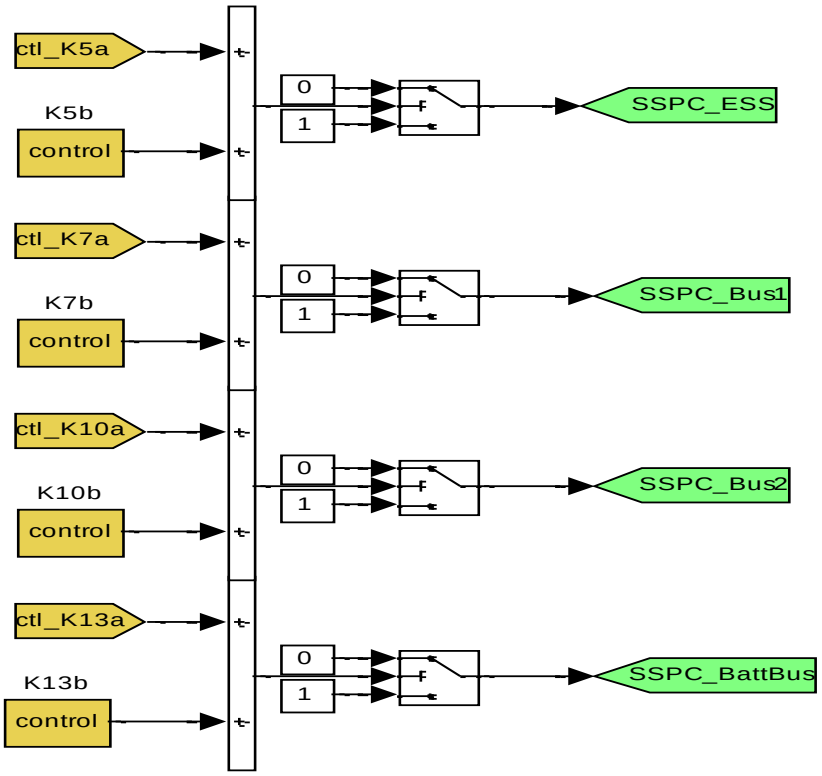

Figure 2.25. DCSCC implemented in Simulink

DCSCC detects any single loss of VFGs by using external switching time control for the ACPC switches K5, K7, K10 and K13, and then sends binary signals, according to failure of the VFG. The binary signals are sent to the external switching time control for the SSPC blocks, which are in fact single 25 VDC ideal sources. The idea is to provide 25VDC to the DC busses, 2 ms after failure within the 50 ms time delay for the ACPC breakers. Once ACPC reconfigures the power supply, the SSPC stops to operate.

CHAPITRE 3 GLOBAL EXPRESS AIRCRAFT ELECTRIC POWER SYSTEM SIMULATION AND ANALYSIS

The objective of this chapter is to summarize the implementation and validation tests executed on the Global Express aircraft electric power system model. Figure 3.1 shows the first part of the schematic for the Global Express electric power system, including the AC part of the system.

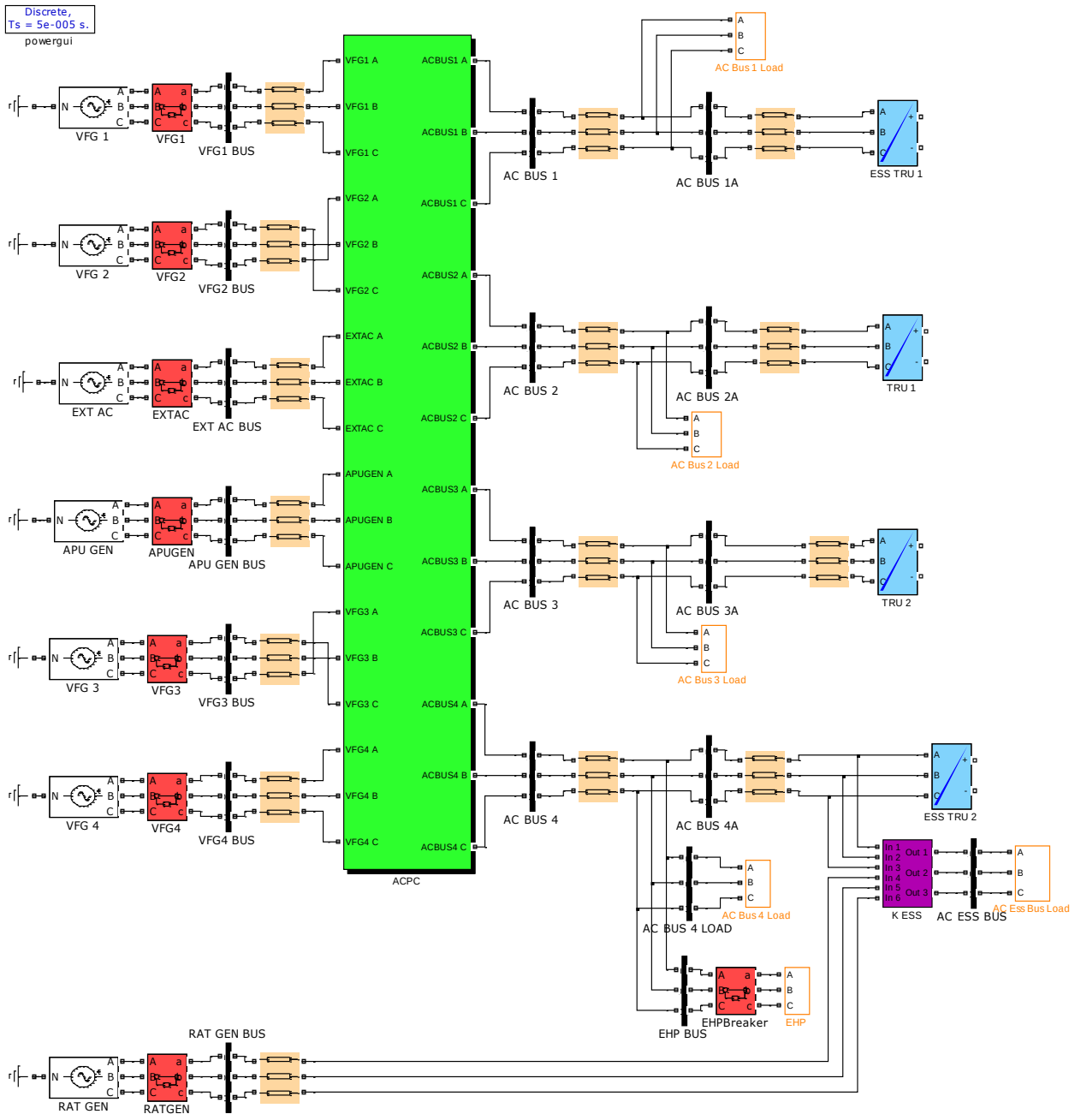

Figure 3.1. Complete aircraft electric system implementation in Simulink (first part)

Figure 3.2 shows the second part of the schematic for the Global Express electric power system, including the DC part of the system.

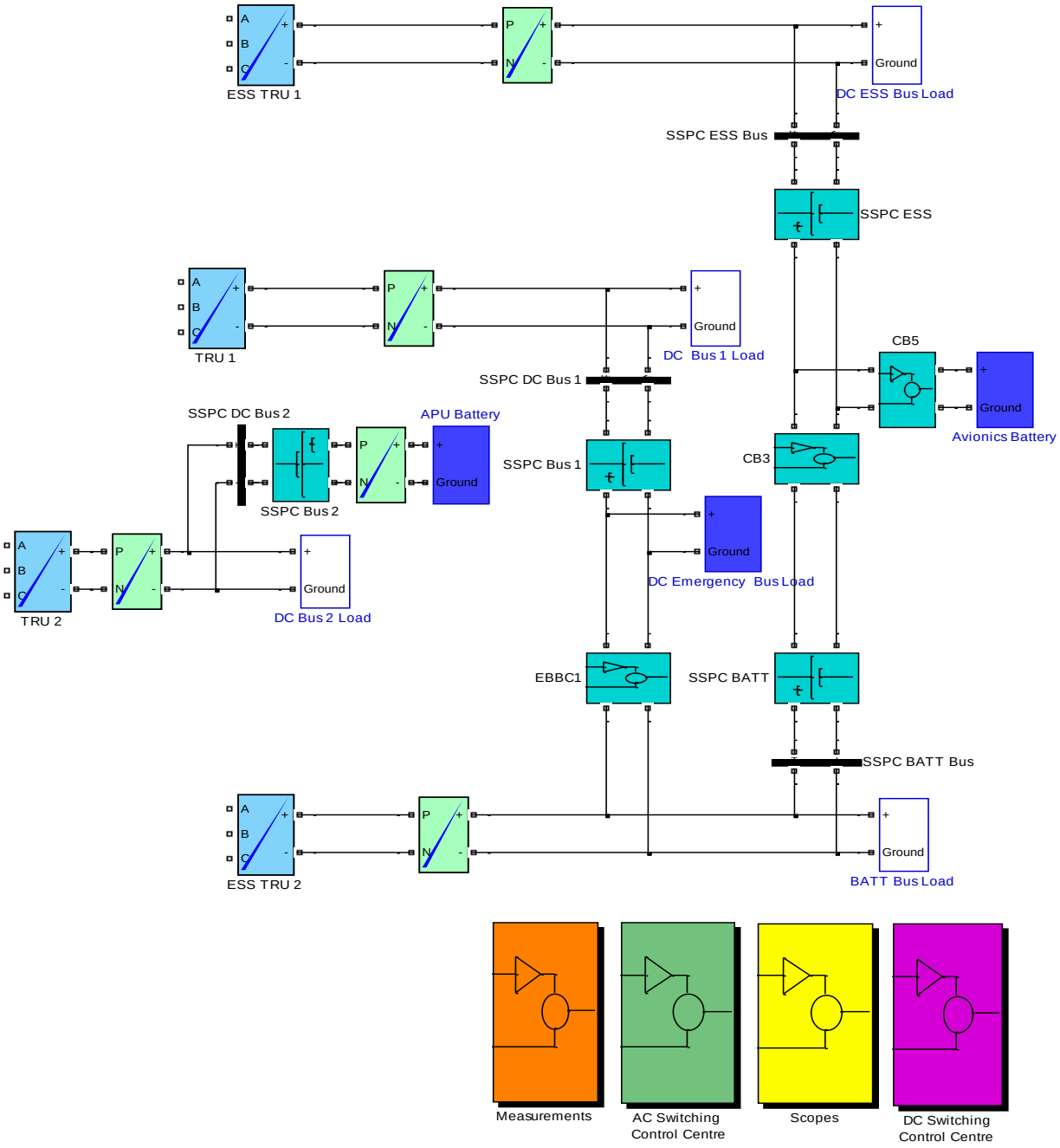

Figure 3.2. Complete aircraft electric system implementation in Simulink (second part)

As mentioned before, the model is implemented in Simulink and the validation tests are performed using EMTP-RV and actual measurements available from Bombardier. The schematic

of the model implemented in EMTP-RV is not presented here. However, it is based on the Figure 2.1 as same as the model implemented in Simulink.

The electrical system is separated into AC and DC systems. The AC system is a variable frequency type system, powered by four engine-driven variable frequency generators (VFGs). An auxiliary generator, called Auxiliary Power Unit (APU), operates at a fixed frequency. In the event of an emergency, a Ram Air Turbine Generator (RAT) is provided for Essential Bus feed. The generator outputs are supplied to the AC Power Center (ACPC), which in turn distributes the power to the aircraft subsystems [18].

The DC power system supply consists of four Transformer Rectifier Units (TRUs) for normal power distribution and two NiCad batteries (a nickel-cadmium battery). The batteries are used for initial system power-up but are then put in the standby mode for emergency power requirements. On the other hand, the TRUs receive power from the AC system, transform and rectify that power into DC power, which is supplied to the DC Power Center (DCPC). The DCPC in turn distributes the power to the aircraft subsystems.

Due to the fact that Global Express has ten different operating conditions listed in Table 2.1 of Chapter 2, ten different models were created to allow studying all operating conditions. The differences between the models reside in the operating frequency and both AC and DC loads. This chapter summarizes only the results and analysis obtained for the G7 operating mode at 500 Hz.

Each simulation is performed using a discrete fixed-step solver with a fixed-step size (fundamental sample time) of 50e-06 s. The simulations were executed on a Intel (R) Core(TM) 2 Duo processor (T9600, 2.80 GHz, 2.80 GHz), 64-bit operating system, where 2 s of simulation represents an elapsed CPU time of 199.2190 s.

3.1 Voltage Frequency Generators (VFGs) and phase sequence

Figure 3.3 presents voltage waveform simulation results taken from each VFG bus when the aircraft presents maximum loading and there is no failure condition. All buses maintain a voltage of 115 V RMS phase-to-ground during the whole simulation period of 0.5 s.

a)

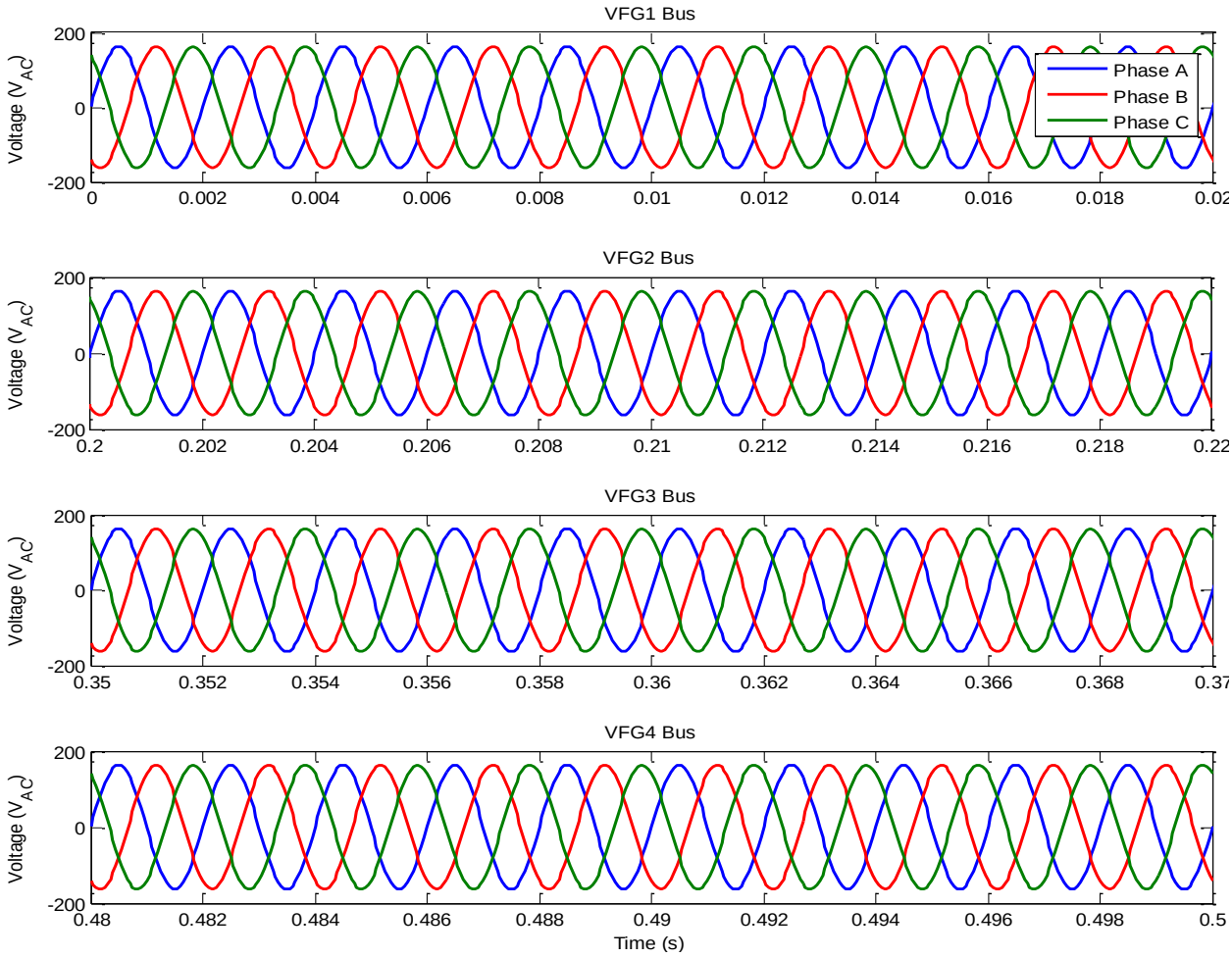

b)

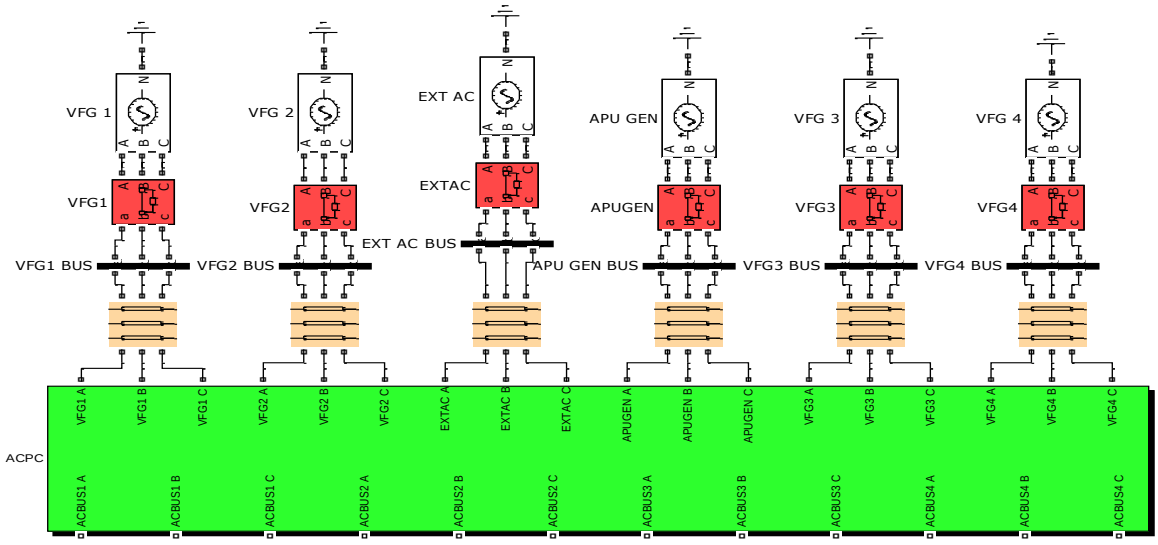

Figure 3.3. a) Voltage simulation results from VFG busses and b) VGF busses location

Figure 3.4 presents current measurements taken from each VFG bus. Figure 3.4 shows the presence of an unbalanced power system, since every bus has different load values. In addition, every phase of a respective AC bus has different load values as well, where the busses served by VFG2 and VFG3 are the most loaded busses. There is some distortion at the beginning due to the start-up of the EHP.

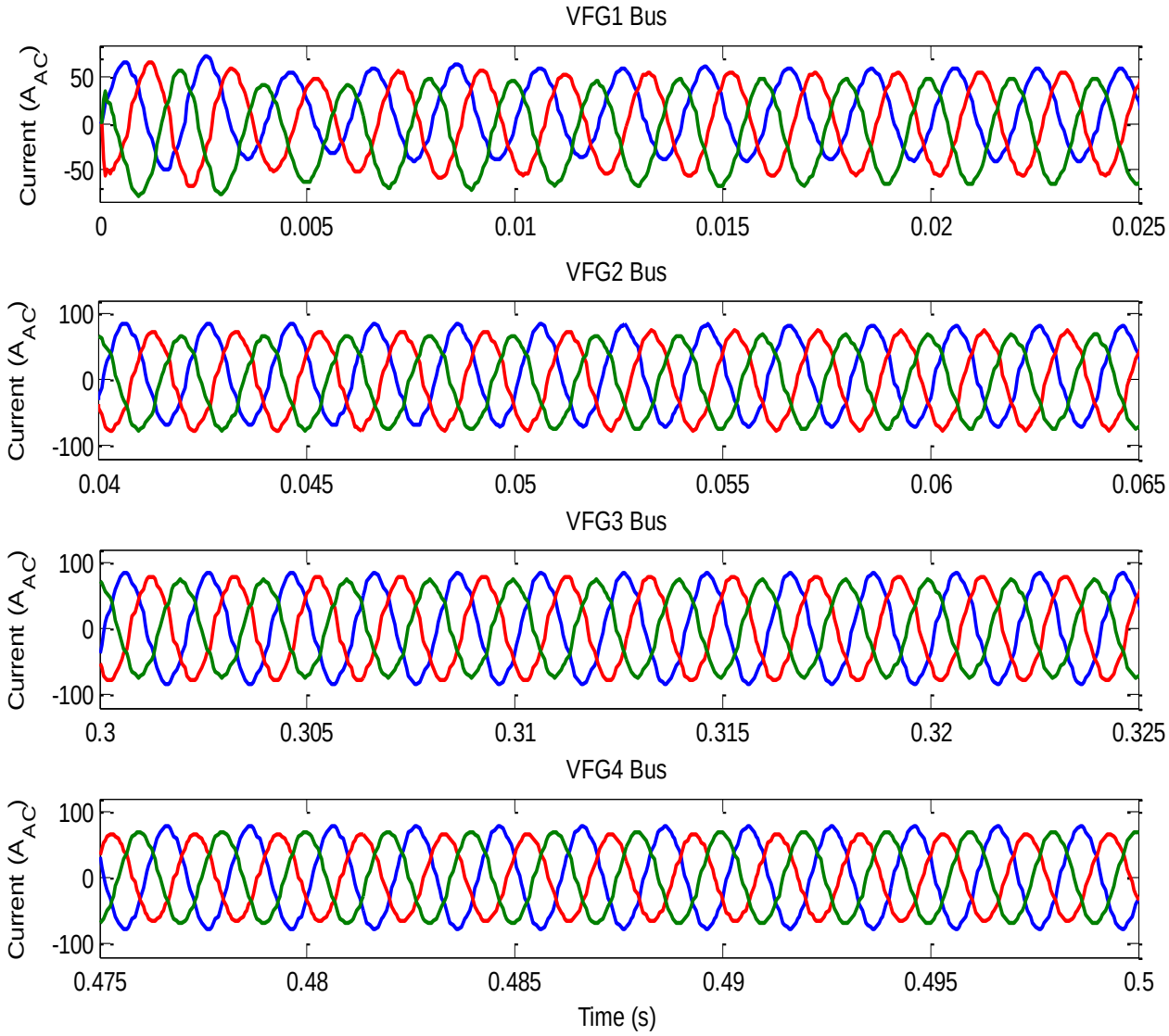

Figure 3.4. Current simulation results from VFG busses

Figure 3.5 presents a FFT analysis performed on the current measurements. Results meet the MIL-E-7016F requirements [20], in which at higher frequencies, the THD of the generator current must be less than 5% [20]. In addition, the fact of having an unbalanced systems, introduces different values of THD per phase, since each phase is not equally loaded.

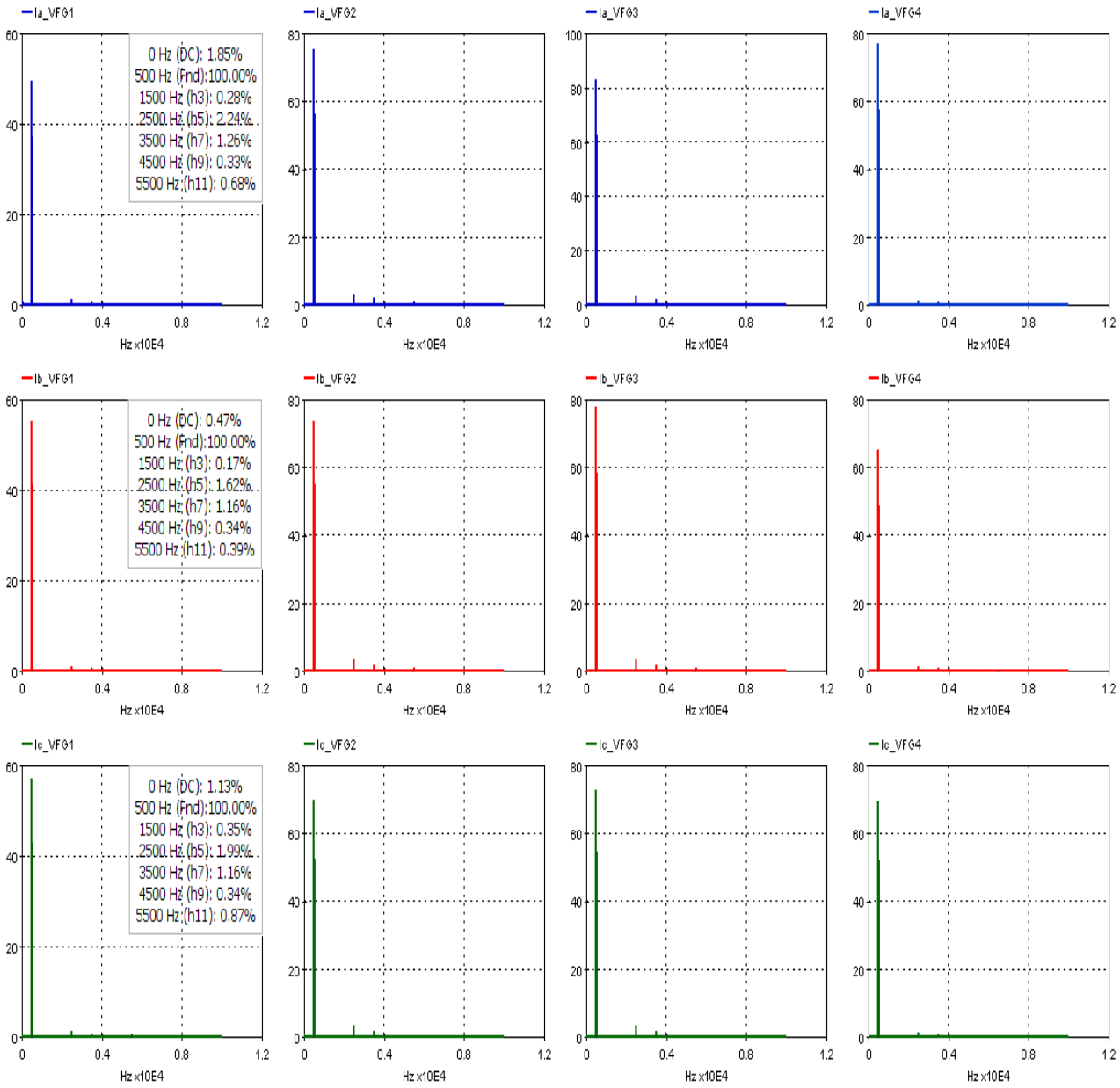

Figure 3.5. FFT analysis of current simulation results from VFG busses

As it is explained in section 2.2.2, generators rotate in opposite directions depending on their location. The phase sequence of generators 1 and 4 is A, B, C. The phase sequence of generators 2 and 3 is C, B, A. This is implemented in the aircraft electric power system modeled in Simulink. Implications of not modeling this phase sequence are presented in Figure 3.6.

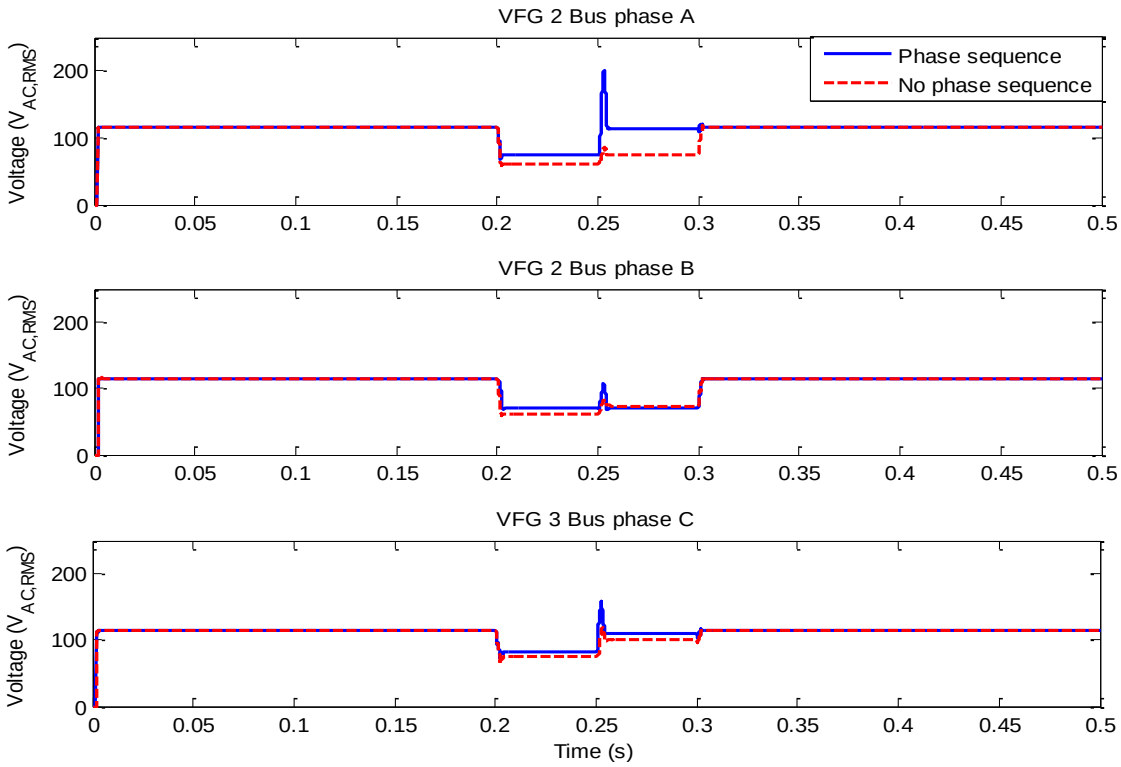

Figure 3.6. Effect of phase sequence in ACPC network reconfiguration

Figure 3.6 presents the RMS voltages from VFG2 while VFG2 and VFG3 fail at the same time. In this case, VFG2 and VFG3 fail at 200 ms of simulation time, so that ACPC reconfigures itself to transfer energy from VFG4 to AC BUS2, while VFG1 supplies energy to AC BUS3, as indicated in [18]. After 100 ms, VFG2 and VFG3 return to operation and ACPC restores the power supply between VFG2 and AC BUS2, and VFG3 and AC BUS3. There is a 50 ms delay between switching operations caused by the commutation times of protective devices found on the aircraft.

While system is working at normal operation, the generators are feeding independent circuits and when ACPC reconfigures the power supply while failure, a couple between two generators and one bus (or circuit) can be created during fault elimination or power transfer. While ACPC reconfigures the aircraft power system at 250 ms, a voltage spike, which is a fast and short duration electrical transient in voltage, is observed, since the maximum voltage is mainly determined by the closing instant of the breaker in relation to the voltage of the supply system. This overvoltage usually occurs when the breaker is closed at the maximum of the voltage.

Therefore, this voltage spike observed in phases A and C is related to the time where the switch is changing its state instead of the fact of modeling the phase sequence. In addition, phase sequence is implemented since the generators are designed to rotate in either direction. This is a design criteria to support the installation where one generator is installed on either side of the gearbox, so that this phenomena is just a mechanic design criteria.

3.2 AC Busses

Figure 3.7 presents voltage simulation results taken from each AC bus. Every bus reaches around 115 VRMS phase-to-ground during all the simulation time of 0.5 s.

a)

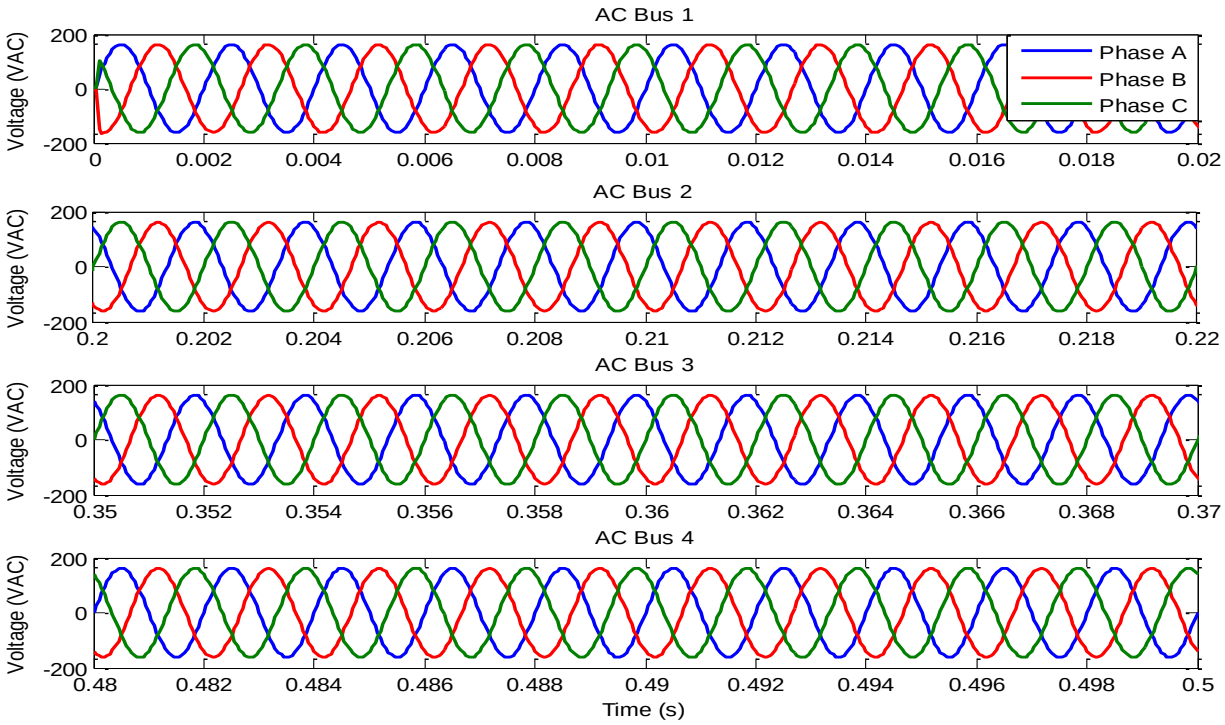

b)

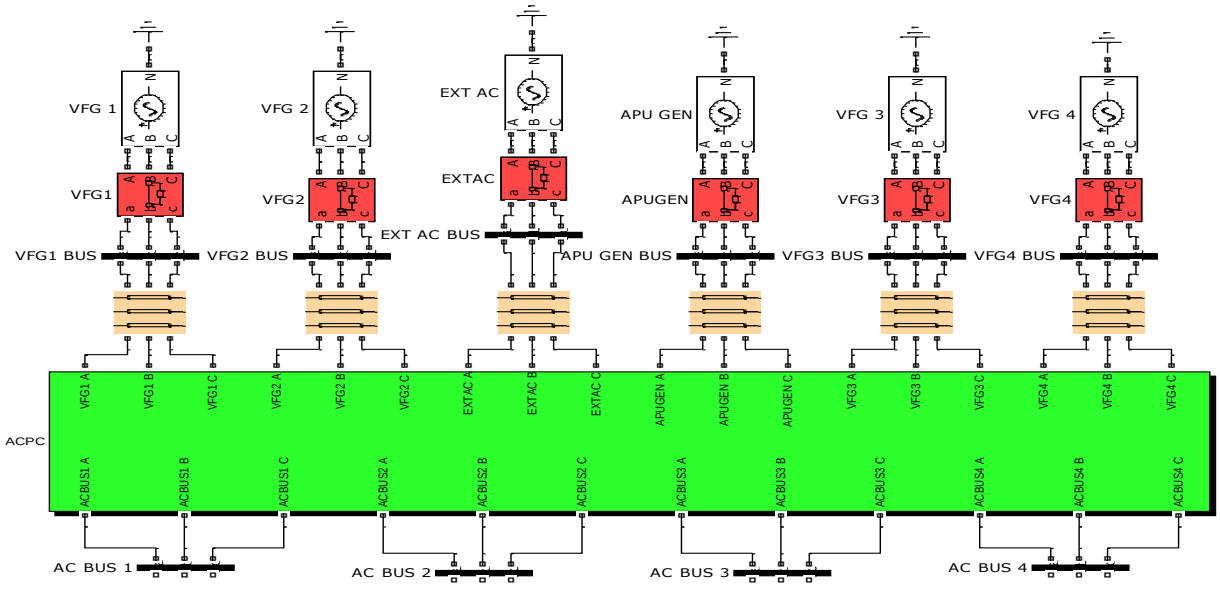

Figure 3.7. a) Voltage simulation results from AC busses and b) Busses location

Figure 3.8 presents current simulation results taken from each AC bus within the same network conditions than in Figure 3.7.

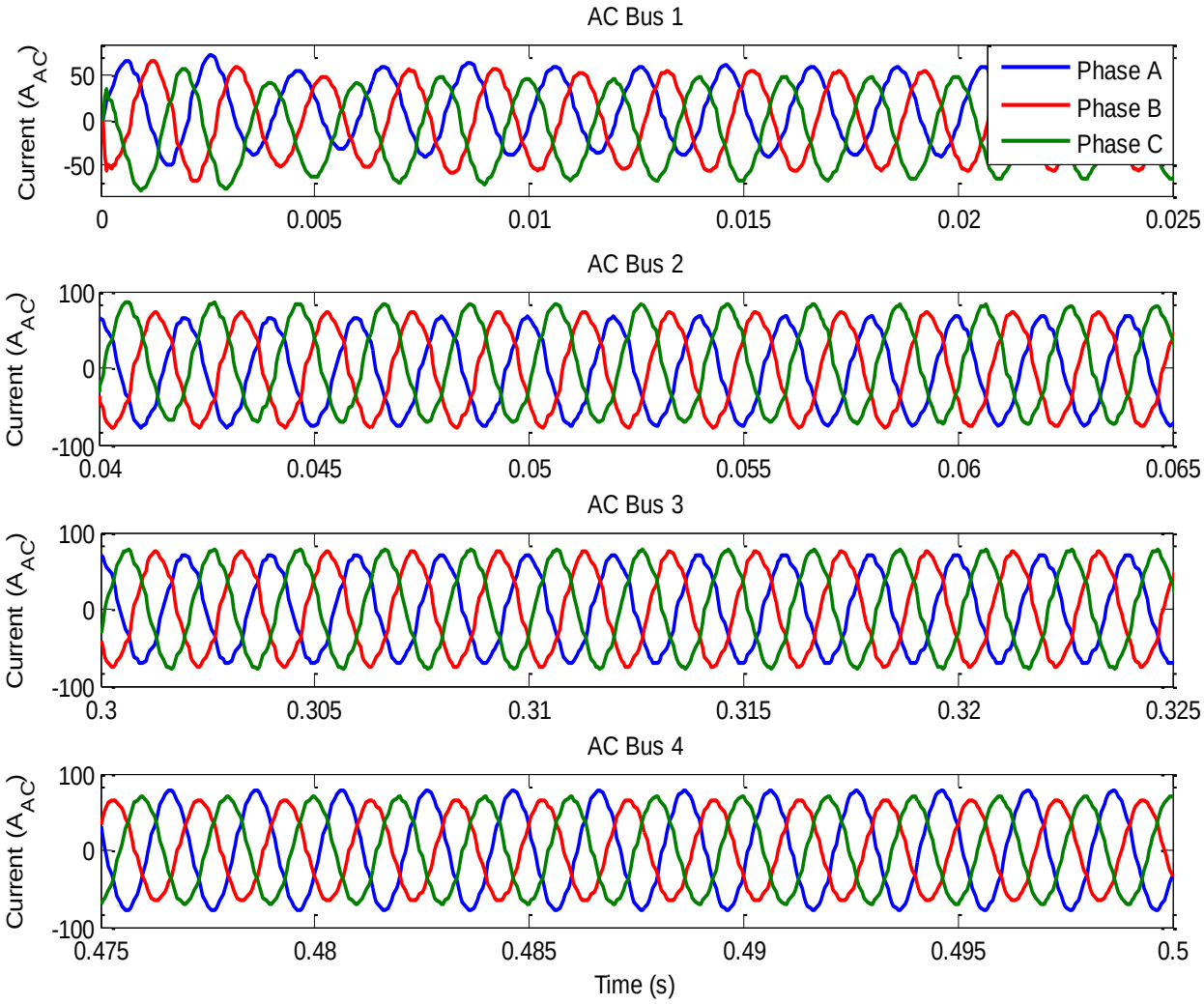

Figure 3.8. Current simulation results from AC busses

Figure 3.9 presents a FFT analysis performed to the current measurements. Results meet the intent of [20], and the percentages of harmonic distortion are lower than the limits in [20]. In addition, the fact of having an unbalanced systems, introduces different values of THD per phase, since each phase is not equally loaded. The source of harmonics can be related to the AC/DC converter (diode bridge) presented in the TRU, the three-phase (two windings) transformer in the TRU, since the magnetizing characteristics of the core (saturable core) is taken into account. Finally, the motor implemented for modeling the EHP, uses variable load torque based on rotor speed, so that it can introduce zero sequence harmonics, commonly called "Triplens" (There are odd multiples of the 3rd harmonics).

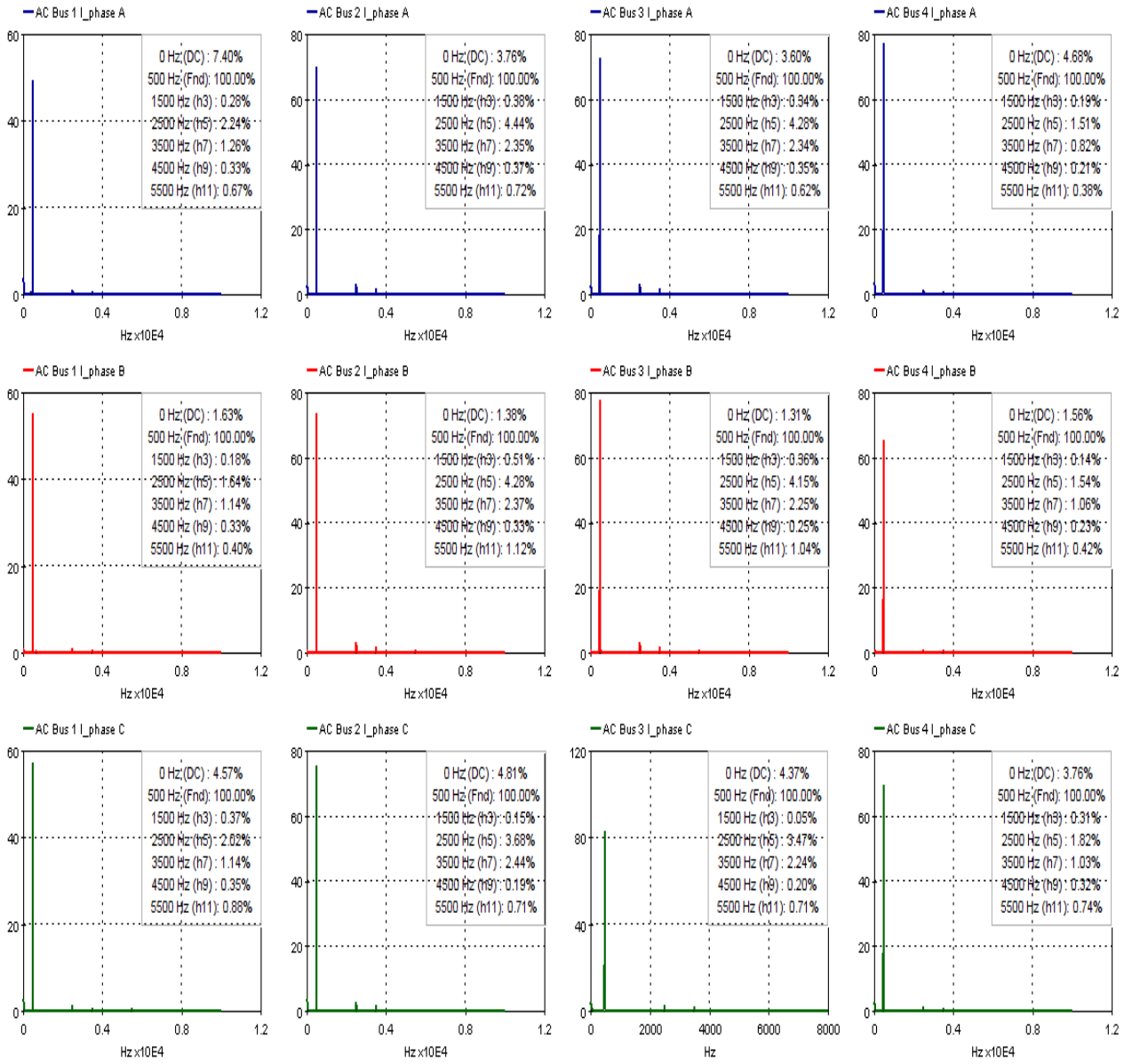

Figure 3.9. FFT analysis of current simulation results from VFG busses

3.3 Electric Hydraulic Pump (EHP)

Regarding EHP loads, available measurements on the steady-state performance of these machines allow the validation of the developed models when EHP is connected to the entire electric network. Concerning the start-up performance, the measurements present what appears to be noise. There is no description of the state of the aircraft electric system when these measurements were taken. Figure 3.10 only shows the first 0.040 s from the beginning of the measurements. The only information available is the operation frequency of 320 Hz. It is not

clear if the given measurements begin from the EHP start-up or from the steady-state performance.

In addition, the ASMs should account for variable frequency even if it is designed for 400 Hz. Figure 3.10 shows current and voltage validation between the Simulink model and available measurements when connected to the network. Differences between both current and voltage waveforms can be explained by the applied torque model and the network representation to which the ASM is connected. Accurate models of hydraulic loads must be implemented through the analysis of mechanical performance equations.

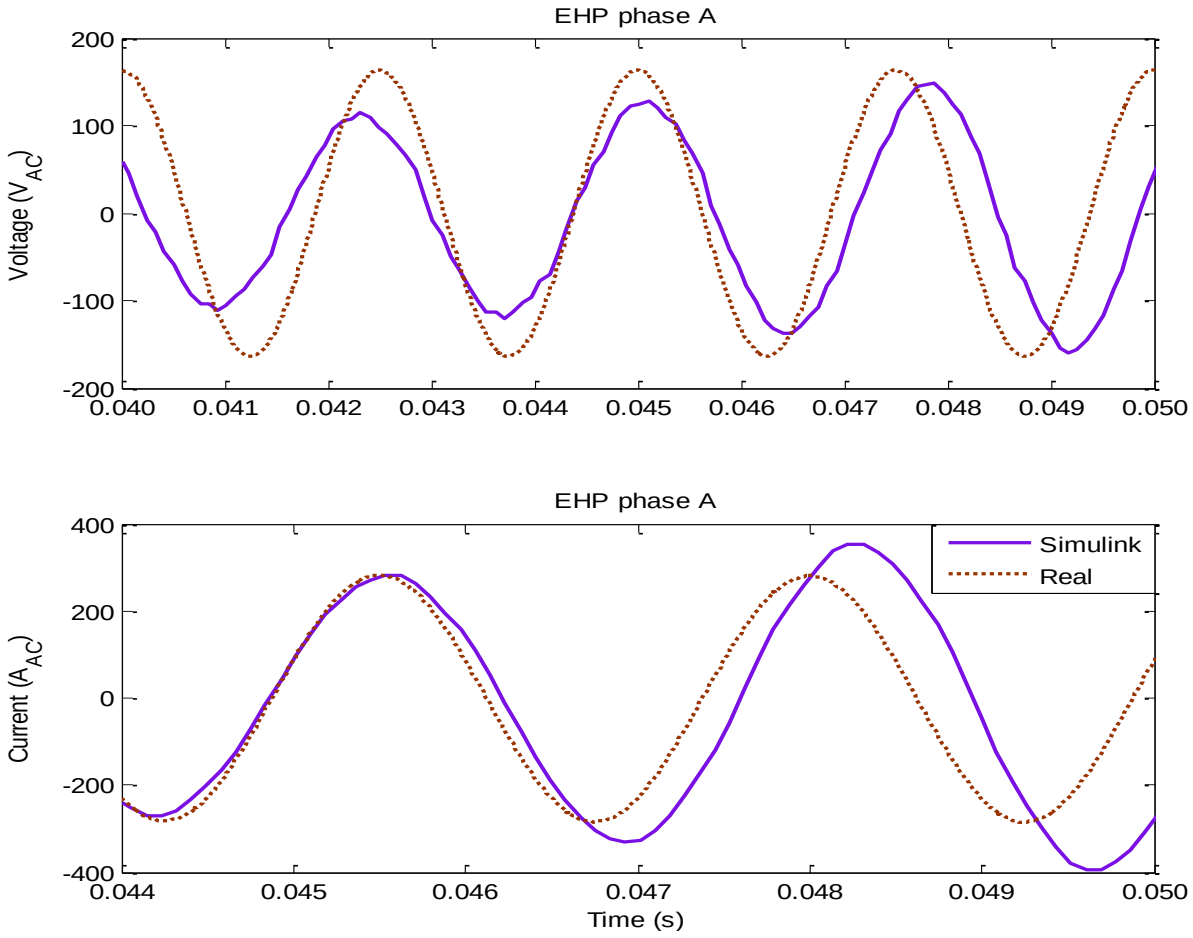

Figure 3.10. Voltage and current measurements between Simulink model and available data

A possible explanation for the growing mismatch between voltage waveforms is related to the modeling of the feeding VFGs. The inclusion of VFG controls and model details should improve the precision of transient and steady-state performance. Figure 3.11 shows the electromagnetic torque, the active and reactive power waveforms between Simulink and EMTP-RV EHP models,

as both models show similarities in their dynamic behaviour. Differences before the first 100ms of simulation can be found due to the way Simulink resolves internal equations of the asynchronous machine model.

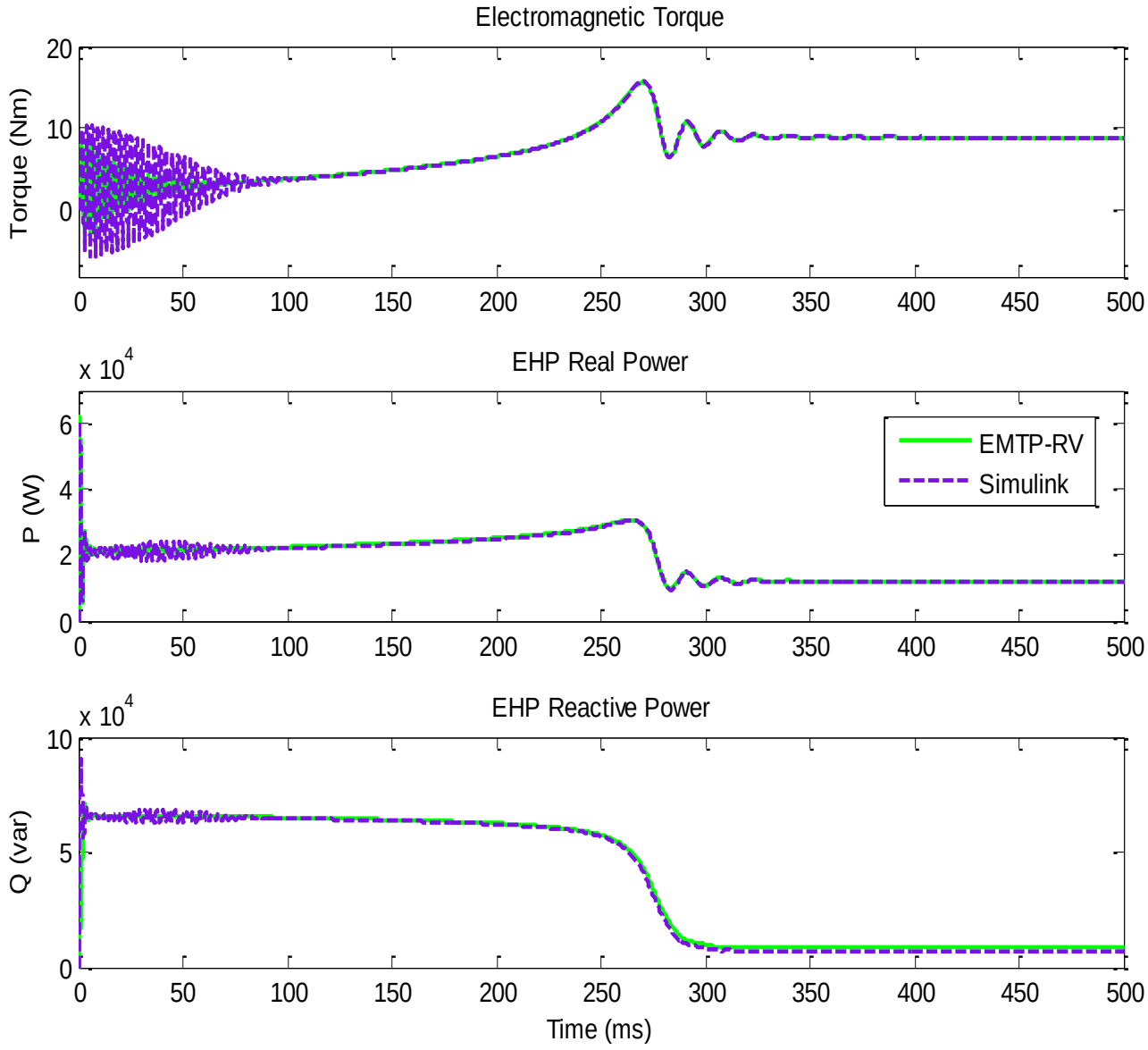

Figure 3.11. EHP comparison between Simulink and EMTP-RV

Figure 3.12 shows the current waveforms when EHP starts-up and it is connected into the network.

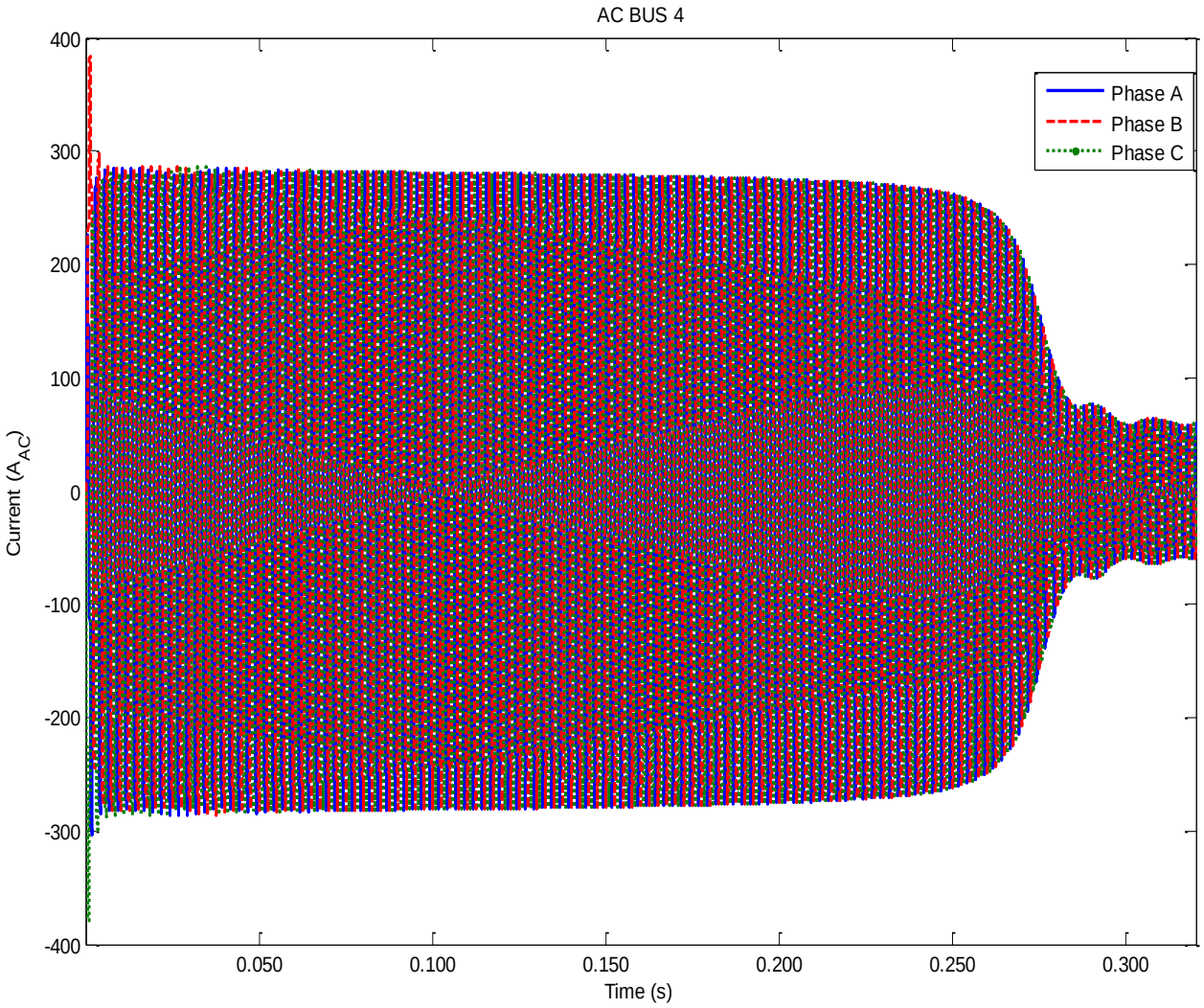

Figure 3.12. Waveforms of the EHP current's start-up

3.4 Transformer Rectifier Unit (TRU)

Figure 3.13 shows the TRU model output of 28 VDC voltage steady-state value for an operation at 500Hz operation, when simulating within the entire network.

a)

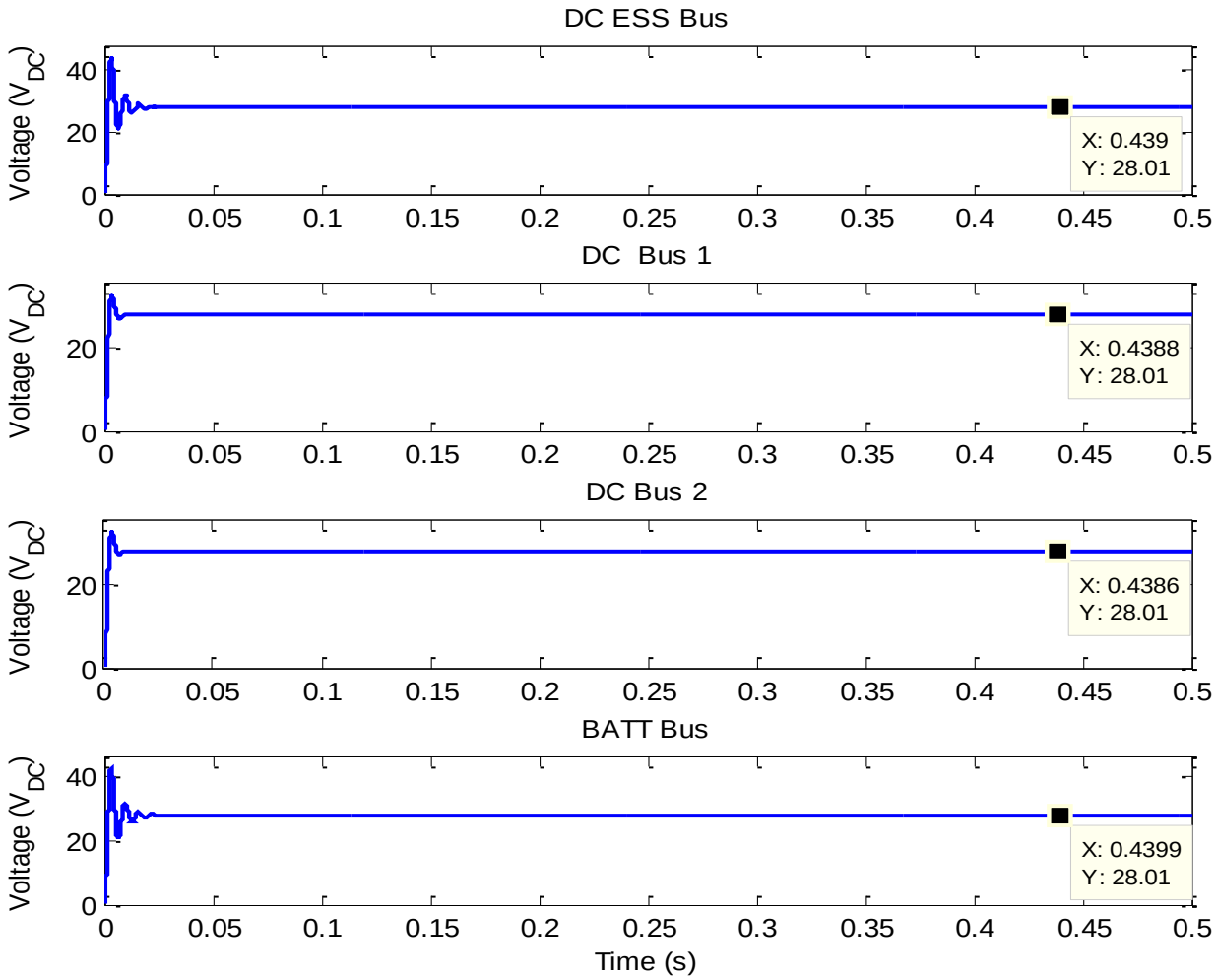

b)

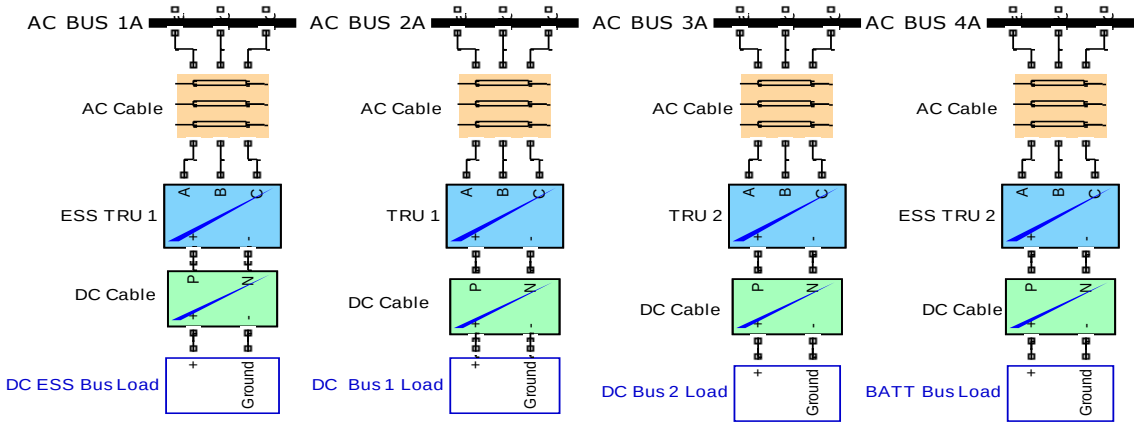

Figure 3.13. a) TRU steady-state voltage behaviour and b) TRUs location

The transient at the beginning is due to start-up of the EHP connected to its respective AC bus serving the TRU, which links the AC part and the DC part of the system and the inrush current from the three-phase transformers. In addition, Figure 3.14 shows that the voltage ripple within 0.6 ms at the DC busses is less than 5% of the nominal voltage. This is within the military standard MIL-STD-704F [26].

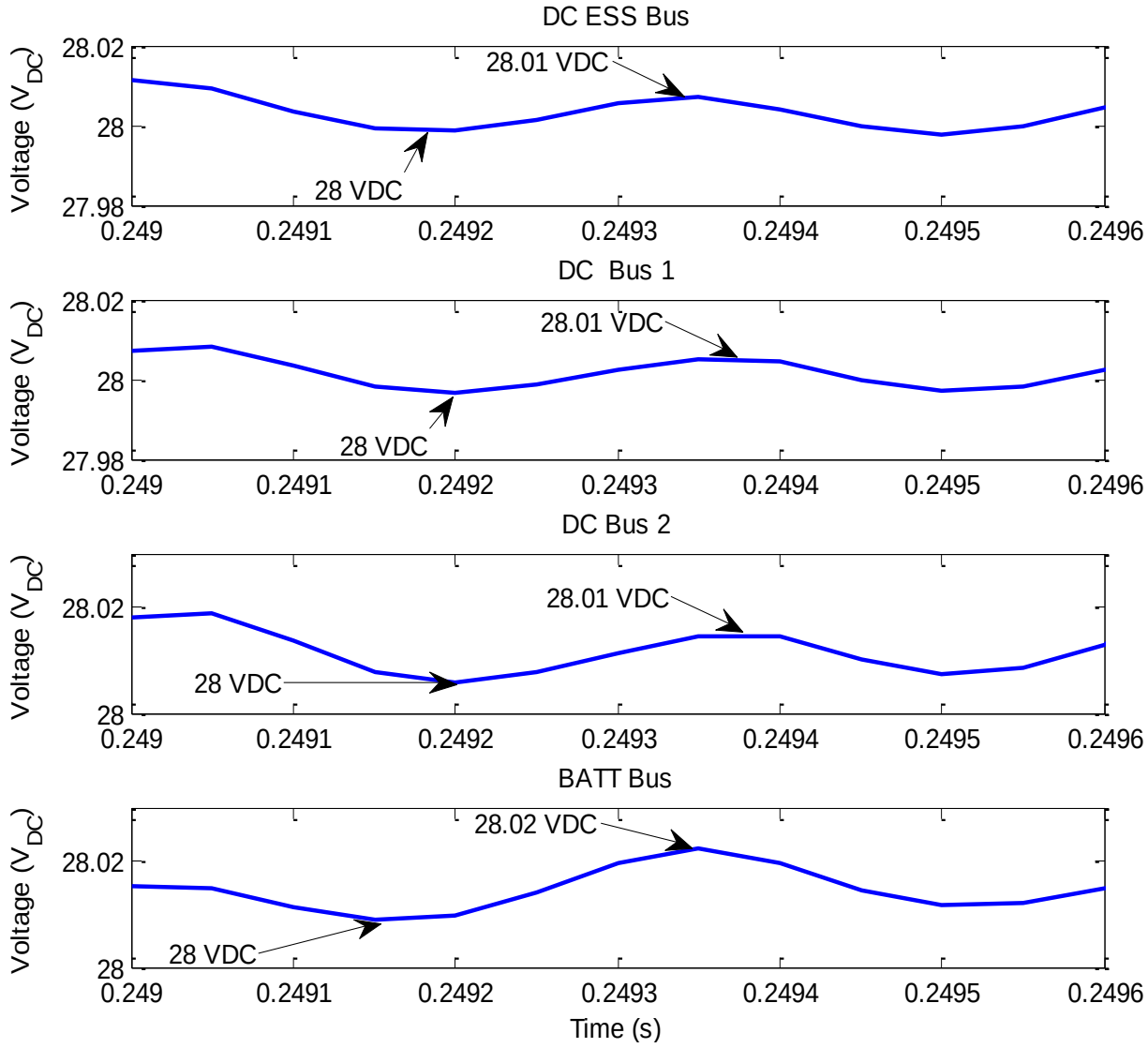

Figure 3.14. TRU voltage ripple

It is important to analyze TRU behaviour before and after a switching event. In this case, VFG4 fails at 200 ms of simulation, so that VFG1 supplies energy to AC BUS4 as indicated in [18]. After 100 ms, VFG4 returns in operation and restores the power supply with AC BUS4, as EHP starts-up at 350 ms. There is 50 ms delay between switching operations and the voltage drop

is detected by the controls implemented in Simulink for triggering the closure of the SSPC in 2 ms, in order to supply battery power to the DC bus. In addition, the minimum voltage sag reaches 14.31 VDC in less than 2 ms, while the maximum overvoltage reaches 43.06 VDC during 2.95 ms. Both voltage levels are within the requirements of MIL-STD-704F [26] as shown in Figure 3.15.

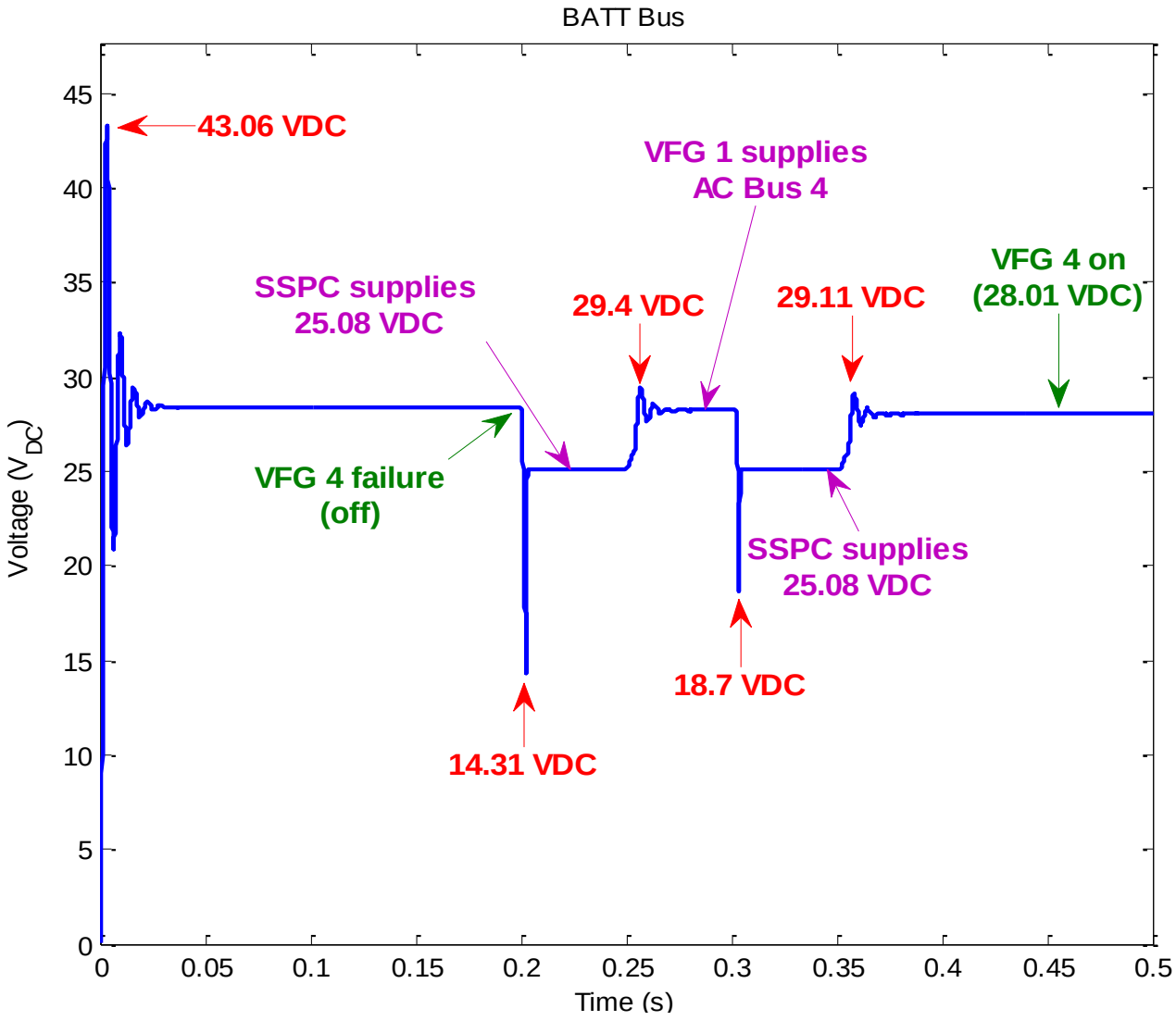

Figure 3.15. TRU voltage transient behaviour during VFG4 failure

3.5 DC Busses

Figure 3.16 presents voltage and current simulations taken from each DC bus. All busses reach steady-state values according to [19] (as shown in Table 3.1).

Table 3.1. Comparison between theoretical and simulated values from DC busses

DC BUS	**VOLTAGE**			**CURRENT**		
	Measured (V_{DC}) [16]	**Simulated (V_{DC})**	**Error (%)**	**Measured (A_{DC}) [16]**	**Simulated (A_{DC})**	**Error (%)**
DC ESS	28.00	28.00	0.00	46.36	46.38	0.04
DC BUS 1	28.00	28.00	0.00	137.00	137.00	0.00
DC BUS 2	28.00	28.01	0.04	140.04	140.10	0.04
BATT BUS	28.00	28.00	0.00	51.41	51.57	0.31

Figure 3.16 shows the transient at the beginning due to start-up of the EHP connected to the AC bus serving the TRU, and the inrush current from the three-phase transformers of the TRU.

a)

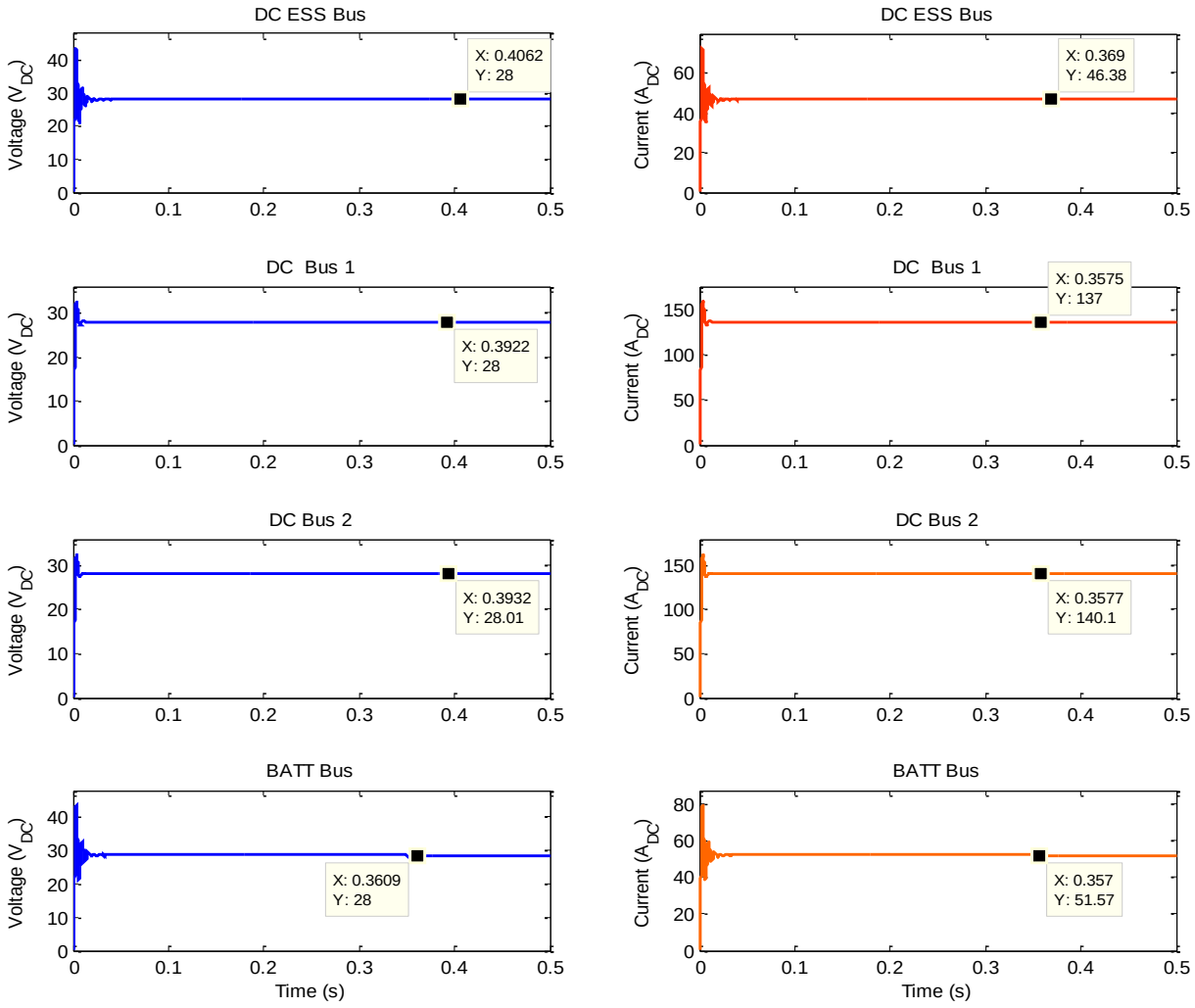

b)

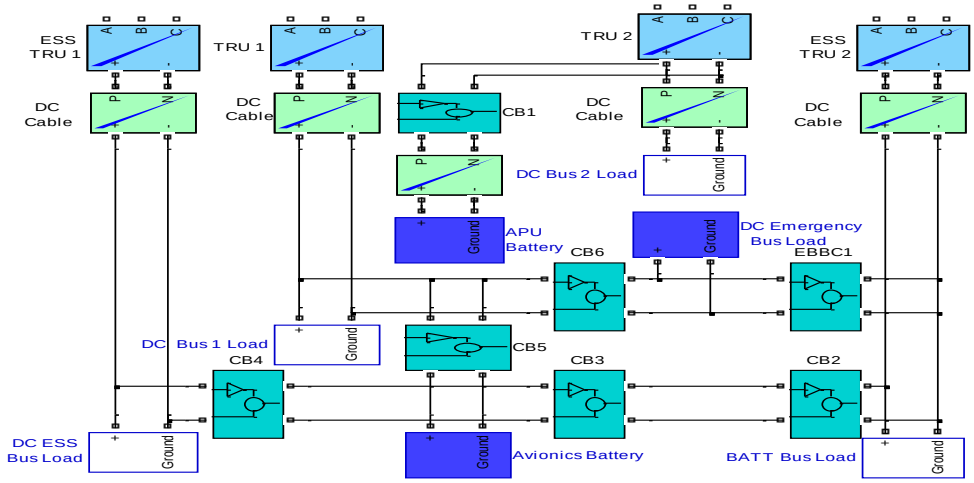

Figure 3.16. a) DC voltage and current steady-state simulation results and b) DC busses location

3.6 Switching Time Delay

As it is explained in Chapter 2, each switch has a 50 ms time delay which is in fact the maximum switching operation time for power interruptions, so that as soon as a VFG failure occurs at a specific time, the switches related to the event operate 50 ms after the failure. This value can be easily changed, since the time delay could be less than 50 ms, depending on the characteristics of the switch. Figure 3.17 shows the implications, on the DC ESS bus voltage, when changing the switching time delay from 50 ms to 30 ms and to 10 ms. In this case VFG1 fails at 200 ms, so that VFG4 supplies energy to AC BUS1 which supplies energy to DC ESS Bus as indicated in [18]. After 100 ms, VFG1 returns in operation and restores the power supply to AC BUS1.

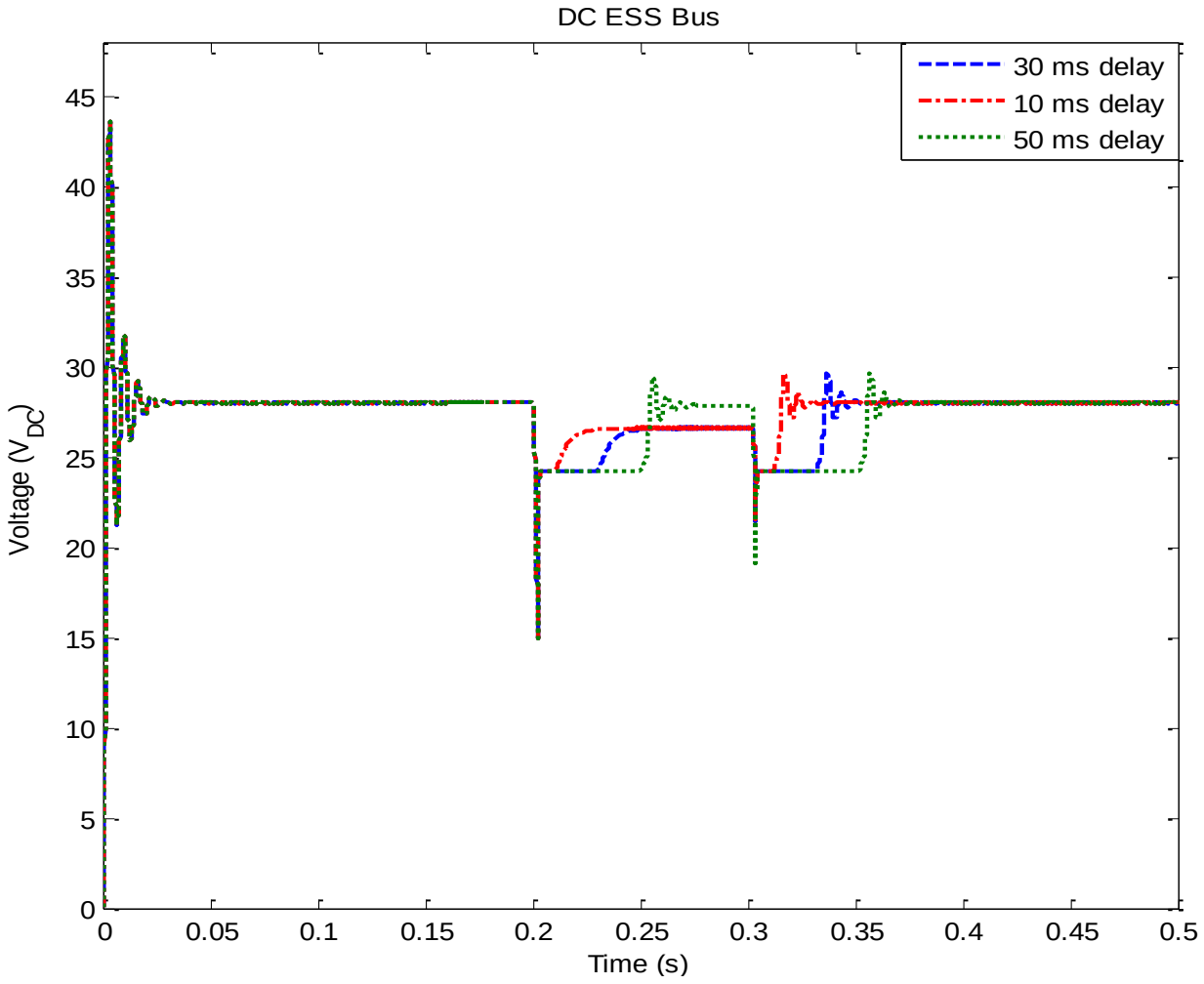

Figure 3.17. Effects of changing the switching time delay on the DC ESS bus voltage

The study of switching time delay impacts can be performed using statistical analysis methods. The control architecture implemented in the Simulink model allows the switching time delay to be easily modified within the simulation. As in EMPT-RV, a random data law can be added to the switch operation time, so that both the switch closing and opening times become randomized. In Figure 3.18, when the switching time delay is set to 50 ms, a voltage transient is observed when the switch recloses. This is due to the switch closes at a time other than as the voltage waveform crosses zero, so that a sudden "jump" or discontinuity in the voltage and current waveforms on the load side of the switch is presented. This is not observed when the switching time delay is set to 30 ms or even 10 ms. The different stages observed in Figure 3.18 are due to network reconfiguration performed by the ACPC.

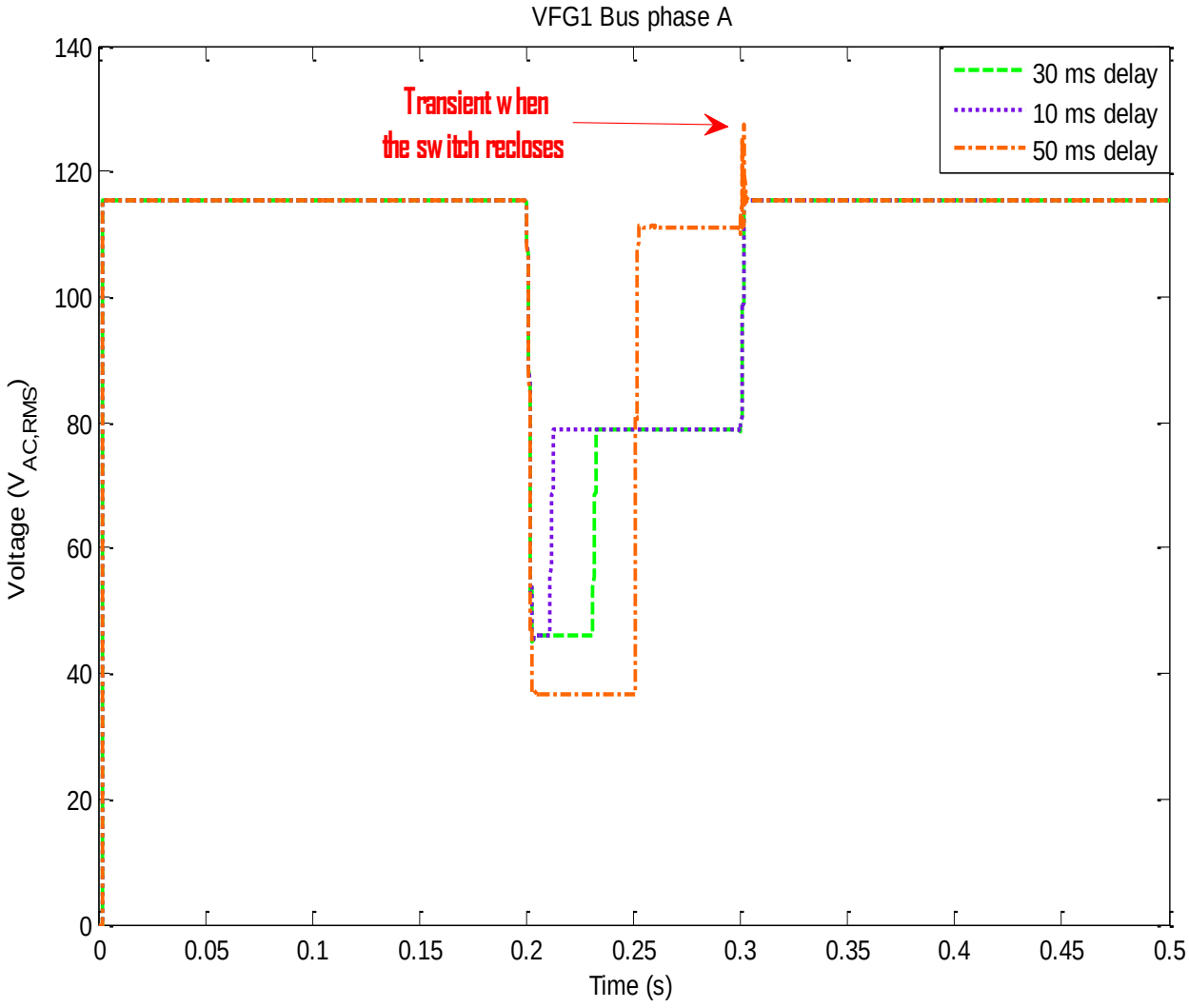

Figure 3.18. Effects of changing the switching time delay on the VFG1 bus RMS voltage

3.7 Case Study 1: VFG4 fails at 200 ms and restores operation at 300 ms

In this case, VFG4 fails at 200 ms of simulation, so that ACPC reconfigures itself to transfer energy from VFG1 to AC BUS4 as indicated in [19]. After 100 ms, VFG4 returns in operation and ACPC restores the power supply between VFG4 and AC BUS4, as AC BUS4 power supply is no longer provided by VFG1. This causes VFG1 to supply more current during VFG's failure (100 ms). Due to the 50 ms delay in switching operations, VFG1 supplies energy to AC BUS4 at 250 ms and VFG4 restores power supply at 350 ms. All the current outputs of the VFG busses supply nominal loads. Figure 3.18 summarizes what is stated above.

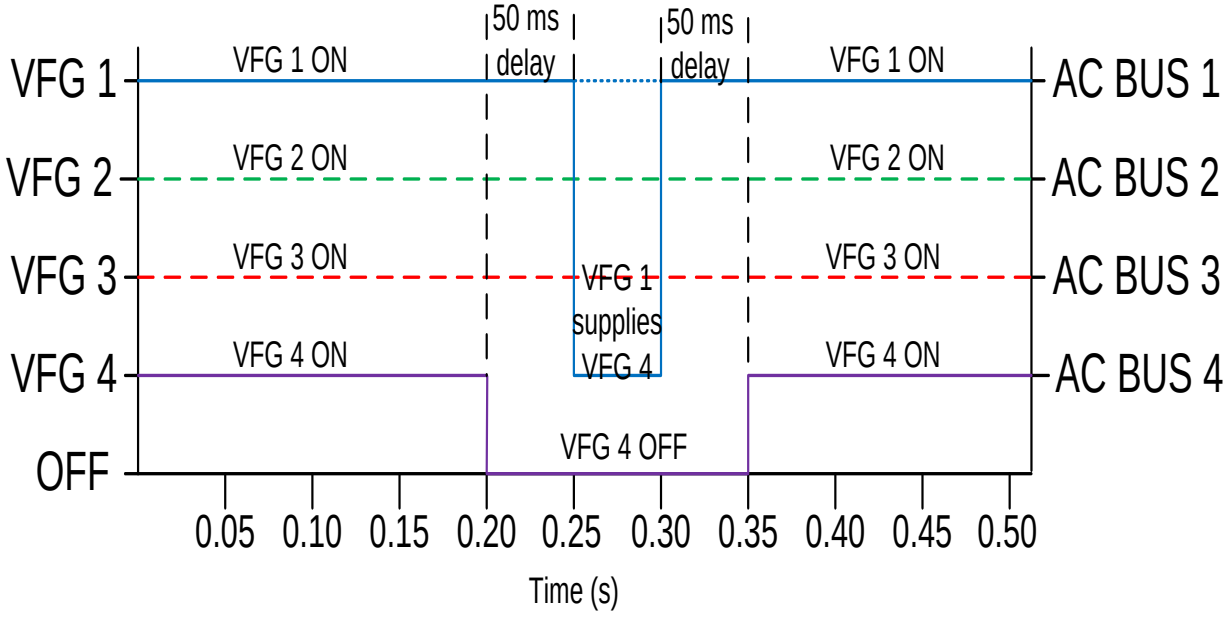

Figure 3.19. VFGs supplying AC busses in case study 1

Figure 3.20 shows current simulation results for all VFG busses. It is observed that VFG1 supplies more current when VFG 4 is off. In addition, ACPC transfers and restores communication between VFG4 and AC BUS4 within the 50 ms delay.

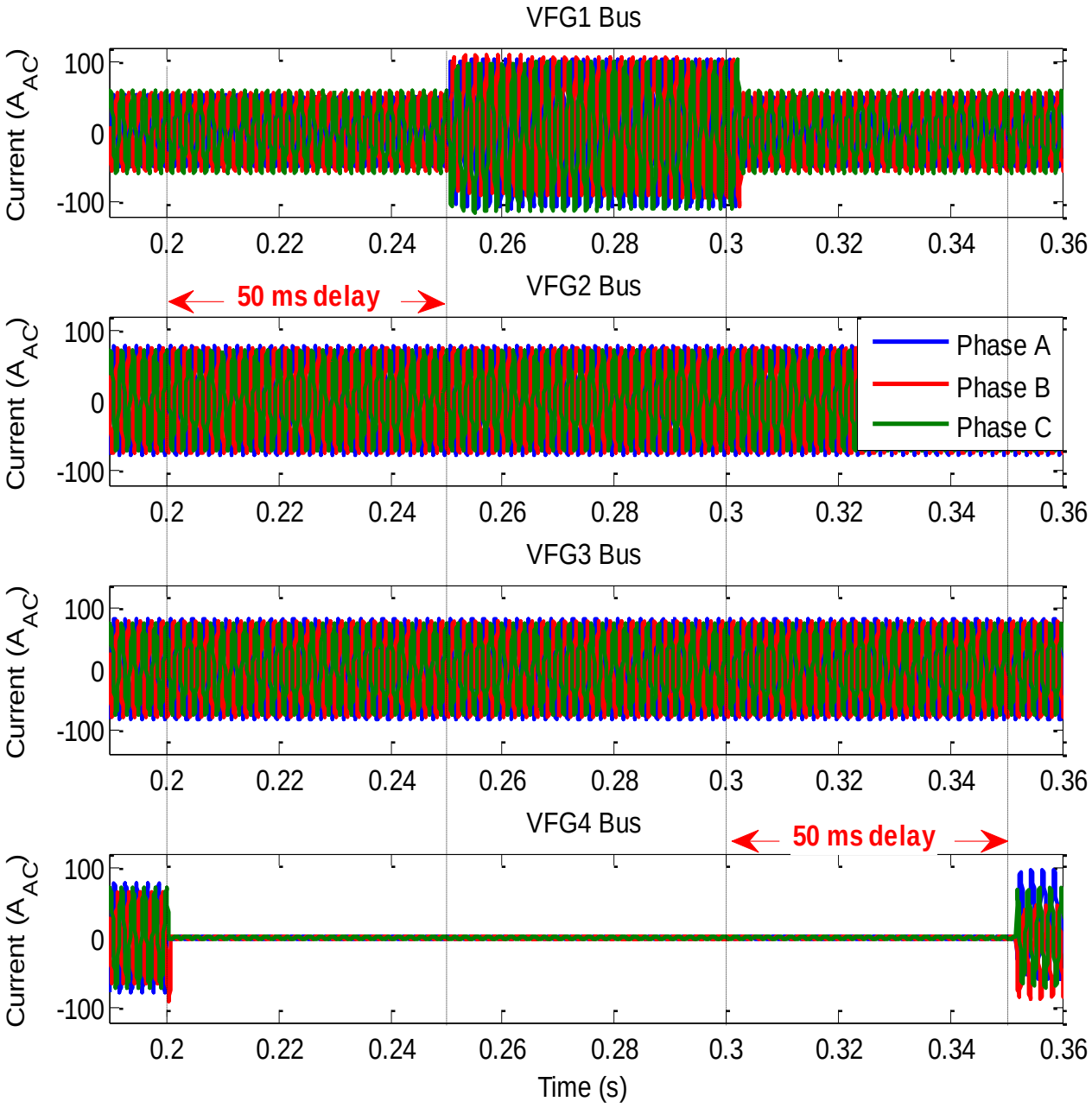

Figure 3.20. Current simulation results from VFG busses when VFG4 fails at 200 ms

Figure 3.21 shows the VFG1 bus current waveforms from both EMTP-RV and Simulink models. Both models have the same steady-state behaviour before and after VFG4 fails. When VFG1 supplies energy to AC BUS 4, 50 ms after SSPC actuation, both models have similar transient behaviour. Some differences are related to the way that EHP and TRU are modeled. While in EMTP-RV, EHP and TRU are designed and simulated for 400 Hz, in Simulink EHP and TRU were designed for 400 Hz, but simulated in 500 Hz, as required for this case study.

Modifications in VFG1 currents related to switching operation are clearly presented in both models.

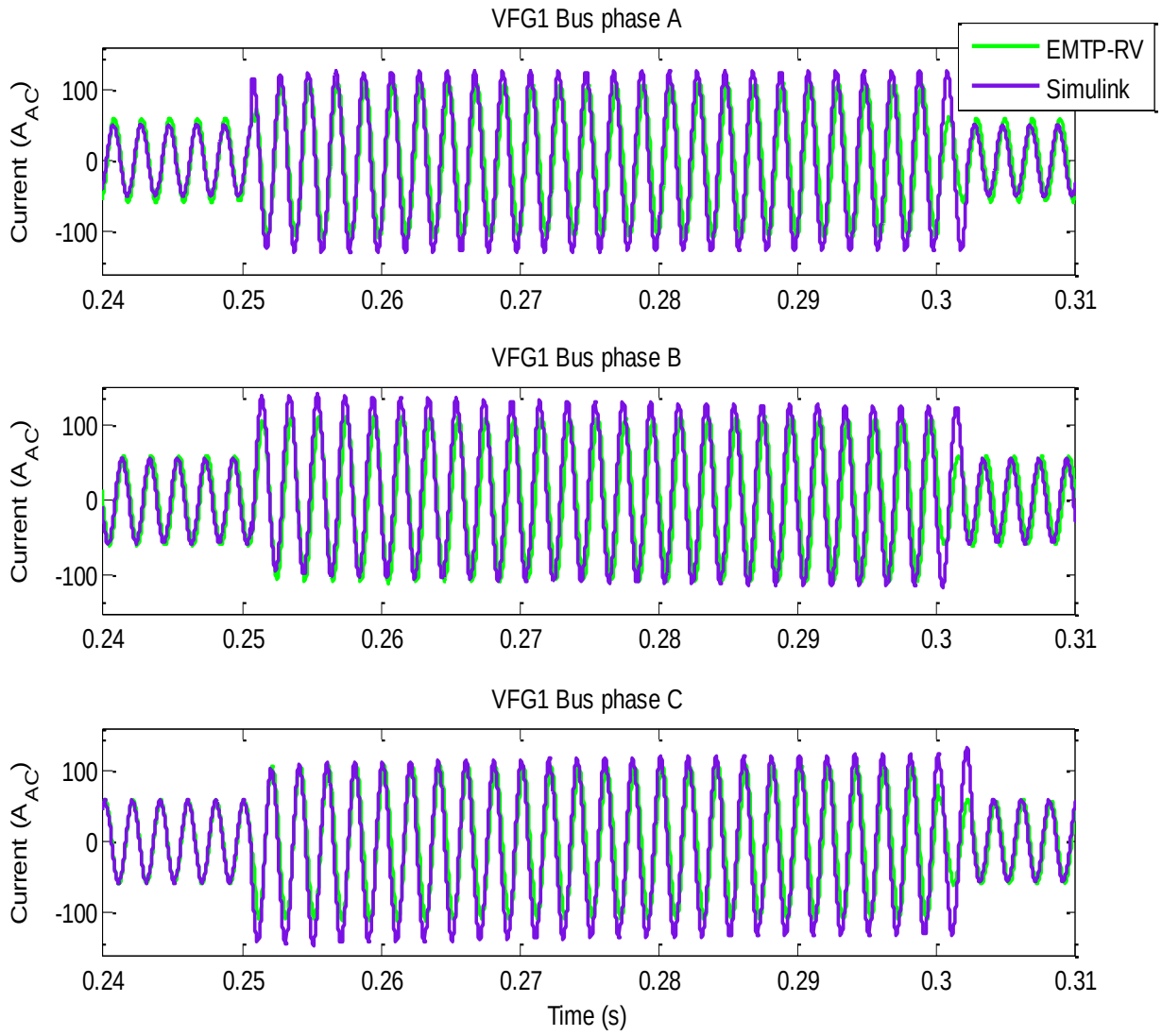

Figure 3.21. VFG1 Bus current waveforms from Simulink and EMTP-RV

Figure 3.22 shows that all DC busses achieve a constant near 28 VDC voltage. Even if VFG4 failure is produced at 200 ms, VFG1 supplies both AC BUS1 and AC BUS4 after 250 ms (50 ms switching delay). At 300 ms, VFG1 stops to supply AC BUS4 while VFG4 waits 50 ms before starting to supply AC BUS4.

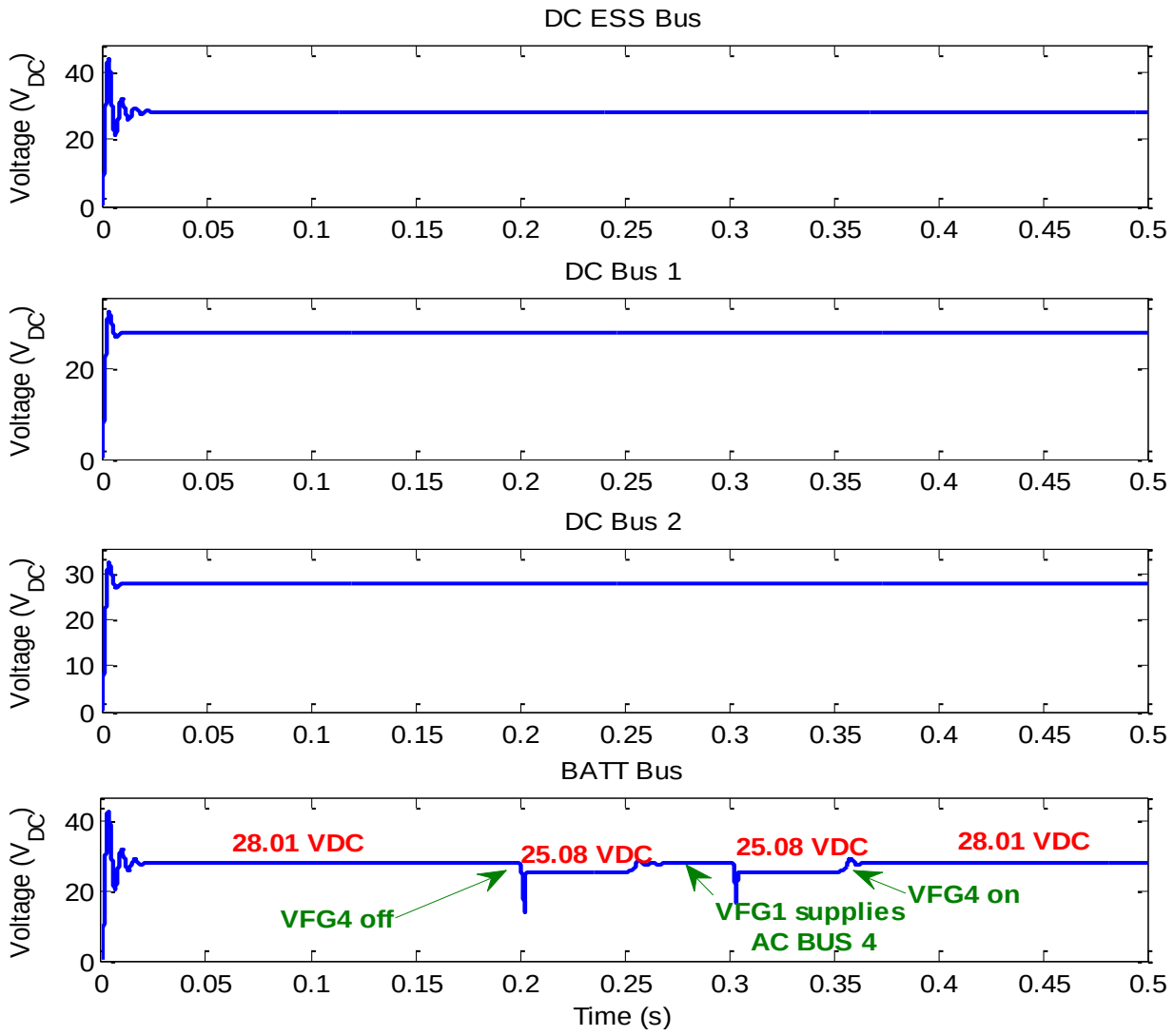

Figure 3.22. DC voltages when VFG4 fails

Figure 3.23 shows the differences in DC waveforms between both platform models, which are due to the implementation of SSPCs and TRUs in EMTP-RV model. While breakers need 50 ms to switch, SSPCs can switch within 2 ms, so that BATT BUS voltage do not drop down to zero when VFG4 fails. While in Simulink model, the BATT Bus voltage drops to 14.31 VDC, in EMTP-RV the BATT Bus voltage drops down to 2 VDC, which is inferior to the lower limit permitted by [18]. This can be easily adjusted by setting the SSPC's voltage trigger to 20 VDC as in Simulink. Once the DC voltage decreases below that limit, SSPC closes and puts the DC busses on battery supply. In terms of overvoltage, both models are far from the upper limit.

The Simulink model shows a less oscillatory behaviour while the switch closes as well as a less voltage spike, due to how the magnetizing characteristics of the core are modeled in both platforms. In addition, the model in EMTP-RV does not reach 28 VDC in fact it reaches 27.19 VDC, even though, it is within the voltage lower limit established in [18], this can be easily adjusted by increasing the secondary winding voltage in the EMTP-RV model. In addition, it is important to mention that when the EMTP-RV model works with the SSPC DC back-up the voltage is 22.58VDC, which must be increased in order to reach the 25 VDC according to the requirements expressed by Bombardier.

It is worth noticing that these tests constitute a preliminary attempt to compare both models, but some little variations concerning how some elements are modeled, prevent a better analysis.

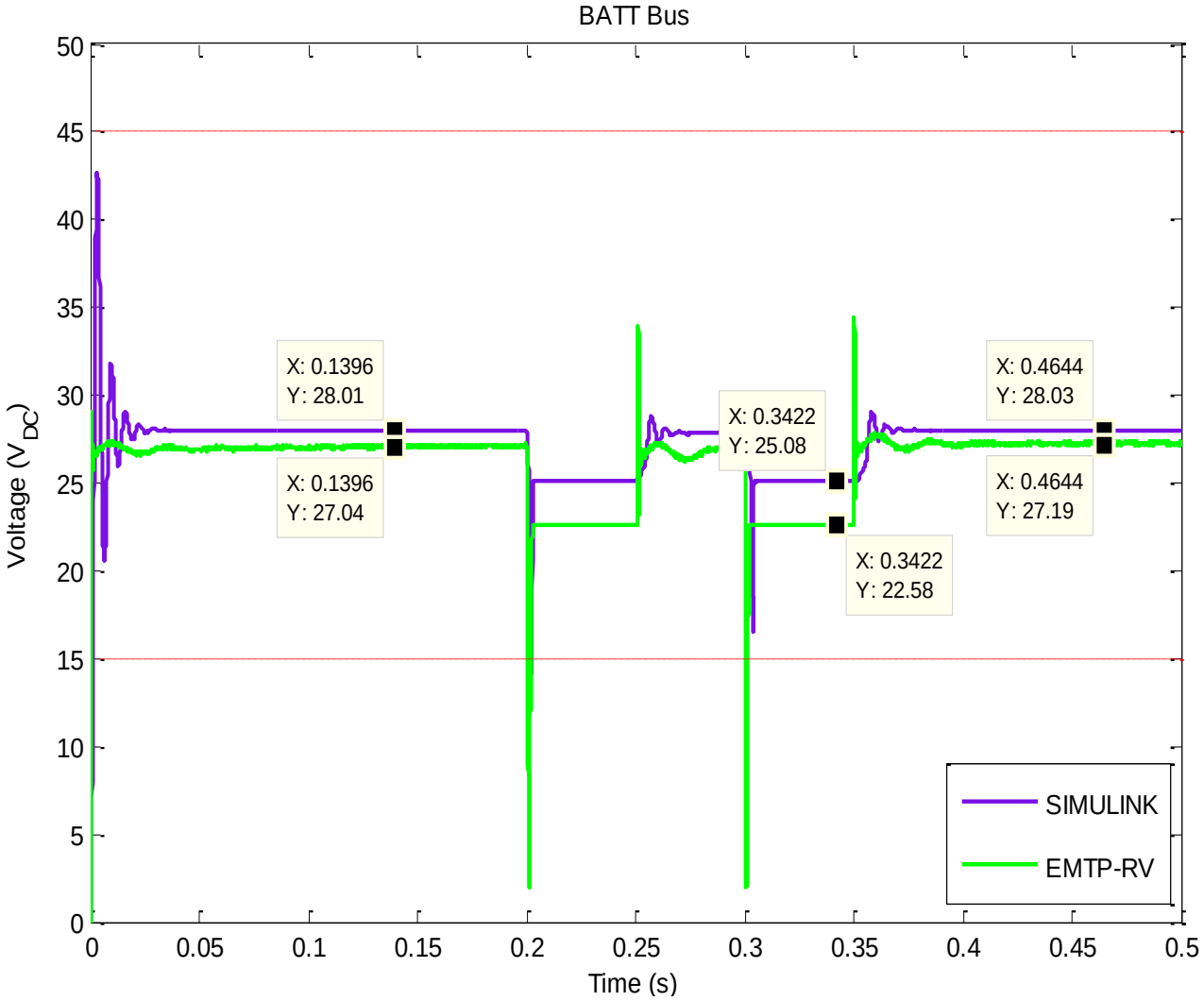

Figure 3.23. BATT Bus voltage in Simulink and EMTP-RV during VFG4 failure

3.8 Case Study 2: VFG1 and VFG4 fail at 200 ms and restores operation at 300 ms

In this case, VFG1 and VFG4 fail at 200 ms of simulation, so that ACPC reconfigures itself to transfer energy from VFG3 to AC BUS1, and from VFG2 to AC BUS4 as indicated in [18]. After 100 ms, VFG1 and VFG4 return to operation and ACPC restores the power supply between VFGs and AC Busses, as AC BUS1 power supply is no longer provided by VFG3 and AC BUS4 is no longer provided by AC BUS4. This causes VFG2 and VFG3 to supply more current during VFG's failure (100 ms). Due to the 50 ms delay in switching operations, VFG3 supplies energy to AC BUS1 at 250 ms, as well as VFG2 supplies ACBUS 4 at the same time. Both VFG1 and VFG4 restores power supply at 350 ms. Figure 3.24 summarizes what is stated above.

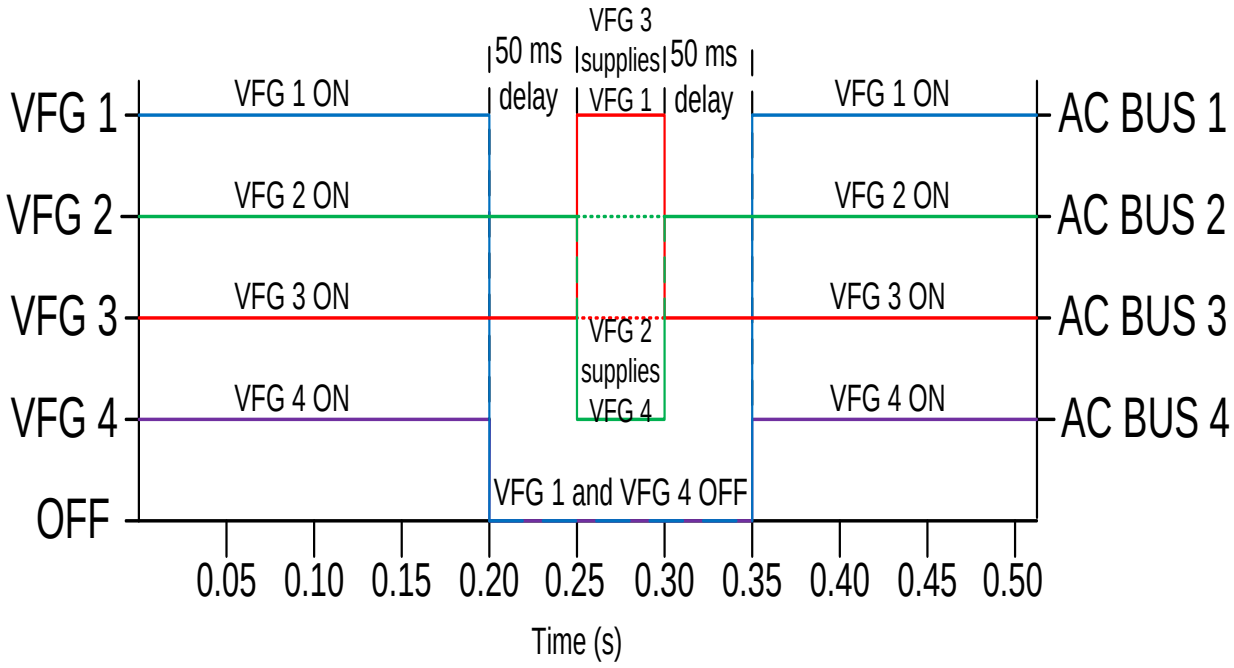

Figure 3.24. VFGs supplying AC busses in case study 2

Figure 3.25 shows current simulation results for all VFG busses. VFG3 supplies more current when VFG1 is off. Same case when VFG2 supplies AC BUS 4 when VFG2 is off.

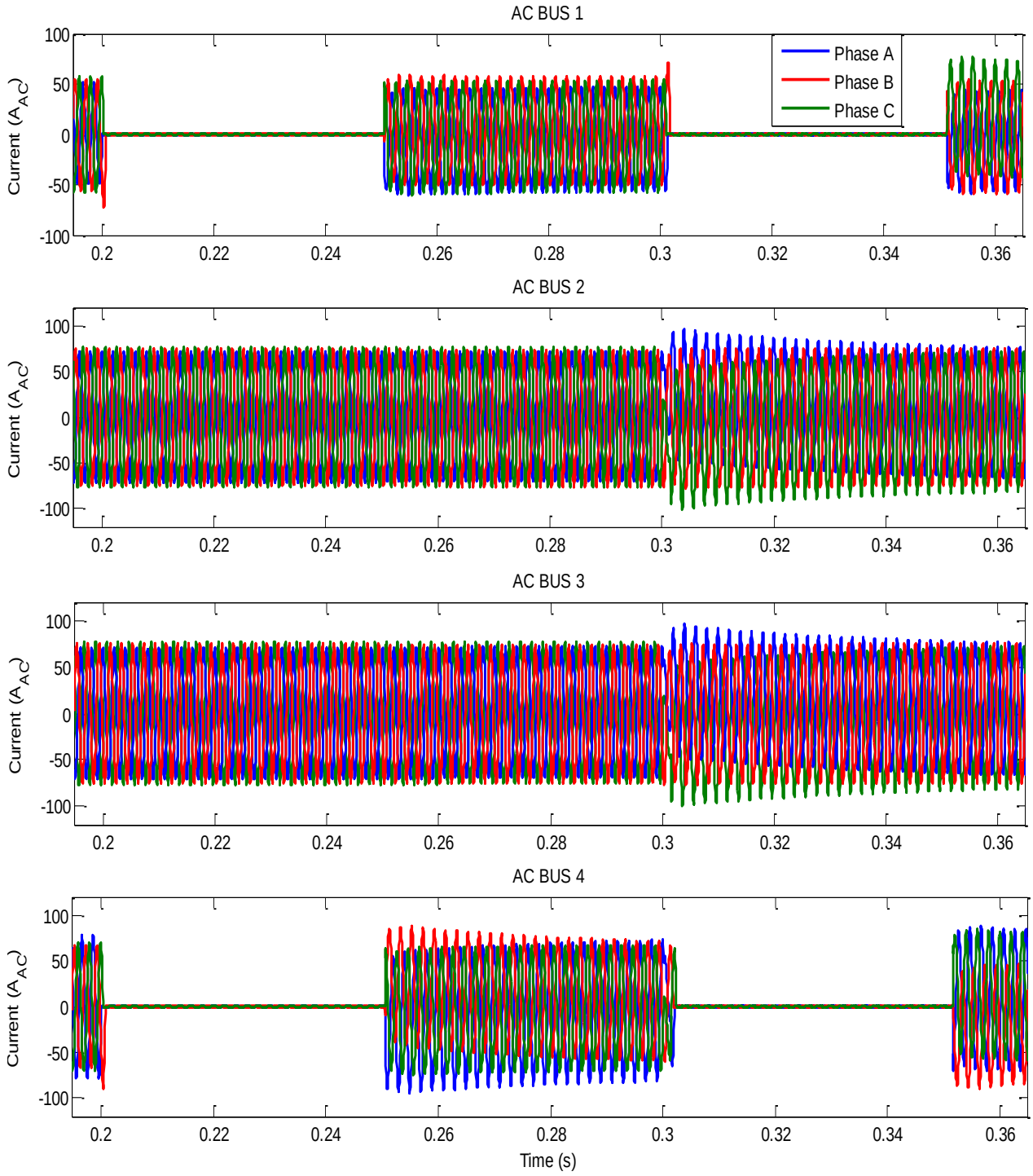

Figure 3.25. Current simulation results from VFG busses when VFG1 and VFG4 fail at 200 ms

Figure 3.26 shows AC busses during the time of VFG1 and VFG4 fail. It also shows how AC Bus 2 currents are affected when VFG3 stops to supply AC BUS 1 (at 300 ms), so that phase A and phase C suffer a power quality event due to the uncontrolled closing. It is important to reduce

this issue since a scenario of fault clearing and unsuccessful reclose due to the switching transient, may cause system swing from a VFG to another. In addition, the study of is type of event can be useful when designing the VFG's protective equipment.

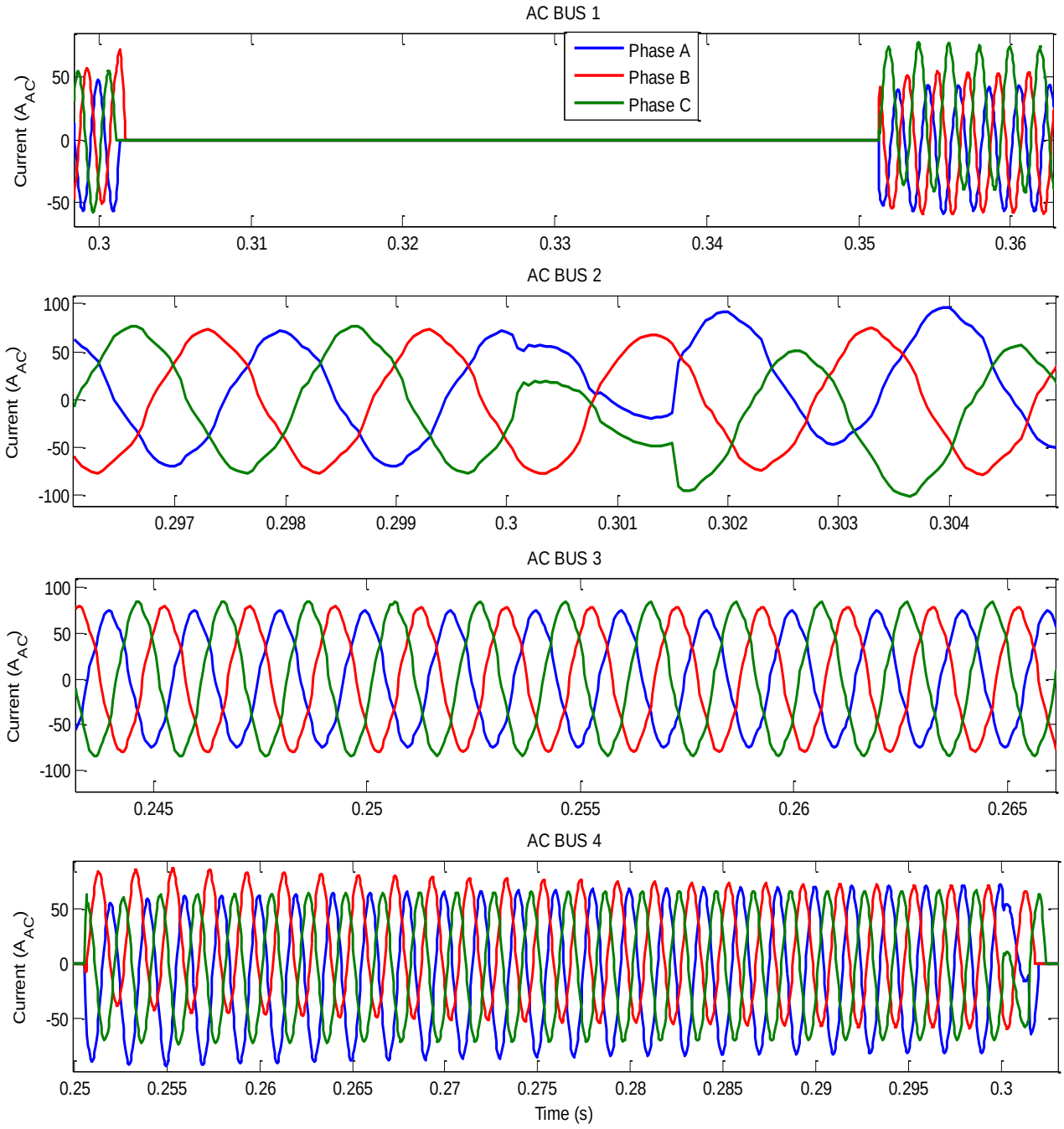

Figure 3.26. Zoom in to the current simulation results from VFG busses

Figure 3.27 shows the DC ESS Bus and the BATT Bus achieve a constant near 28 VDC voltage. In addition, SSPCs switch within 2 ms, so that the DC ESS Bus and the BATT BUS

voltage do not drop down to zero when VFG1 and VFG4 fail respectively. During the 50 ms delay, the DC ESS Bus reaches 25,85 VDC, while the BATT Bus reaches 25.08 VDC.

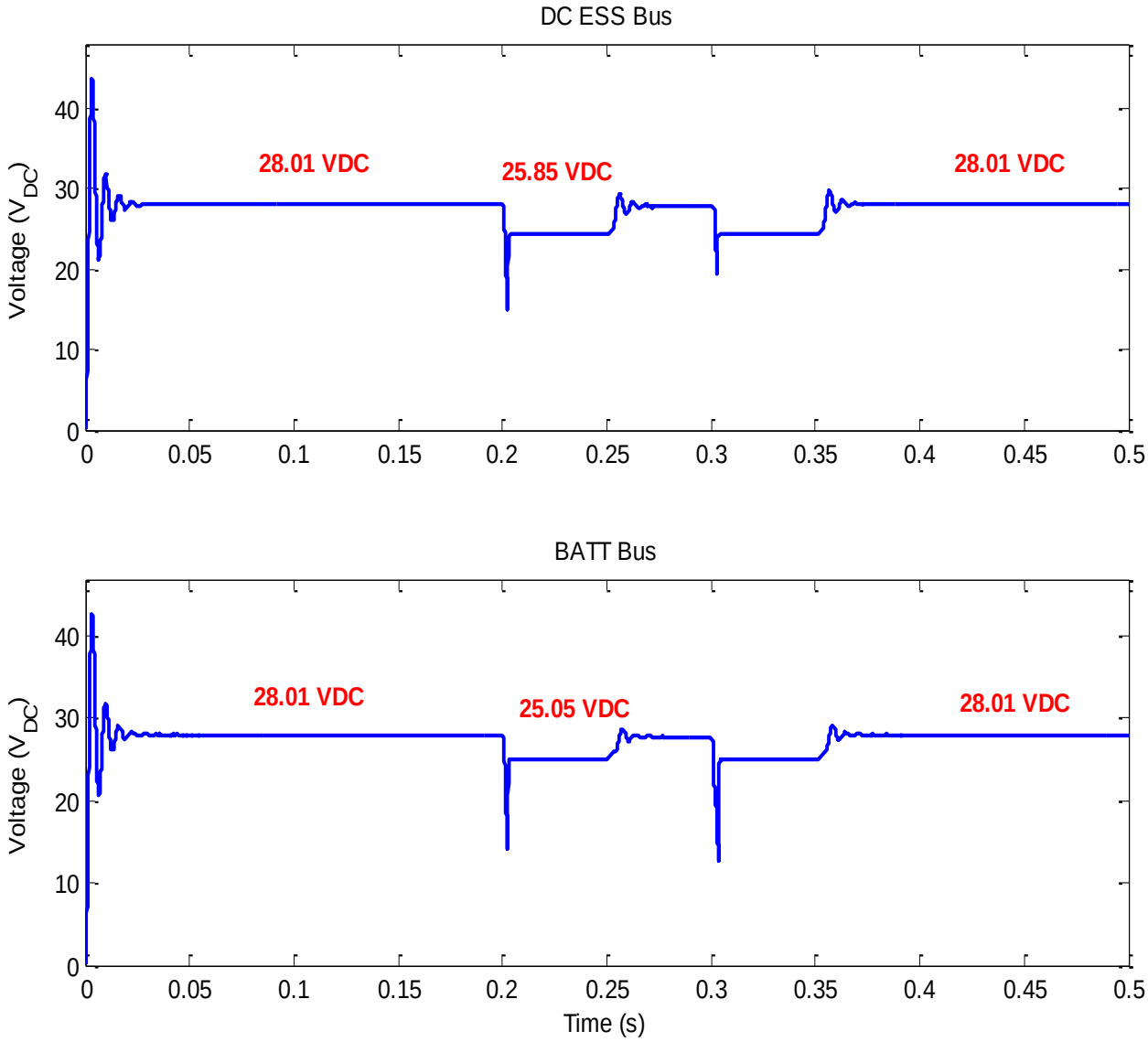

Figure 3.27. DC voltage simulation results when VFG1 and VFG4 fails at 200 ms

3.9 Case Study 3: VFG1 phase A, VFG4 phase B and phase C fail at 200 ms while VFG4 phase A, VFG1 phase B and phase C remind connected

In this case the phase A of the VFG4 switch reminds connected while VFG4 fails at 200 ms. In addition, the phase B and phase C of the VFG1 switch remind connected while VFG1 fails at the same time than VFG4. The idea of this case study is to simulate a possible problem while a switch does not operate properly.

Figure 3.28 zooms the period when the fault occurs. Since two phases of the VFG4 are OFF, ACSC sends a fault signal to the ACPC in order to command VFG1 to supply AC BUS 4. Therefore, AC Bus 1 shows an overcurrent when failure occurs. In addition, a transient in AC BUS 4 is observed at 250 ms when ACPC tries to restore the power supply.

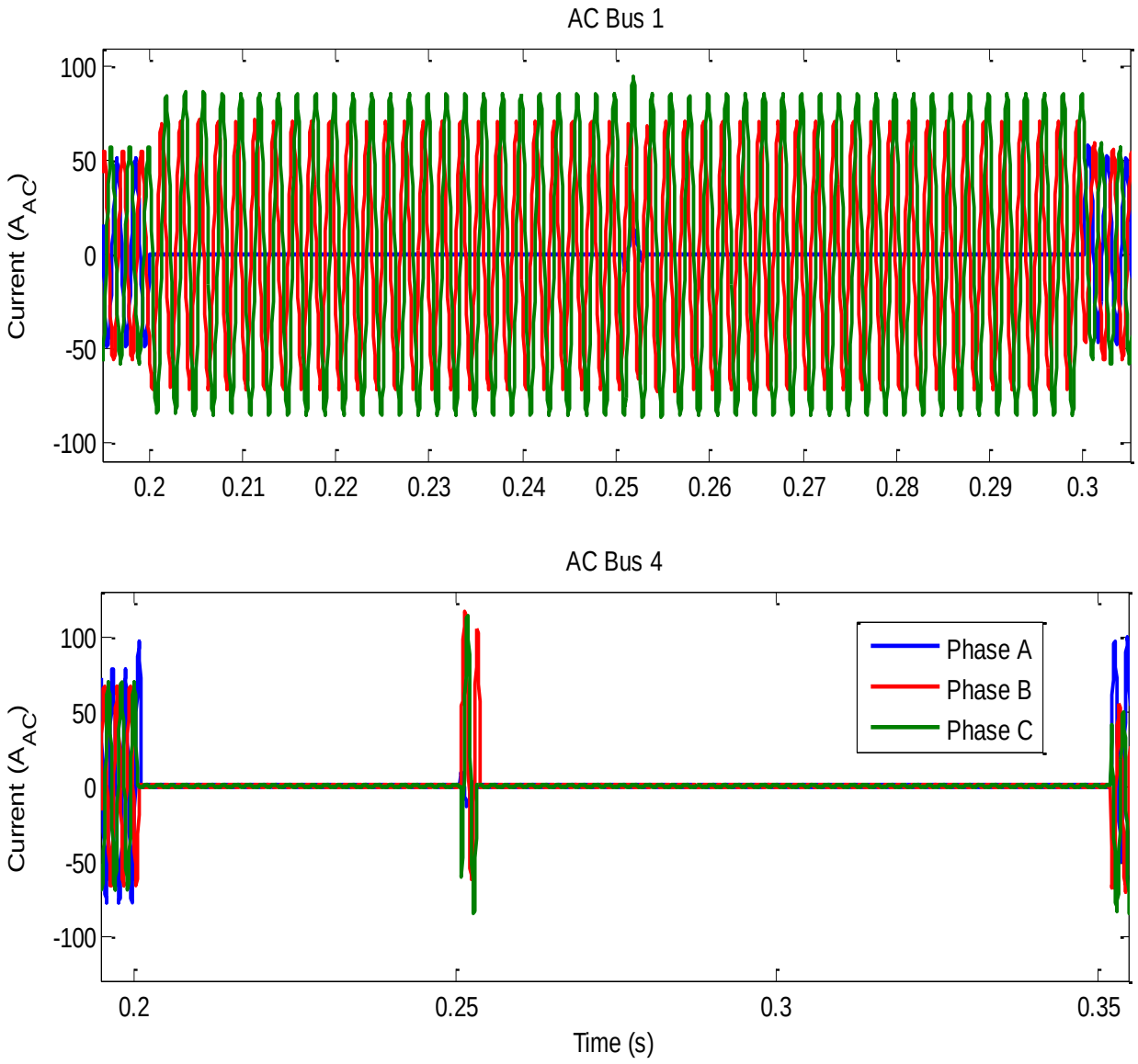

Figure 3.28. Zoom in to the current simulation results from VFG busses in case study 3

Regarding the DC busses, DC ESS Bus shows a 7.7% voltage drop during failure, since there is an overcurrent in AC Bus 1. In this case, SSPC does not work during failure since DCSCC does not see any fault signal because there is only one phase OFF.

On the other hand, DC BATT Bus does work on battery back-up during failure, since two phases are OFF and DCSCC interprets it as a failure. Both DC voltages reach steady-state values before and after transients.

Figure 3.29 shows the DC voltages from DC ESS Bus and BATT Bus under the conditions stated above.

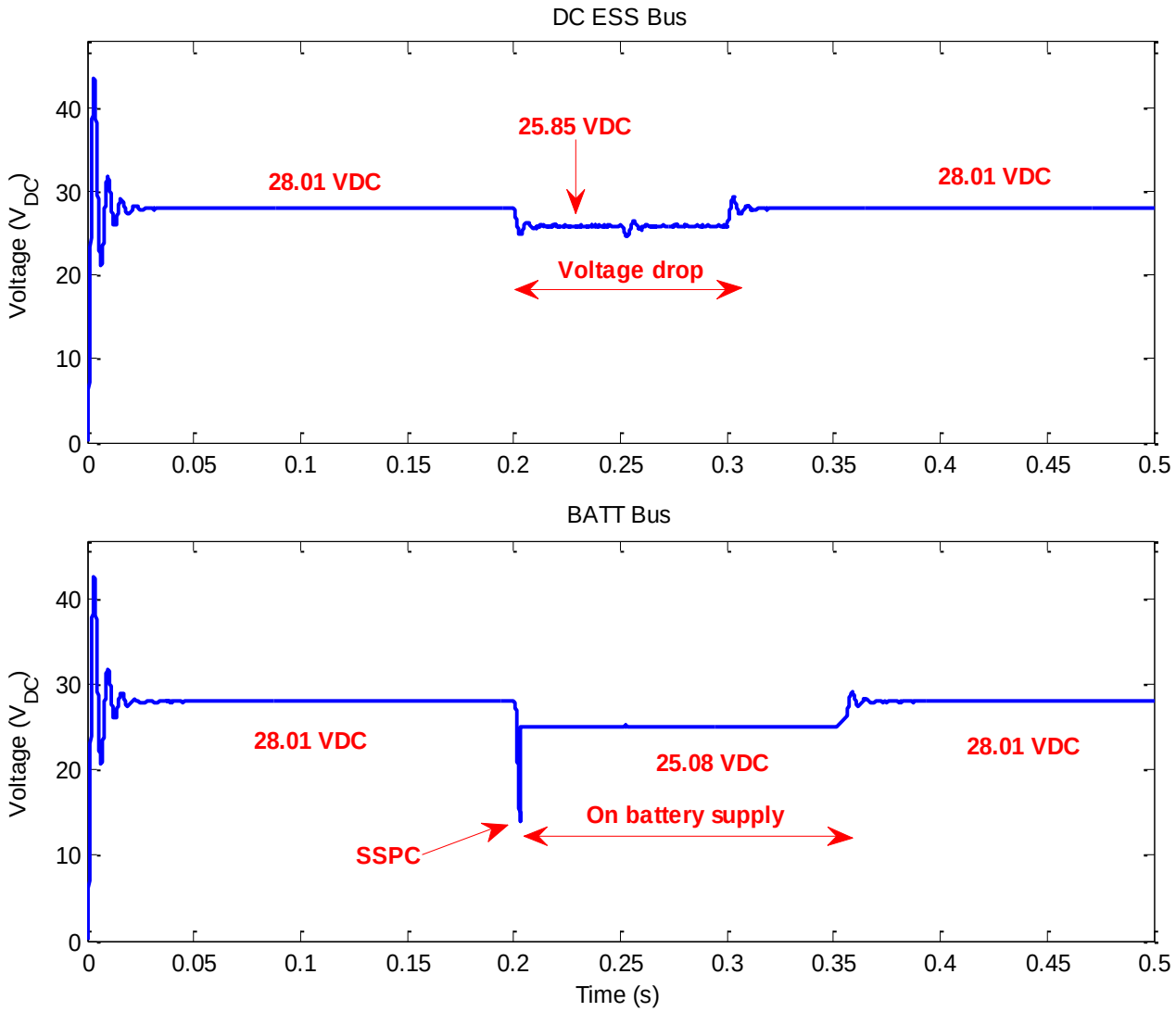

Figure 3.29. DC voltages simulation results when a malfunction occurs while switching

CHAPITRE 4 GLOBAL EXPRESS AIRCRAFT ELECTRIC POWER SYSTEM IN A REAL-TIME ENVIRONMENT

The goal of this chapter is to test the Simulink model of the Global Express aircraft presented in the previous sections in the real-time environment of the Opal-RT real-time simulator [15].

The objective is to explain how the electric power system is regrouped into subsystems for real-time execution and to study various constraints and limitations discovered during the real-time conversion. In addition, the selection of time step, results and analysis as well as potential practical application are also developed.

4.1 Real-time Simulation Fundamentals

In a real-time system, the time-step is a predetermined parameter, for example $\Delta t = 10\ \mu s$ or $50\ \mu s$. Inside this time-step, the processor has to read input signals, such as sensors, to perform all necessary calculations, such as control algorithms, and to write all outputs, such as control actuators. For that reason, one of the most important issues in real-time simulations is how to define a time step. Decreasing the time step increases the accuracy of the results while increasing the time required for simulating the system. A simple rule is to use 10 samples for the highest frequency period of simulated system transients. This frequency is the highest frequency content in the simulated waveforms.

Due to the fact that digital simulations are performed, a simulation with discrete-time and constant step is assumed. During discrete-time simulation, time moves forward in steps of equal duration, which is commonly known as fixed time-step simulation. It is worth noticing that other solving techniques exist that use variable time-steps. Such techniques are used for solving high frequency dynamics and non-linear systems, but are unsuitable for real-time simulation [15].

As mentioned before, real-time digital simulation is based on discrete time-steps where the simulator solves model equations successively. Proper time-step duration must be determined to accurately represent system frequency response up to the fastest transient of interest. Simulation results can be validated when the simulator achieves real-time without overruns [15]. In addition, for each time-step, the simulator first read inputs and generates outputs, and then it solves model

equations, exchanges results with other simulation nodes. Finally, the simulator waits for the start of the next step.

A real-time model in Opal-RT can only run in Fixed-Step mode. The Fixed-Step size (fundamental sample time) must be chosen carefully regarding the needs of the simulation, the dynamics of the model and must take into account the software/hardware capabilities [27]. In addition, in a real-time system, when a predetermined time step is too short and could not have enough time to perform inputs, model calculations and outputs, there is an overrun. When an overrun occurs, one time-step will be omitted, so that the next computation will be performed at the next time step [27].

The main use of real-time simulators is for testing physical devices interfaced with a simulation model. It is possible, for example, to test actual physical control systems submitted to measurements and activating various switches in the real-time simulator network. Real-time simulation can be also used to identify model parameters through actual waveforms extracted physical external devices submitted to the network model solved in real-time mode.

Another important advantage for performing real-time simulations is the ability of lowering costs for testing a new device under real operational conditions. Real-time simulators allow testing in real-time a very large number of cases. This offers dramatic computational speed advantages.

4.2 From Simulink to Real-Time: Global Express Electric Power System Real-Time Modeling

In order to use a Simulink model in real-time with Opal-RT's software and hardware, some modeling concepts must be followed when building the application. One of the most important concepts in real-time simulation using Opal-RT is regrouping the model into subsystems, so that the real-time model can be computed on multiple cores for achieving real-time performance. Each top-level subsystem created by the user will be computed on one core, except the Console Subsystem (SC, in Opal-RT nomenclature).

In a Simulink model that is to be used with RT-LAB [27], no mathematical content can be found in the top-level of the model. Therefore, subsystems are needed. A prefix must be added to all the top-level subsystems, in order to allow RT-LAB to manage them. There are 3 types of

subsystems: the Master Subsystem (SM, in Opal-RT nomenclature), the Slave Subsystem (SS) and the Console Subsystem (SC). Figure 4.1 presents the Global Express aircraft electric power system regrouped in one SM and several SSs.

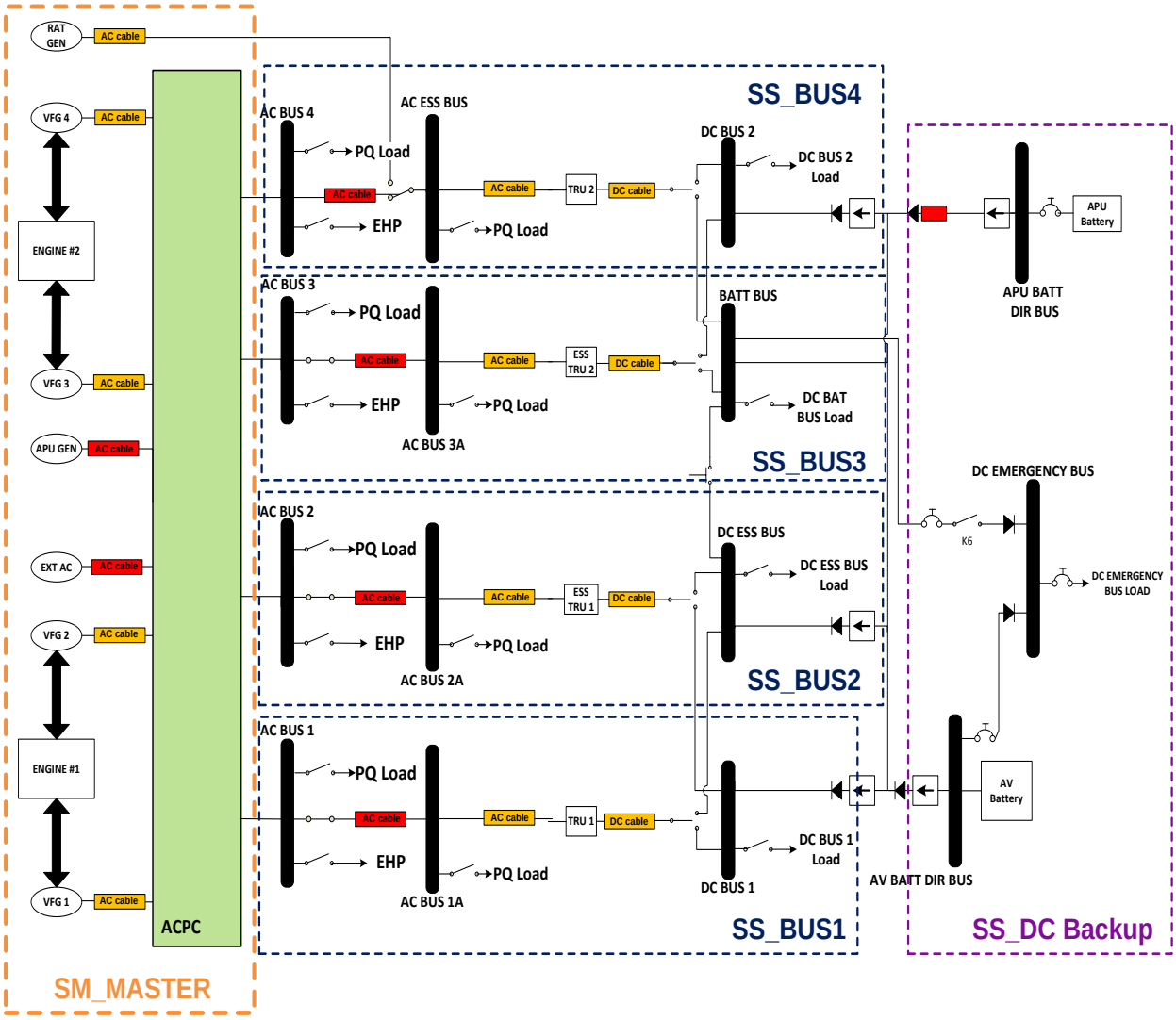

Figure 4.1. Separation of the Global Express electric power system for real-time environmental

Figure 4.2 shows the implementation of the model for real-time purposes. It takes into account the fact that the AC power system and its DC branches form a radial network, as the generators feeds independent circuits. This is the case in the real-time model. Each AC bus, its related load, its related TRU and DC load are regrouping in a single subsystem SS, in order to improve efficiency and achieve real-time. In addition, each subsystem is computed on a different computation node in the simulator hardware. No Goto/From tags are allowed between top-level

subsystems to exchange data, only “wires”. In terms of the DC backup, it is implemented as a separated subsystem in order to facilitate the manipulation of the model.

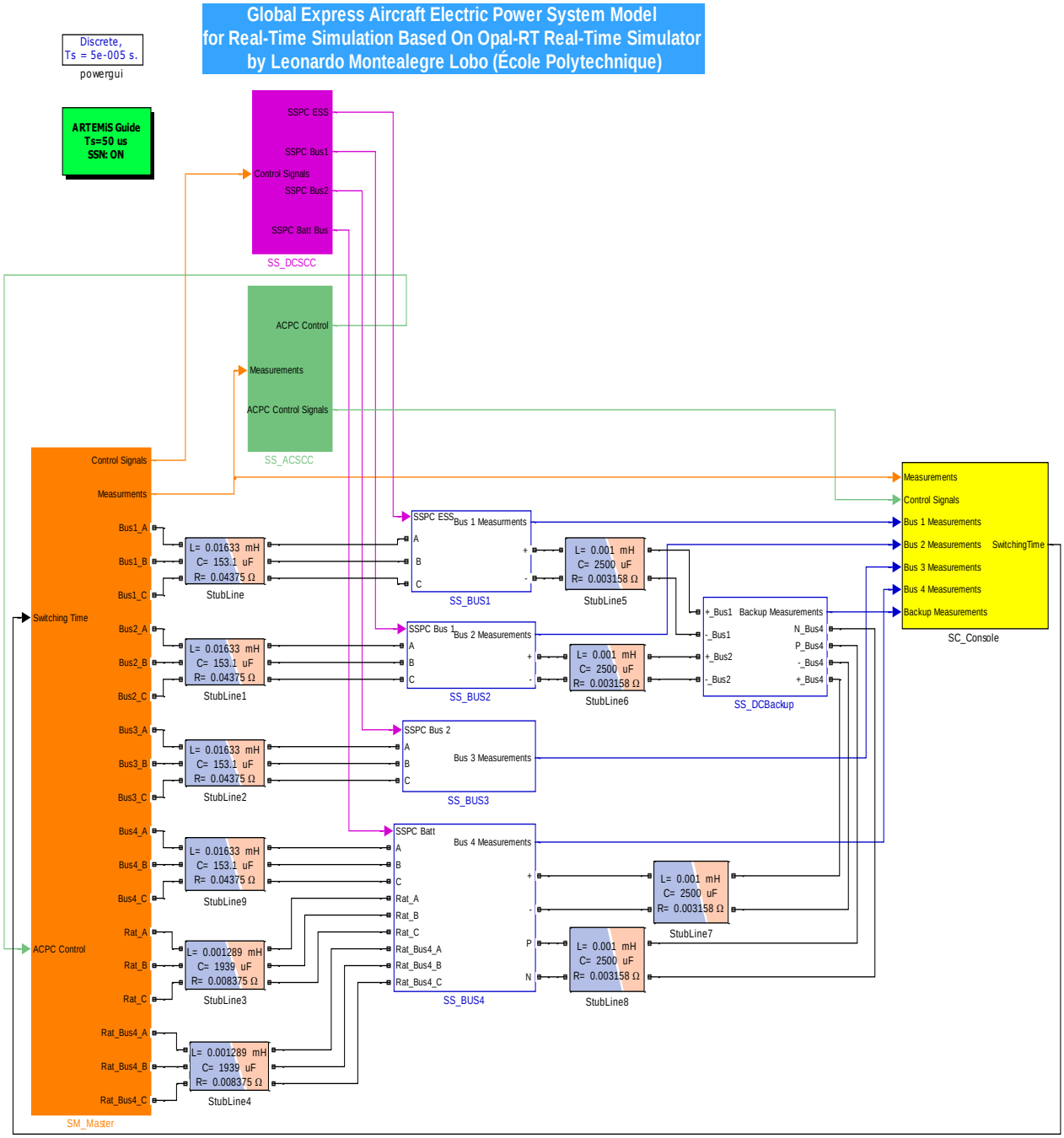

Figure 4.2. Global Express aircraft electric power system for real-time simulation

There is only one SM allowed in a real-time model. Inside this subsystem, all the computational elements of the model, the mathematical operations, the I/O blocks, the signal

generators must be placed. That is the reason for adding the VFG's, the APU GEN, the EXT GEN, the RAT GEN and the ACPC to the SM. Meanwhile, there is no limit on the number of SS. This subsystem is needed only if the computational elements must be distributed across multiple nodes. In order to improve real-time modeling accuracy and to achieve real-time performance, the Global Express aircraft electric power system is regrouping into seven SSs. Finally there is only one SC and it contains all user interface blocks (scopes, displays, switches, controls, etc.). This is the only subsystem that is available to the user during execution, so that the user can control some parameter of its model as well as observe the waveforms or data that is generated while executing. In other words, SC enables the user to interact with the system while it is running. The console runs asynchronously from the other subsystems. It is also the only subsystem that is not linked to a computation node (core) [27]. Therefore, there must be no signal generation or important mathematical operations included in this subsystem.

4.2.1 SM_Master Subsystem

Figure 4.3 shows all the elements of the SM. It includes the seven generators (four VFGs, APU GEN, EXT GEN and RAT GEN) of Global Express, thirty-six three-phase breakers (twenty-six three-phase breakers inside the ACPC and ten other three-phase breakers), seven stub lines and more than fifty signals going from SM to SC and SSs. The main aspects of the SM are listed next:

1. SC sends switching time control signals to each generator breaker, in order to simulate any fault or loss of operation.
2. SS_ACSCC subsystem sends to the ACPC, control signals for power system reconfiguration due to failure simulation as shown in Figure 4.2.
3. SM sends voltages and currents for all busses to SS_ACSCC in order to send binary signals to the external switching time control for the ACPC switches, and SC_Console for user manipulation.
4. SM sends control signals from ACPC to SS_DCSCC, which is responsible for sending binary signals to the external switching time control for the SSPC blocks, that commands the closure of the SSPC needed for supplying battery power to a specific DC bus (DC Backup subsystem).

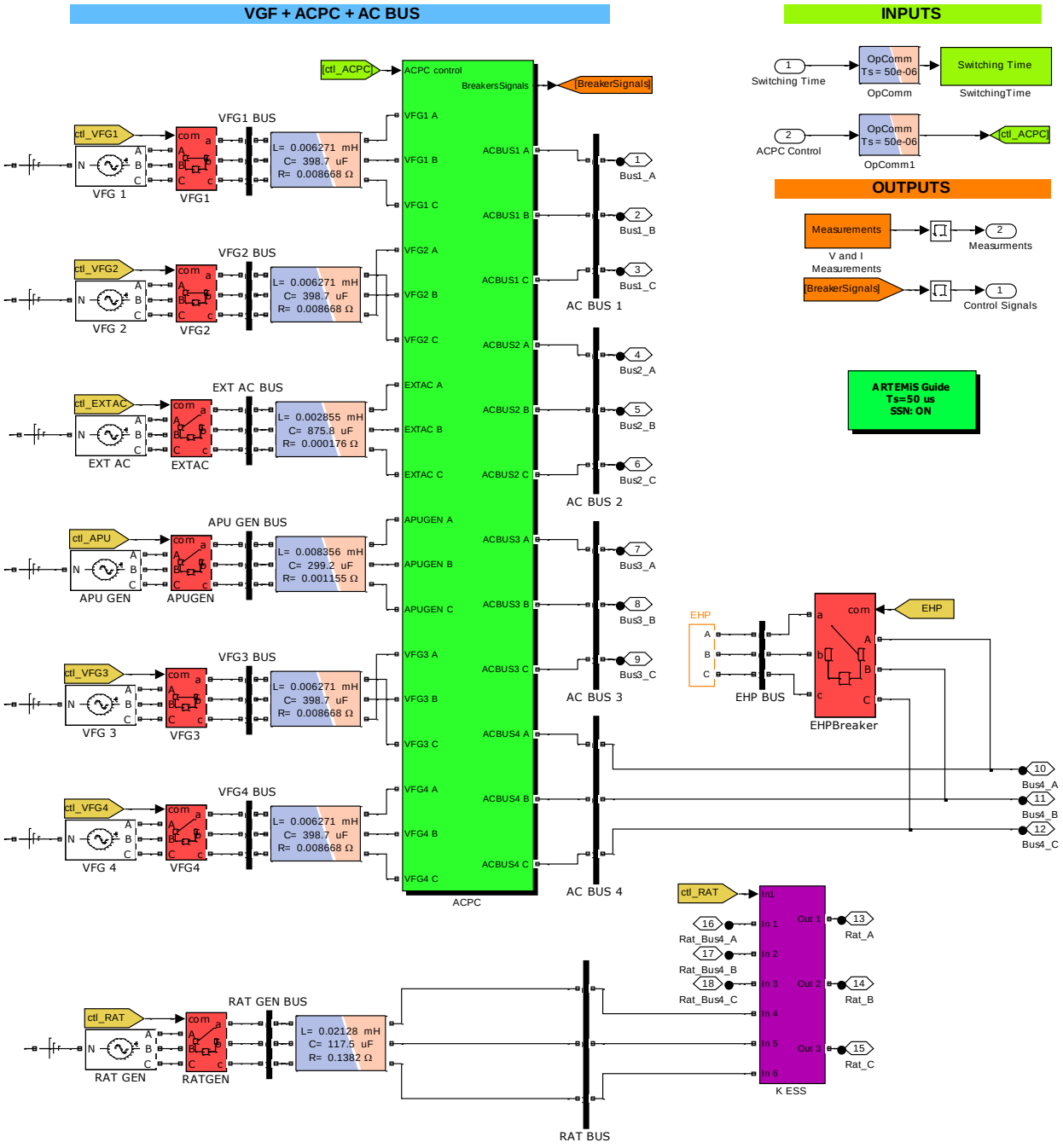

Figure 4.3. SM_Master subsystem model for real-time simulation

In terms of input signals, it is need to use the OpComm blocks. RT-LAB uses OpComm blocks to enable and save communication setup information. This includes both communication between the console and the computation nodes and the communication between the multiple computation nodes in a distributed simulation scenario. All subsystem inputs must first go

through an OpComm block before any operation associated with the input signals. In general, only one OpComm block must be used even if there are multiple inputs in one subsystem. However, there is a set of rules to be followed when placing the OpComm blocks [27].

- In the real-time subsystems (SM or SS): One OpComm receives real-time-synchronized signals from other real-time subsystems, and one OpComm receives asynchronous signals from the SC.
- In the console subsystem (SC): One or more OpComm blocks may be inserted to receive signals from the real-time subsystems. Multiple OpComm blocks define unique "acquisition groups" with their own data acquisition parameters.

Finally, Figure 4.4 summarizes what is stated above. There is one OpComm for the Switching Time signals at the SM_Master subsystem, receiving real-time asynchronous signals from the CS, while there is one OpComm for the ACPC switching control signals, receiving real-time synchronized signals from SS_ACSCC.

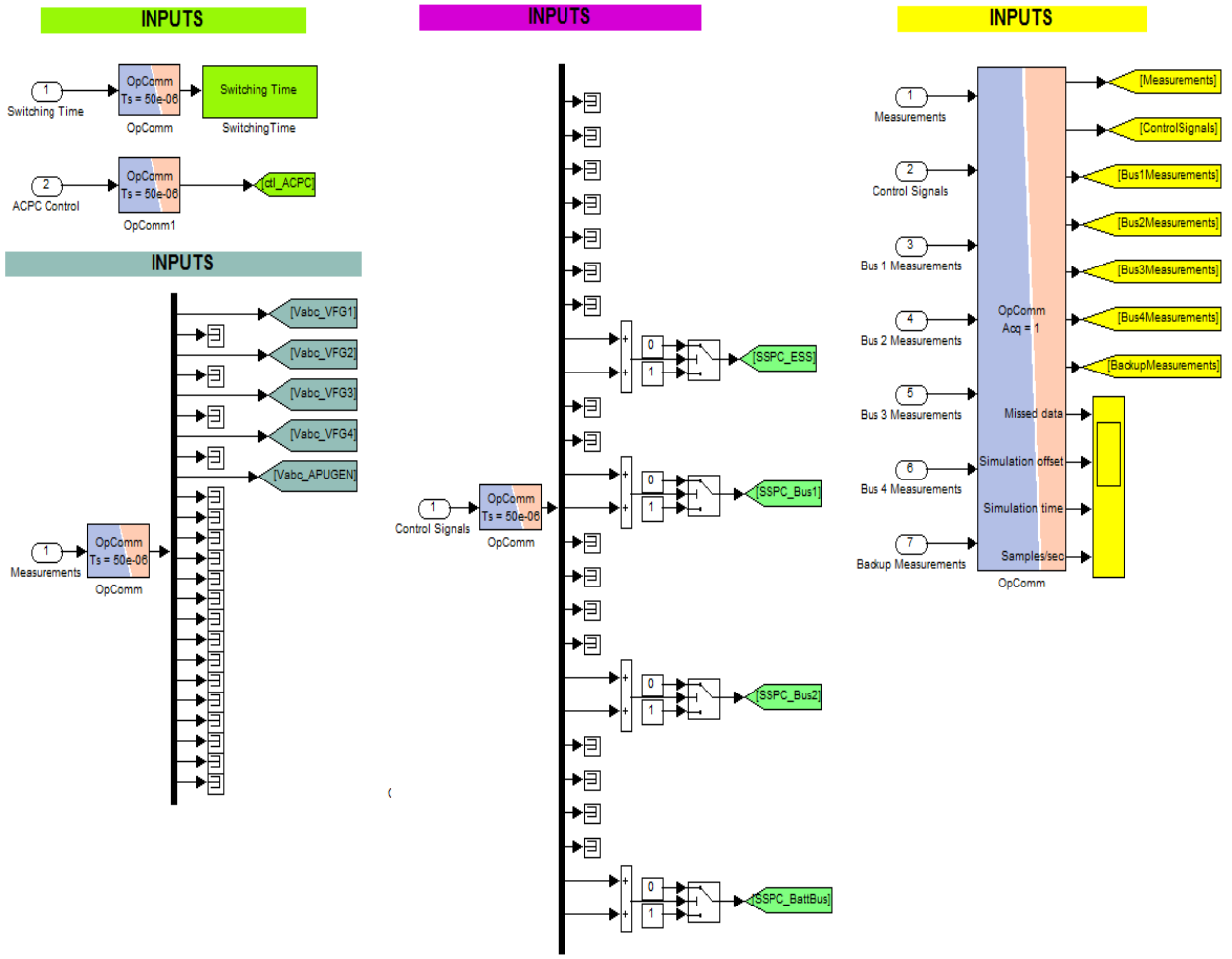

Figure 4.4. OpComm implementation according to subsystem type

On the other hand, RT-LAB maximizes parallelism when computation nodes exchange only priority signals. For this, real-time subsystems (SM and SS) must be computed and must send their outputs before they read their inputs (within the same time-step), so that the state must be identified in order to enable parallel subsystem computation [27]. Examples of blocks which introduce a state are the integrator and the memory blocks. For that reason, models are separated in order to exchange only priority signals between real-time subsystems, so that is why a memory blocks is added at every real-time subsystem's outputs. Careful placement of delay blocks can eliminate algebraic loops; however delay blocks must be handled with care because they can alter model dynamics. Figure 4.5 shows DC voltage measurements from the DC ESS Bus after a switching operation, before and after adding the memory blocks. The results are compared in order to make sure that the impact of the delay is acceptable, that is, the effect of adding the memory block should be negligible, as it is the case in Figure 4.5.

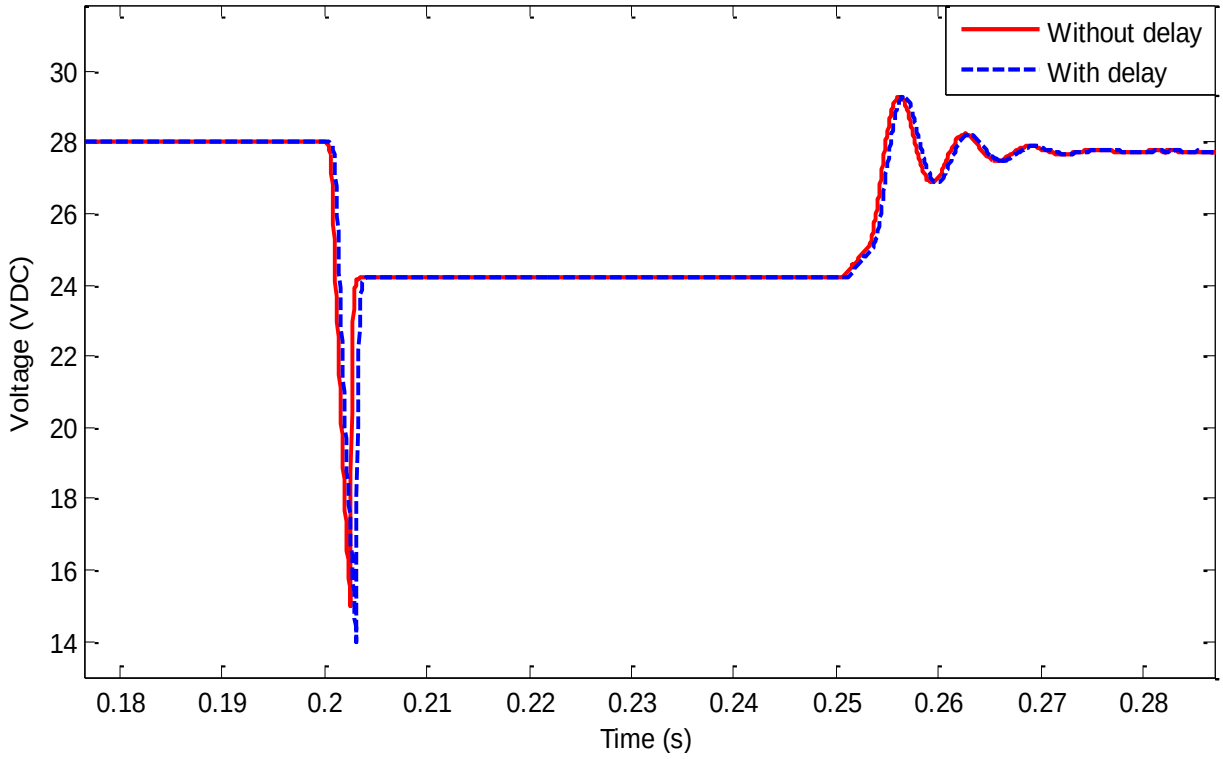

Figure 4.5. Effect of adding the memory blocks to real-time subsystem outputs

Another element important to consider is the addition of the stub lines, which are part of the ARTEMiS library [28]. ARTEMiS is a suite of fixed-step solvers and algorithms that optimize Simulink models of elecromechanical systems, created using the SimPowerSystems (SPS), for real-time execution[1].

The uses and benefits when using ARTEMiS are listed next [28]:

1. ARTEMiS takes advantage of the sparse matrix properties to optimize the computation time, so that in SPS and ARTEMiS, each independent sub-circuit has its own smaller set of ABCD state-space equations. This allows a faster iteration since SPS S-functions are not sparsely-optimized, so that the switches located on different sub-networks are pre-computed independently.
2. ARTEMiS can pre-compute circuit topologies and store them in memory. In other words, while SPS re-computes system matrix in the real-time loop each time a switch change

[1] Information consulted on September the 7th at www.opal-rt.com/node/288

conduction state (On/Off), ARTEMiS pre-computes all system matrix for all possibilities of switch conduction states before the beginning of the real-time loop. This allows performing a real-time simulation with no overruns during real-time execution.

3. ARTEMIS solvers have intrinsic immunity to numerical oscillations produced by inductive circuit opening. In addition, ARTEMiS solvers are designed to improve the accuracy of simulation of power system at large time steps.
4. ARTEMiS applies unique interpolation techniques, such as Inlined Thyristor Valve Compensation (ITVC), Inlined Voltage Inverter Compensation (IVIC) and Impulse Event Detection. In addition, ARTEMiS provides special tools to decouple a large/complex circuit, and enable parallel computation through PC clusters
5. ARTEMiS adapts a few blocks from the SPS library from real-time simulation, such as Switched Linear-Segment MOV, Transformers with Switched Saturable Core.

One of the powerful elements presented in the ARTEMiS Library are the ARTEMiS Lines. The ARTEMiS lines are the standard Bergeron line model with lumped losses[2]. An element of the ARTEMis lines is the so called Stubline, which is the same model as the ARTEMiS line except that the transmission delay is set exactly to 1 simulation step to permit subsystem decoupling [28]. In the ARTEMiS Distributed Parameter line, the user selects RLC, and then the model computes the transmission delay. In the stubline, the user selects RL and the transmission delay is set to the model time step, then the equivalent line capacitance is computed internally.

Moreover, the stublines implemented in the real-time model are used for artificial decoupling of power system equations. In general, the sizes of state-space matrices dramatically increase if the number of states, or if the number of inputs and outputs becomes larger. For large electric networks, either interconnected or in radial structure, there could be many inputs and outputs for each state space, as it is the case in the Global Express aircraft power system. In addition, for transient simulation of power systems, the number of circuit breakers required to create faults or

[2] The model is based on the Bergeron's travelling wave method used by the Electromagnetic Transient Program (EMTP), which is based on the paper called “Digital Computer Solution of Electromagnetic Transients in Single and Multiple Networks” by Herman W. Dommel (April, 1969).

load disturbances is also counted into the total number of states. This can cause that the memory may overflow with a large state-space matrix, which results in an error at compilation.

The best solution is to use a proper decoupling tool from the ARTEMiS Library [28] to decouple the model. The decoupled model has a few smaller state-space matrices instead of a single one, so that it is easier and faster to compute in real-time. There are many tools for decoupling presented in the ARTEMiS Library2. One of the tools is called ARTEMiS Lines [28]. When physical modelling signals are transmitted between two subsystems at the root level of the model (SM and SS or SS and SS), ARTEMiS Lines are used to link the physical modelling connectors at the root level of the block diagram [28]. No connection between ARTEMiS Lines is allowed at the root level, though the connection can be done by route the line connector into the subsystems and connected inside the subsystems. If the lines are not long enough for decoupling the stub lines can be used to simulate the resistance and inductance, while it decouples the state-space equation of the networks at both sides of the line. Basically, a stub line is a N-phase (1-6) distributed parameter line model with one time-step propagation delay [28]. Since the inductance and resistance can be specified by either absolute values or per-unit value, the stub lines implemented in this model, takes into account the resistance and inductance values calculated from the AC Cable and DC Cable model block from the off-line model. Extra capacitance value is added automatically based on the equation [28], were Ts is the fundamental sample period.

$$T_s = 2 \cdot \pi \cdot \sqrt{L \cdot C} \tag{4.1}$$

The capacitance value resulting from (4.1) must be carefully observed, since it depends of the time step and the cable inductance, so that if the inductance is too small, the capacitance is too high. This can create stability issues while simulating in real-time. That is why the system dynamic responses must be compared before and after using the ARTEMiS Stub lines to make sure its impact is acceptable.

Returning to the number of three-phase breakers and the implications that can be presented while simulating in real-time, a State-Space Nodal method (SSN) [29] appears to be the perfect solution for that constraint. The rule of thumb is to have around 5 three-phase breakers per subsystem, but in the case of the SM, this number goes up to 30, so that SSN method is the most

practical way to eliminate one of the principal constraints discovered during this research, while converting the off-line model to real-time.

Basically, the SSN method is a solver that uses arbitrary size state-space equations to create clusters of electrical elements and combines them into the nodal admittance matrix using a nodal method [29]. The discrete state-space solvers are inefficient for handling switching events, especially in real-time applications, where pre-calculation methods must be used. The massive pre-calculation of state-space matrix sets for all switch combinations becomes problematic in terms of required memory for large numbers of coupled switches [29]. While extending the state-space solver, the real-time simulation can support a very large number of switching devices, including Simulink three-phase breakers, giving the opportunity to manage the large number of breakers presented in the SM.

Moreover, SSN enables the coupling of complex nodal-based models, such as frequency-dependent lines into a state-space solver and can be used to split a large model on multiple CPUs that does not contain long transmission lines without artificial delays [29].

A description of the SSN algorithm is listed next. From the step 1 to the step 4, SSN performs a state-space analysis formulation while from the step 5 to 8, a nodal analysis is executed. There is a loop inside the algorithm, once he arrives to the step 8, he returns to the step 2 and he continues with the next steps.

1. Pre-calculation of discrete state-space matrices and admittance for all switch permutations in each group and initial conditions of states.
2. Update switch position in each group.
3. Select discrete state-space matrix for the switch positions in each group.
4. Compute group nodal injection from past states and known sources.
5. Build global injection vector and global admittance matrix.
6. Solve the nodal equation YV=I.
7. Update state equation of each block from the nodal solution.
8. Output Solutions.

In fact, SSN provides several advantages over the state-space method. The reduction of the size and complexity in the automatic generation of state-space equations for each group is achieved by the clustering approach. In addition, the groups can be solved in parallel and the number of pre-calculated matrix sets for switching topologies can become substantially reduced [29].

Figure 4.6 shows how the SSN blocks are implemented inside the ACPC in the Global Express real-time model. They are used between the SM and each SS_Bus#. The SSN Interface blocks are chosen at a node that decouples the state-space groups of the model, so that instead of having up to 30 three-phase breakers in a subsystem, SSN creates a small group of 6 three-phase breakers.

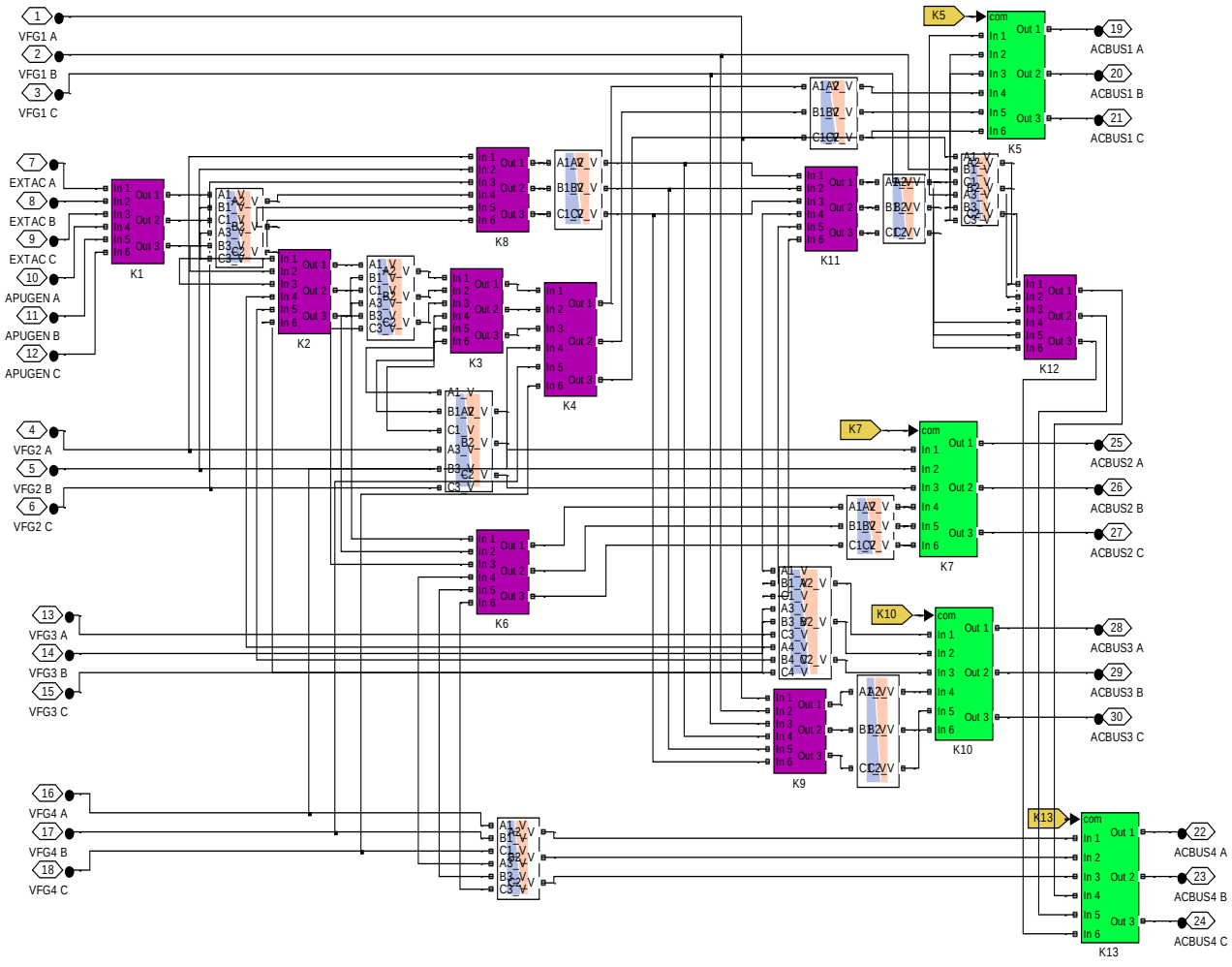

Figure 4.6. SSN Interface blocks implementation in Global Express electric power system real-time model

4.2.2 SS_ACSCC Subsystem

Figure 4.7 shows all the elements of the SS_ACSCC subsystem. It includes the main AC switching control, responsible for sending binary signals to the external switching time control for the ACPC switches, in order to change ON/OFF state positions.

In addition, it includes the secondary AC switching control, which detects when two or more VFG fails and then sends binary signals to the external switching time control for the ACPC switches (K2, K3, K4, K6, K8, K9, K11, K12), according to VFG's failure. Furthermore, it receives voltage measurements from the generator busses VFG 1, VFG 2, VFG 3, VFG 4 and APU GEN. On the other hand, the SS_ACSCC subsystem sends ACPC control signals to the SC_Console for user observation (scopes) and manipulation, and then closes the loop, sending ACPC control signals to the SM for ACPC reconfiguration based on truth tables representing Global Express reconfiguration logic (see Chapter 2 on section 2.2.2). The switch states vary depending on a game of events regarding loss of VFGs and TRUs, so that the AC system architecture alternates to provide electrical power to every bus.

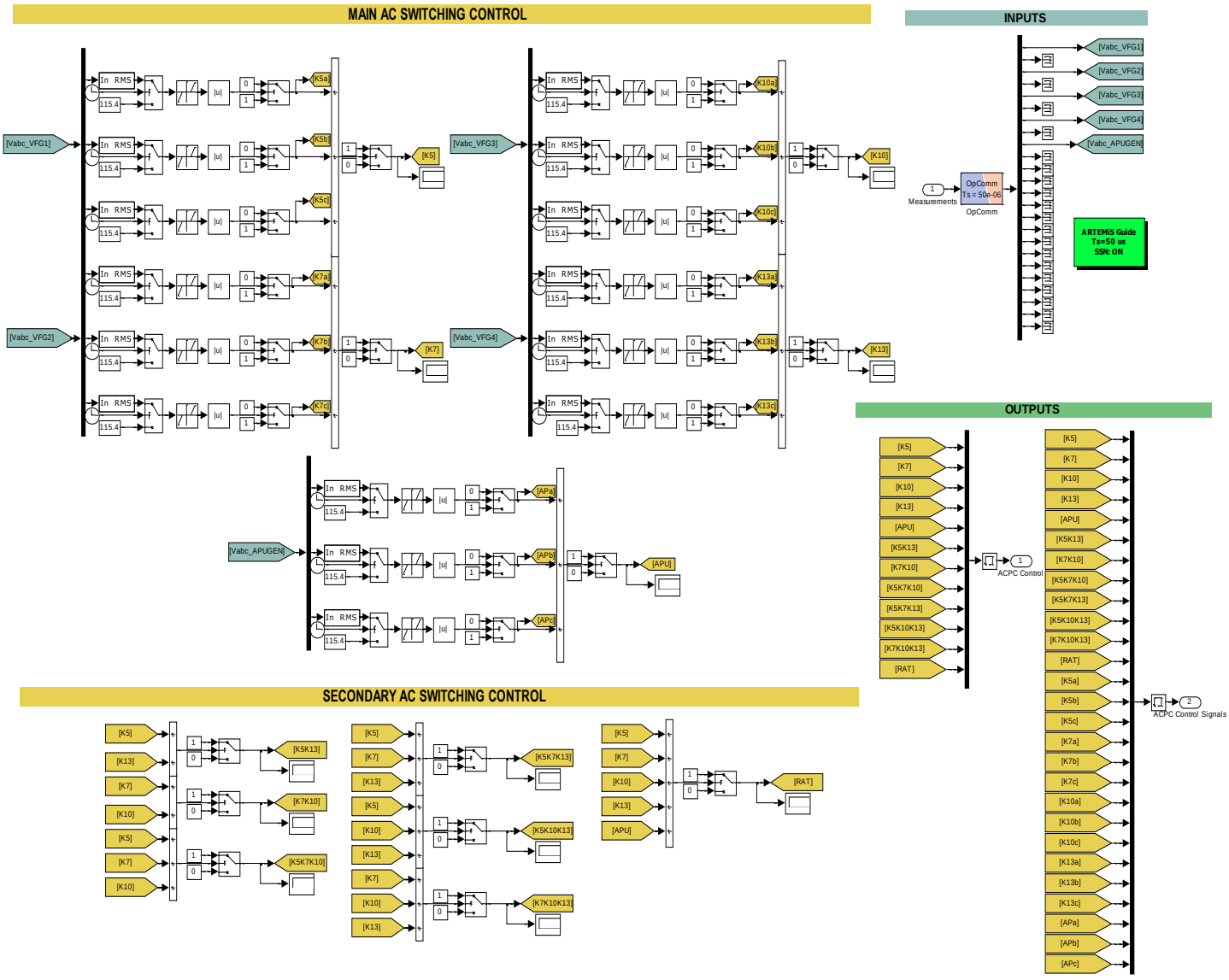

Figure 4.7. SS_ACSCC subsystem model for real-time simulation

4.2.3 SS_DCSCC Subsystem

Figure 4.8 shows all the elements of the SS_DCSCC subsystem. It includes the DC switching control, responsible for sending binary signals to the external switching time control for the SSPC blocks (SS_DCBackup), in order to provide DC voltage in cause of a failure. It receives external switching time control of every three-phase breaker located at the ACPC, and sends control signals to SS_Bus1, SS_Bus2, SSS_Bus3 and SS_Bus4 for SSPC actuation. Hence, the DCSCC commands the closure of the SSPC needed for supplying battery power to a specific bus.

Once AC system reconfiguration is over, SSPCs switch off and disconnect the battery from the bus.

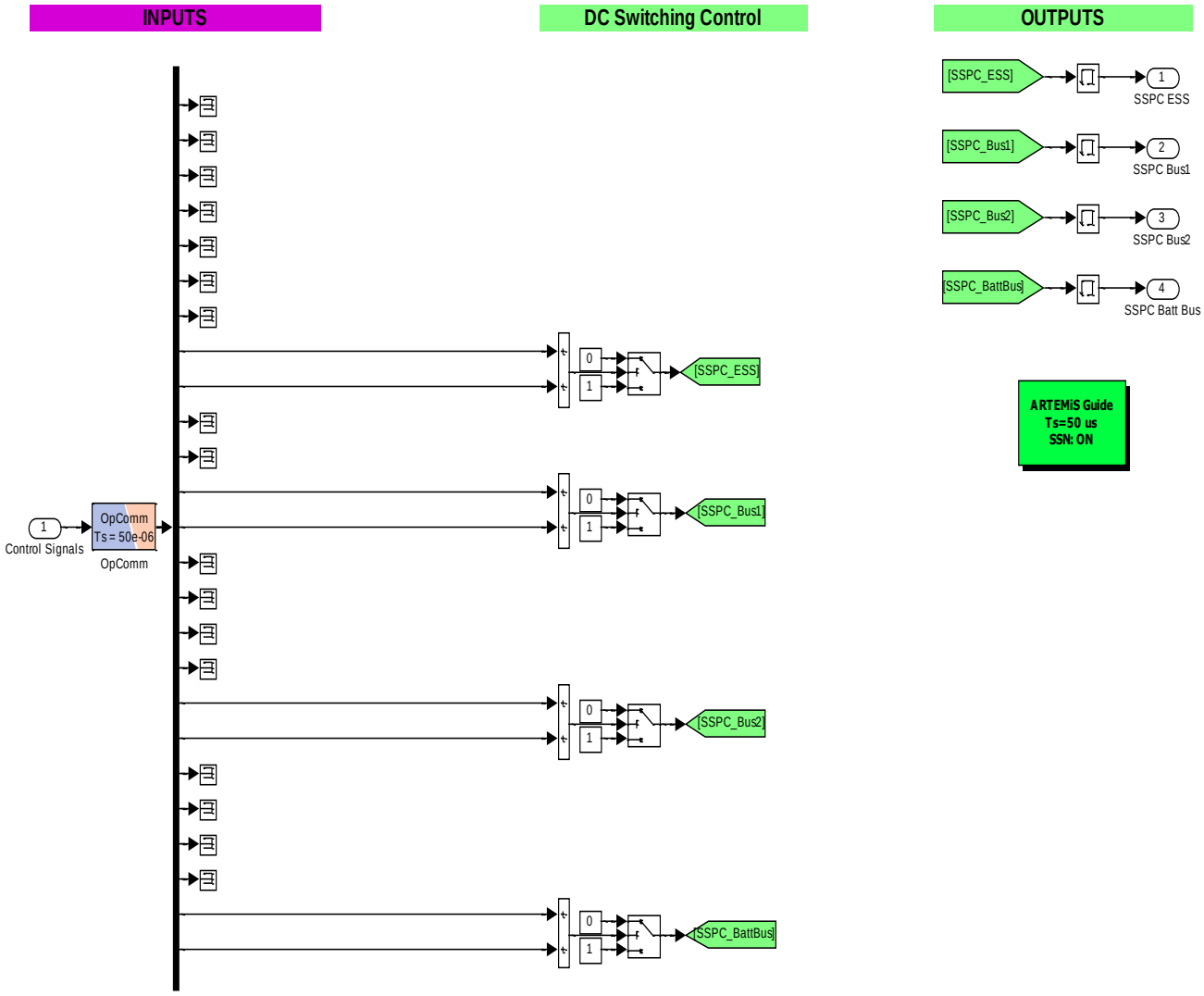

Figure 4.8. SS_DCSCC subsystem model for real-time simulation

4.2.4 SS_BUS1 Subsystem

Figure 4.9 shows all the elements of the SS_BUS1 subsystem. It includes the AC and DC load blocks, as well as the TRU block for AC/DC conversion. It is worth noting that the models mentioned above, are not modified from their off-line versions. Moreover, it presents a stub line linking SM, SSN Interface block and the DC part of the SS_BUS1. It receives SS_DCSCC switching control signals for SSPC actuation. The DCSCC commands the closure of the SSPC needed for supplying battery power to a specific bus when a failure is occurring. It sends to the

SC_Console, voltage and current measurements for every AC and DC bus presented in the subsystem. Finally, it is connected to the SS_Backup for DC reconfiguration when needed.

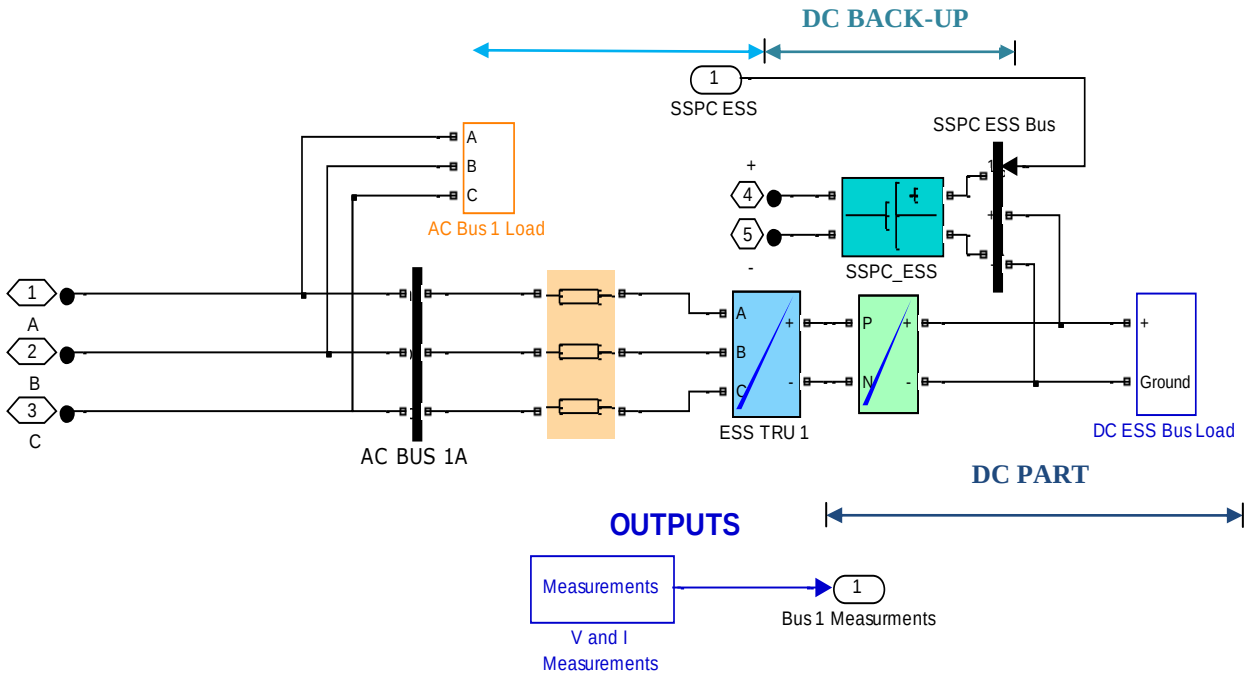

Figure 4.9. SS_BUS1 subsystem model for real-time simulation

4.2.5 SS_BUS2 Subsystem

Figure 4.10 shows all the elements of the SS_BUS2 subsystem. It includes the AC and DC load blocks, as well as the TRU block for AC/DC conversion. Again as in 4.2.4, the models are not adjusted from their off-line versions. A stub line, for network decoupling, links the SM, SSN Interface block and the DC part of the SS_BUS2. It receives from SS_DCSCC, the switching control signals needed for SSPC actuation. Hence, DCSCC commands the closure of the SSPC in order to supply battery power to a specific bus when a failure occurs. It sends to the SC_Console, voltage and current measurements for every AC and DC bus presented in the subsystem. Finally, it is connected to the SS_Backup for DC reconfiguration when needed.

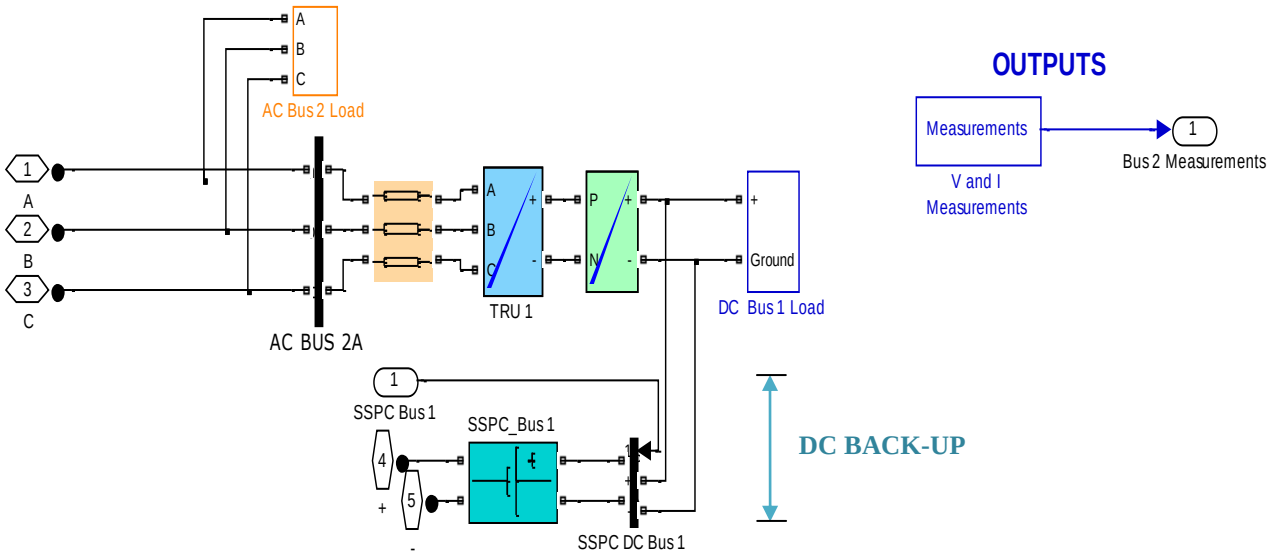

Figure 4.10. SS_BUS2 subsystem model for real-time simulation

4.2.6 SS_BUS3 Subsystem

Figure 4.11 shows all the elements of the SS_BUS3 subsystem. It includes the AC and DC load blocks, as well as the TRU block for AC/DC conversion. Again, the models are not adjusted from their off-line versions. A stub line, for network decoupling, links the SM, SSN Interface block and the DC part of the SS_BUS2. It receives from SS_DCSCC, the switching control signals needed for SSPC actuation. The DCSCC commands the closure of the SSPC in order to supply battery power from APU Battery, to a specific bus when a failure occurs, so that SS_BUS3 is not connected to the SS_Backup, because it requires a special back-up supply provided by the APU Battery. Finally, it sends to the SC_Console, voltage and current measurements for every AC and DC bus presented in the subsystem.

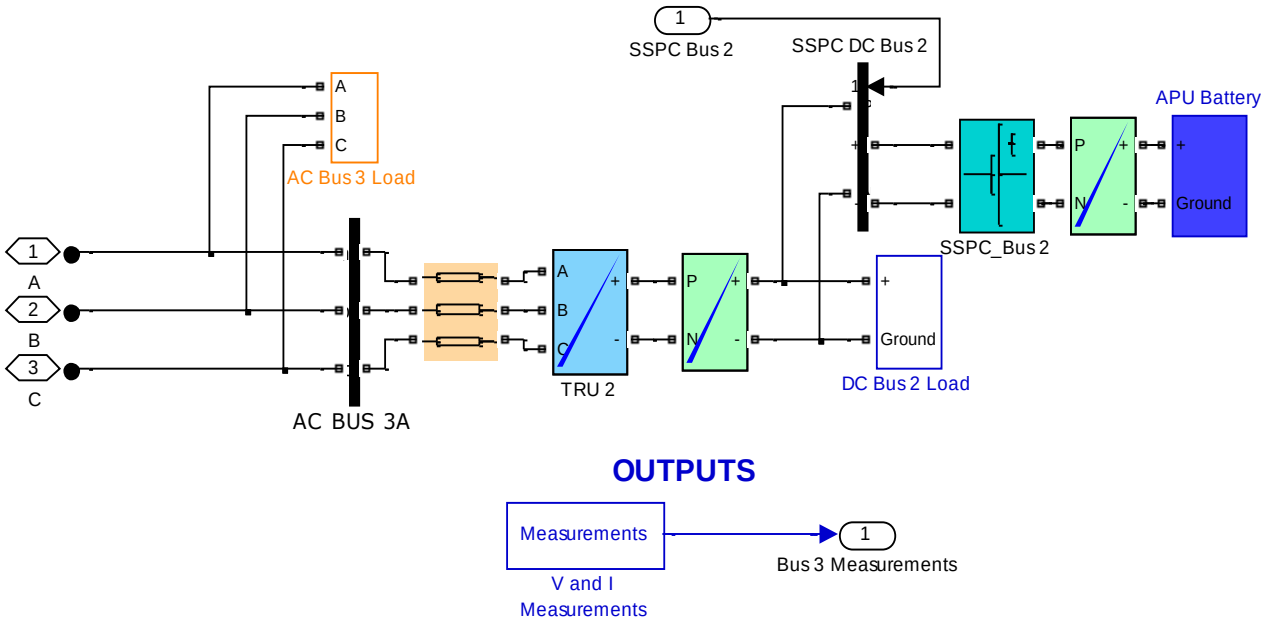

Figure 4.11. SS_BUS3 subsystem model for real-time simulation

4.2.7 SS_BUS4 Subsystem

Figure 4.12 shows all the elements of the SS_BUS4 subsystem. It includes the AC and DC load blocks, as well as the TRU block for AC/DC conversion. A stub line used for network decoupling, links the SM, SSN Interface block and the DC part of the SS_BUS2. It is worth noting, that some AC loads as well as the DC part of the subsystem, present double AC back-up, so that one or more supplies are available (AC ESS BUS receives energy fromVFG4 and RAT GEN. In the event of an emergency, RAT GEN is provided for Essential Bus (AC ESS BUS) feed. The generator outputs are supplied to the AC Power Centre (ACPC), which in turn distributes the power to the aircraft subsystems. SS_BUS4 receives from SS_DCSCC, the switching control signals needed for SSPC actuation. The DCSCC commands the closure of the SSPC in order to supply battery power to a specific bus when a failure occurs. It sends to the SC_Console, voltage and current measurements for every AC and DC bus presented in the subsystem. Finally, it is connected to the SS_Backup for DC reconfiguration when needed.

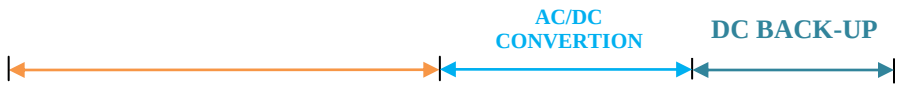

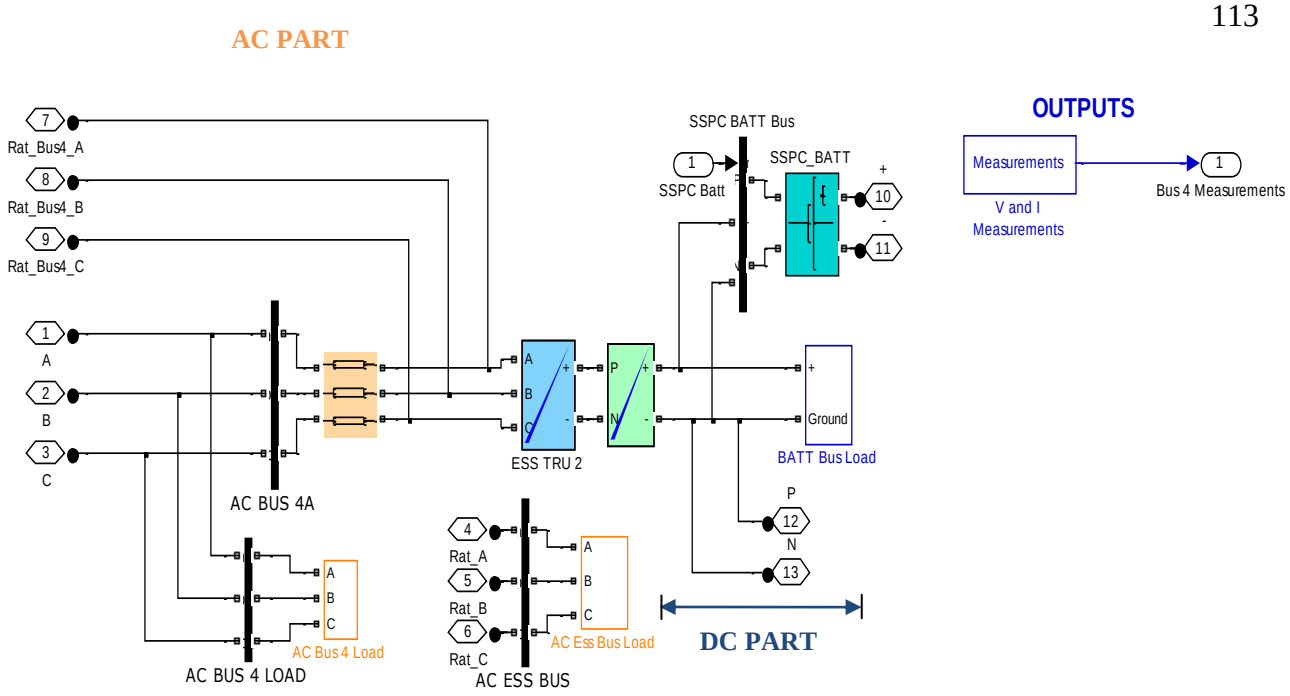

Figure 4.12. SS_BUS4 subsystem model for real-time simulation

4.2.8 SS_DCBackup Subsystem

Figure 4.13 shows all the elements of the SS_DCBackup subsystem. It includes the DC Emergency Bus which is supplied by the Battery Bus and the Avionics Battery Bus, powering the DC Emergency Bus when no TRUs are on-line and supplies the DCPC BATT Bus when the Battery Master switch is selected ON with no TRUs on-line. In addition, the Avionics Battery and the APU Battery are always supplying power to their direct buses as long as their feed receptacles are connected to the battery.

Stub lines link the SSs, SSN Interface block with SS_DCBackup. The goal of the block is to supply energy to critical DC busses when a failure occurs. It sends to the SC_Console, voltage and current measurements for every AC and DC bus presented in the subsystem. Finally, it is connected to the SS_Bus1, SS_Bus2 and SS_Bus4 for DC reconfiguration when needed.

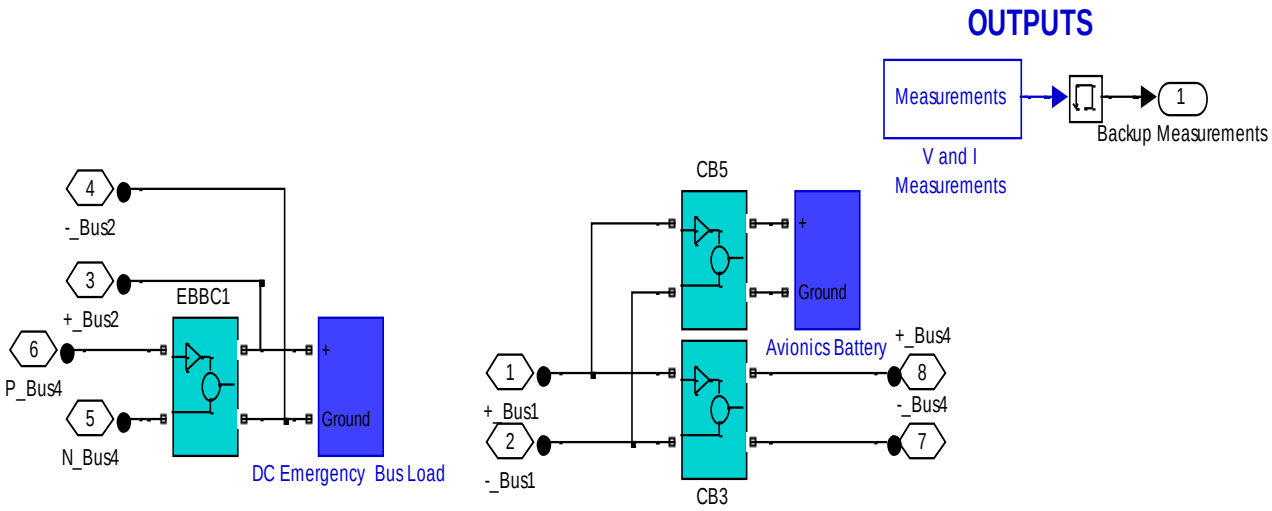

Figure 4.13. SS_DCBackup subsystem model for real-time simulation

4.2.9 SS_Console Subsystem

Figure 4.14 presents the elements of the SC subsystem. It includes the AC voltage and current measurements from all VFG busses, SS_BUS1, SS_BUS2, SS_BUS3 and SS_BUS4, for user's manipulation while real-time execution. In addition, it includes all the switching control signals from SS_ACSCC and SS_DCSCC. The signals mentioned above arrive to one OpComm block, so that only one acquisition group is set.

In addition SC sends switching time control signals to each generator breaker in the SM subsystem, by using the Control Signal Generator, in order to simulate any fault or loss of operation. It generates an OFF/ON switching external control signal changing at specified times. If a signal value is not specified at time zero, the output is kept at 0 until the first specified transition time.

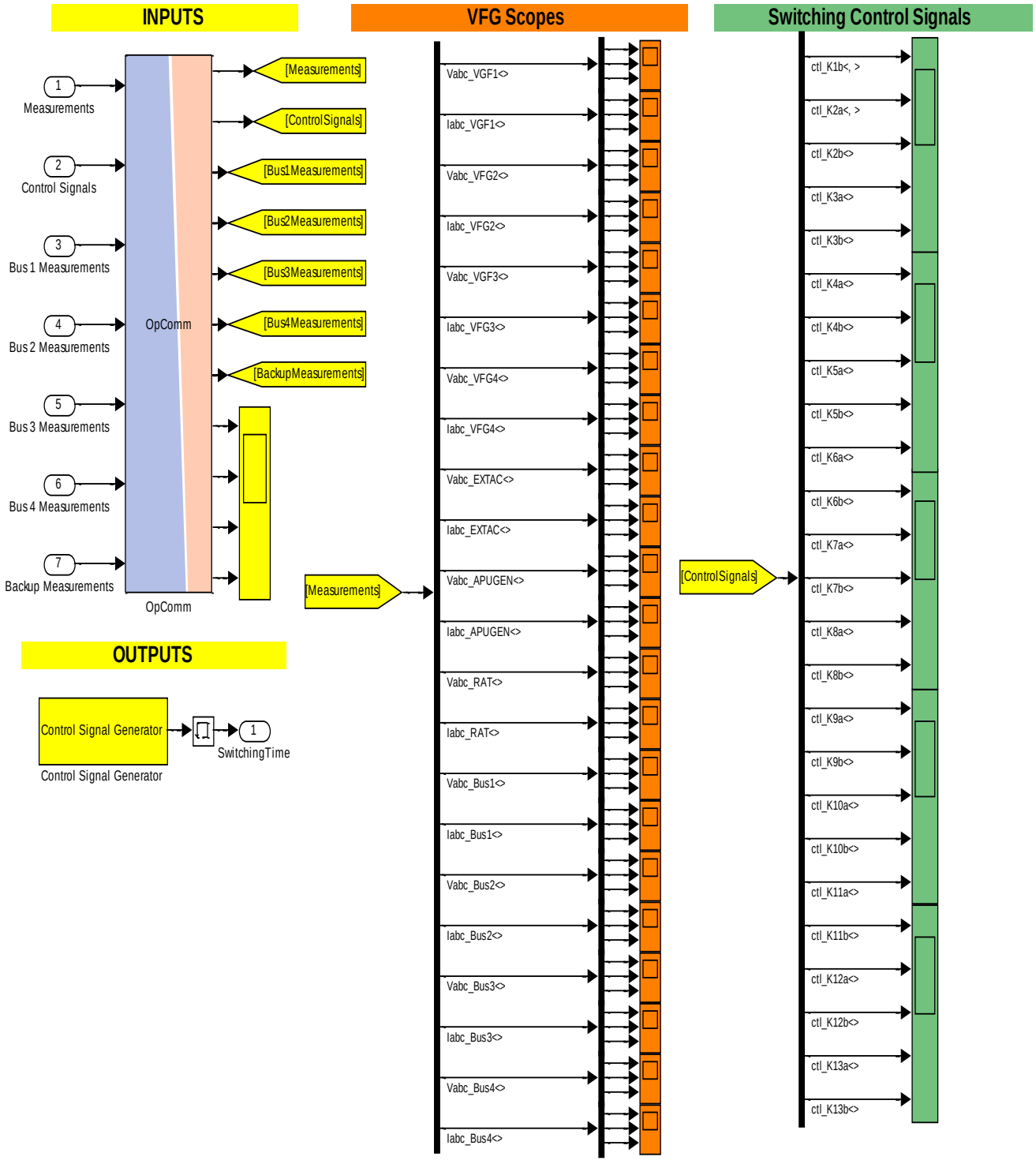

Figure 4.14. SC_Console subsystem model for real-time simulation (first part)

Figure 4.15 presents the rest of elements of the SC subsystem. It includes the DC voltage and current measurements from SS_BUS1, SS_BUS2, SS_BUS3, SS_BUS4 and SS_DCBackup for user's manipulation while real-time execution.

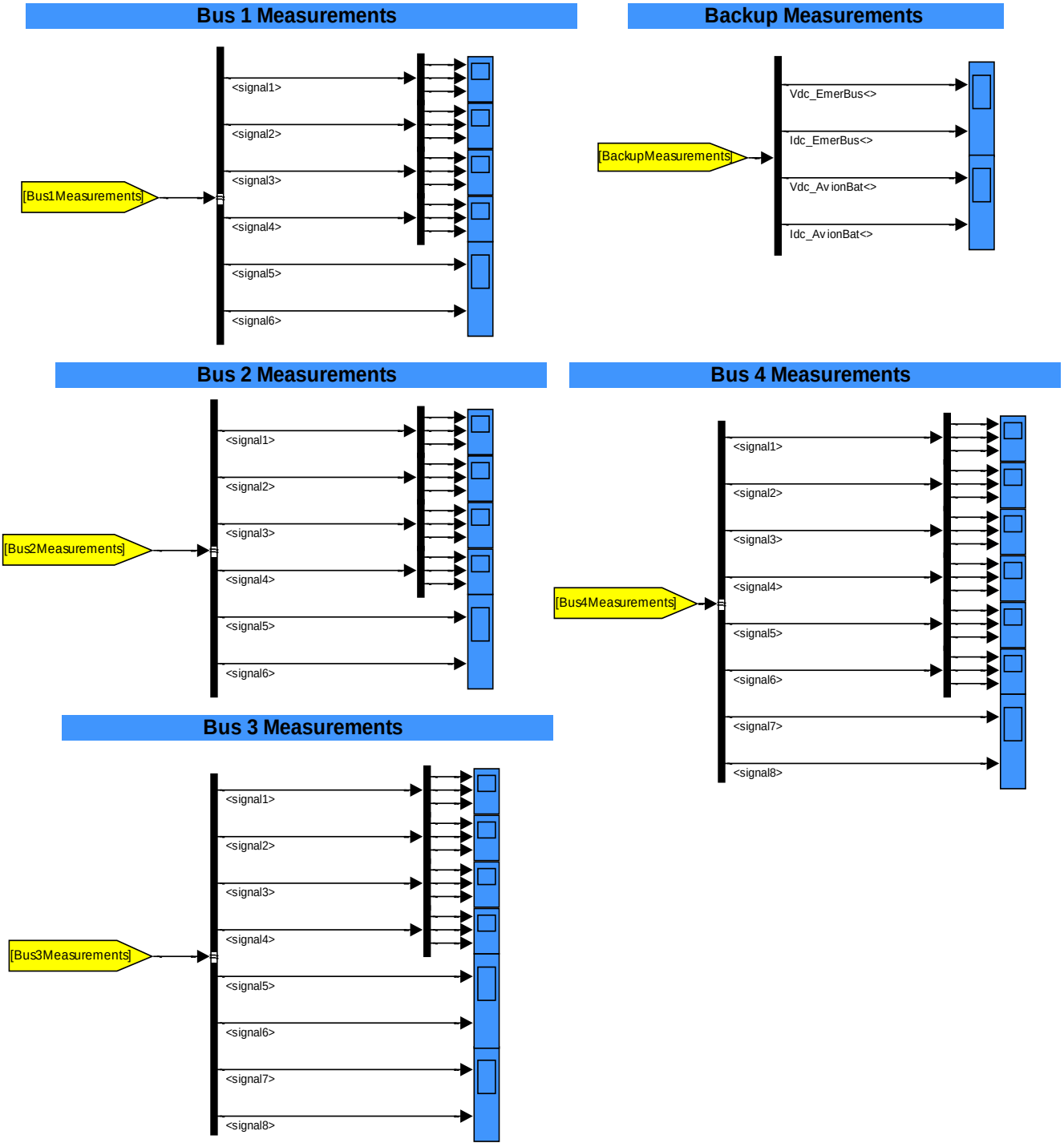

Figure 4.15. SC_Console subsystem model for real-time simulation (second part)

Figure 4.16 shows the implementation of the Control Signals Generation for real-time simulation.

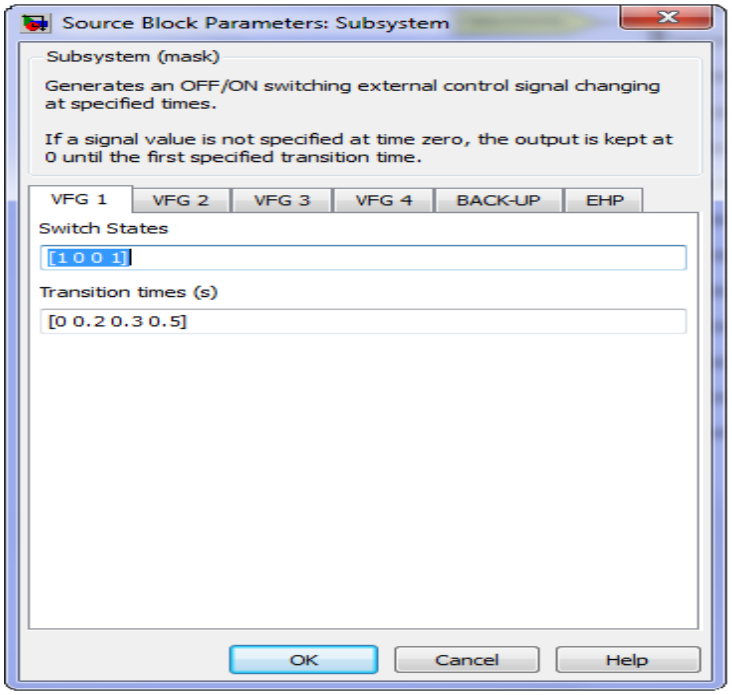

Figure 4.16. Switching Signal Generator subsystem model for real-time simulation

4.3 Testing the Real-Time Model

One of the first aspects is to study the simulation error as a function of the increasing time-step during a real-time simulation.

In this case, VFG1 fails at 200 ms of simulation, so that ACPC reconfigures itself to transfer energy from VFG4 to AC BUS1 as indicated in [18]. After 100 ms, VFG1 returns in operate and ACPC restores the power supply between VFG1 and AC BUS1, as AC BUS1 power supply is no longer provided by VFG4. This causes VFG4 to supply more current during VFG's failure (100 ms) and SSPCs to operate. In addition, there is a 50 ms delay between switching operation caused by the commutation times of protective devices found on the aircraft, so that VFG4 supplies energy to AC BUS1 at 250 ms, and VFG1 restores power supply at 350 ms. This can be observed in Figure 4.17 a). It also shows how DC ESS Bus voltage behaves during these events for different time steps. It is worth noting that the behaviour of the model shown in Figure 4.17 when the time step is higher than 1 µs is very unstable and the voltage value is higher than 28 VDC. This can be related to the high equivalent line impedance from the stubline model, since the

transmission delay is set to the model time step and the cable's reactance affects the transient behaviour of the model.

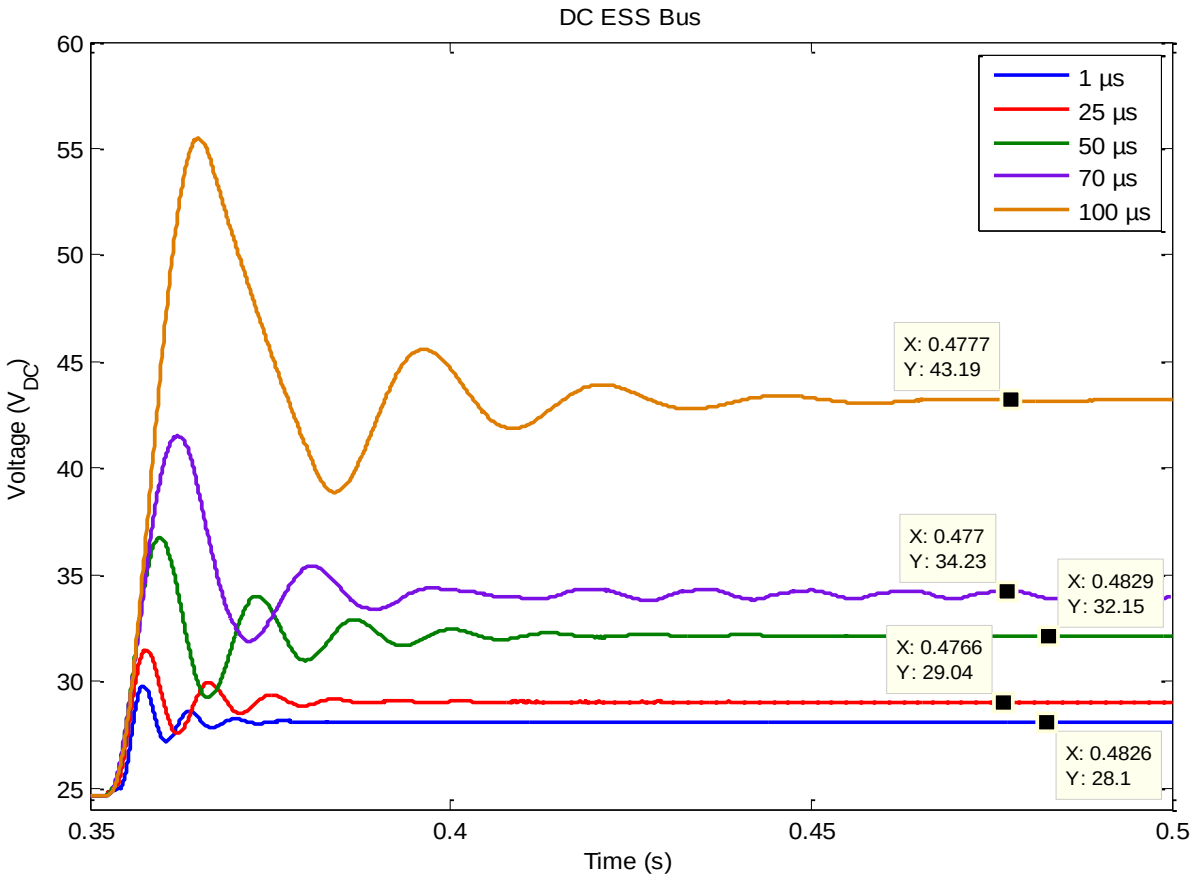

Figure 4.17. DC ESS Bus voltage for different time steps using stublines

Meanwhile, Figure 4.18 shows the same behaviour than in Figure 4.17. The difference is the addition of the SSN blocks causing a little ripple in DC voltages. However, these values are within the limits established in [26]. There are important differences between Figure 4.17 and Figure 4.18, which are listed as follow:

1. In Figure 4.18, all waveforms present similar behaviour for 1 µs, 25 µs, 50 µs and 70 µs. For 100 µs, the voltage reaches out of the lower limit established in [26]. Meanwhile, in Figure 4.17 the waveforms for 1 µs and 25 µs present similar and stable behaviour while the waveforms for 50 µs, 70 µs and 100 µs present an inacceptable behaviour.
2. The voltage spike in Figure 4.17 is up to 55 VDC while in Figure 4.18 the addition of the SSN blocks allows to have a voltage spike less of 30 VDC in all the waveforms.

3. In Figure 4.18, all waveforms present a little ripple after the transient, which is more evident once the time step is increased. This ripple can be observed until the end of the simulation. Meanwhile, Figure 4.17 does not present the same type of ripple and even for 1 µs and 25 µs the ripple is no longer observed 25 after the transient. However, more tests are needed in order to relate this ripple to the addition of the SSN blocks.

4. In Figure 4.17 only the voltage when the time step is set to 1 µs is within the established in [26], while in Figure 4.18 only the voltage when the time step is 100 µs is without the limits in [26]. The rise of the DC voltage in Figure 4.17 can be related to the capacitance values of the stublines.

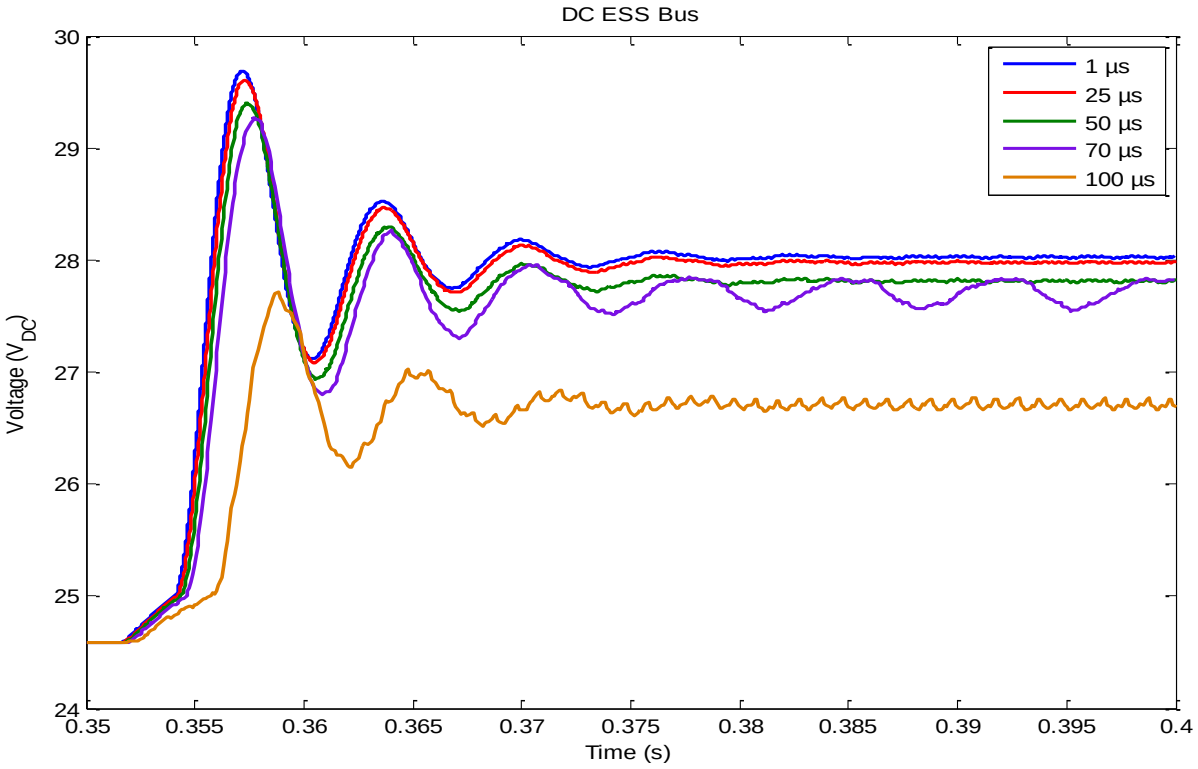

Figure 4.18. DC ESS Bus voltage for different time steps using SSN blocks

In addition Figure 4.19 shows the relationship between the actual Simulink solution for 1 µs without real-time setup modifications, the 1 µs for real-time including the SSN solver blocks and the 1 µs for real-time without SSN solver blocks but with the stublines. The behaviour is quite similar in both simulations allowing validations between off-line and real-time models. In addition, the stublines does not seem to affect the results when simulated for 1 µs, but once the

time step is increased, the results when using stublines are not acceptables. Again it is important to model the capacitance of the AC and DC cables, in order to achieve better and accurate results.

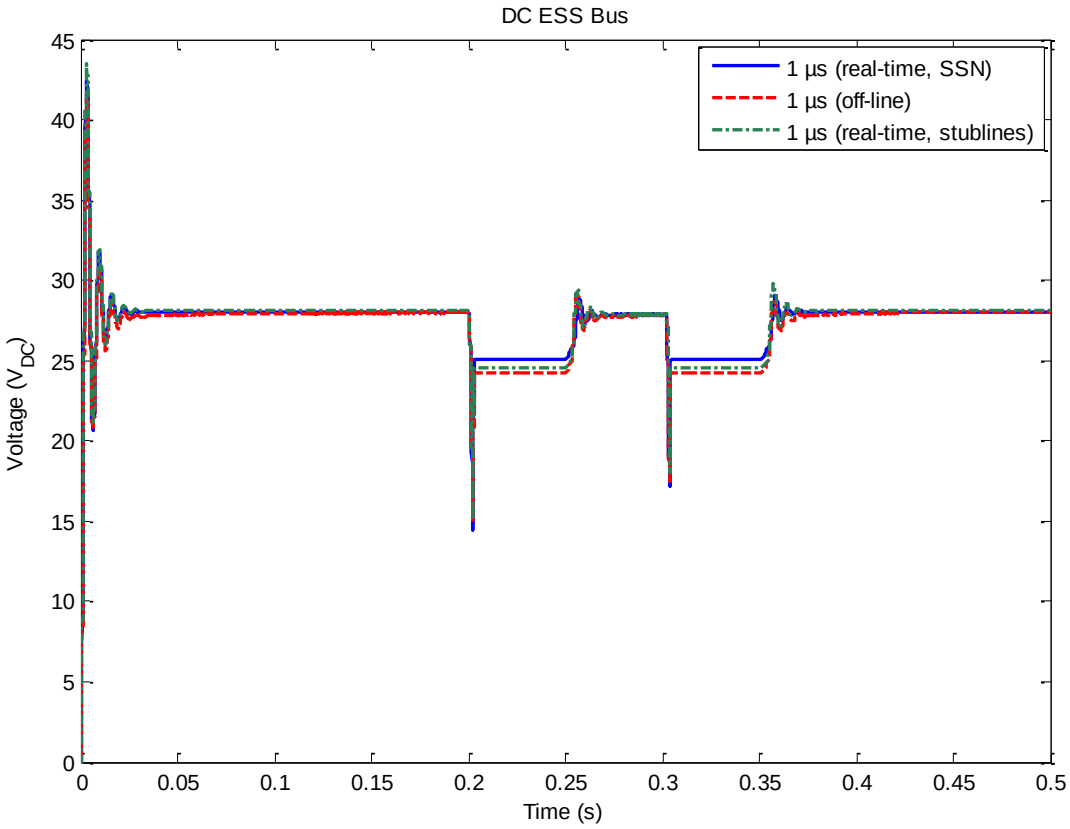

DC ESS Bus for real-time and off-line simulations

Meanwhile, Table 4.1 shows the error in simulation results as the time step is increased. It takes the voltage simulated result for all time steps when $t = 0.378\,s$, sortly after the DC voltages achieve steady-state behaviour. From 1 µs to 70 µs , the error in results is very low, while for 100 µs, the error is significant.

Table 4.1. Comparison between different time steps while the error in results increases

Time Step (µs)	**VOLTAGE**		
	Measured (V_{DC}) [16]	**Simulated (V_{DC})**	**Error (%)**
1	28.00	28.02	0.07
25	28.00	27.98	0.07
50	28.00	27.82	0.64
70	28.00	27.84	0.57
100	28.00	26.76	4.43

In addition, Figure 4.20 shows the real-time AC current simulation results of the VFG1 bus for 1 µs and 70 µs. It shows the current results right before ACPC restore communication betwen VFG1 and AC BUS 1. Despite the differences betwen the time step, both simulations present similar behaviour.

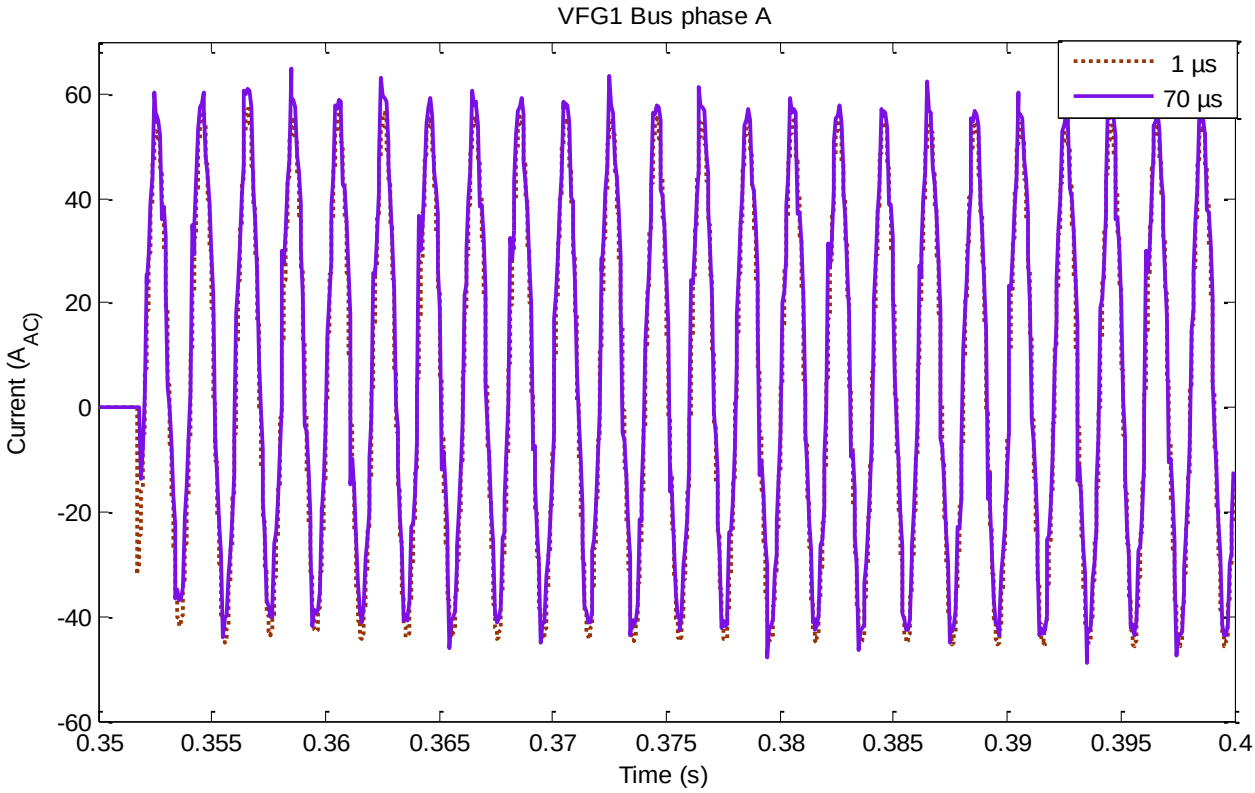

Figure 4.19. VFG1 Bus phase A current for 1 µs and 70 µs

After working with SSN Interface blocks and testing many possible configurations a time step of 70 µs was selected in order to achieve real-time simulations within the acceptable error percentages. This time step is selected since some limitations were found in the SSN solver implementation during the simulation of the Global Express system presented in this work. The Global Express power system possesses a large number of three-phase switches, so that an important number of subgroups are created while using SSN Interface blocks in order to account for real-time simulation. This can create some limitations in terms of memory during the simulation, preventing the simulation to account for real-time. It is worth noticing that there are not theoretical problems when using SSN solver, but its implementation causes some limitations that in addition with the robustness of the Global Express aircraft power system, prevent the possibility to account for better time-steps during real-time simulation.

According to M.Dufour[3] some tests at Opal-RT Technologies "have revealed that the high time step may be caused by inneficient coding of the LU part of the SSN solver". In addition, he mentions that "work is underway to optimise the coding of the LU part of the SSN solver (factorisation and forward-Backward solution) using optimal ordering of the system nodes" based on [30].

Figure 4.21 shows current simulation results for all VFG busses when VFG1 fails at 200 ms and restores operation at 300 ms, as in Case Study 1 (section 3.7) . It is observed that VFG4 supplies more current when VFG1 is off. In addition, ACPC transfers and restores the power supply between VFG1 and AC BUS1 within the 50 ms delay for switching operation. The real-time simulation results show same behaviour as the results presented in the off-line simulation.

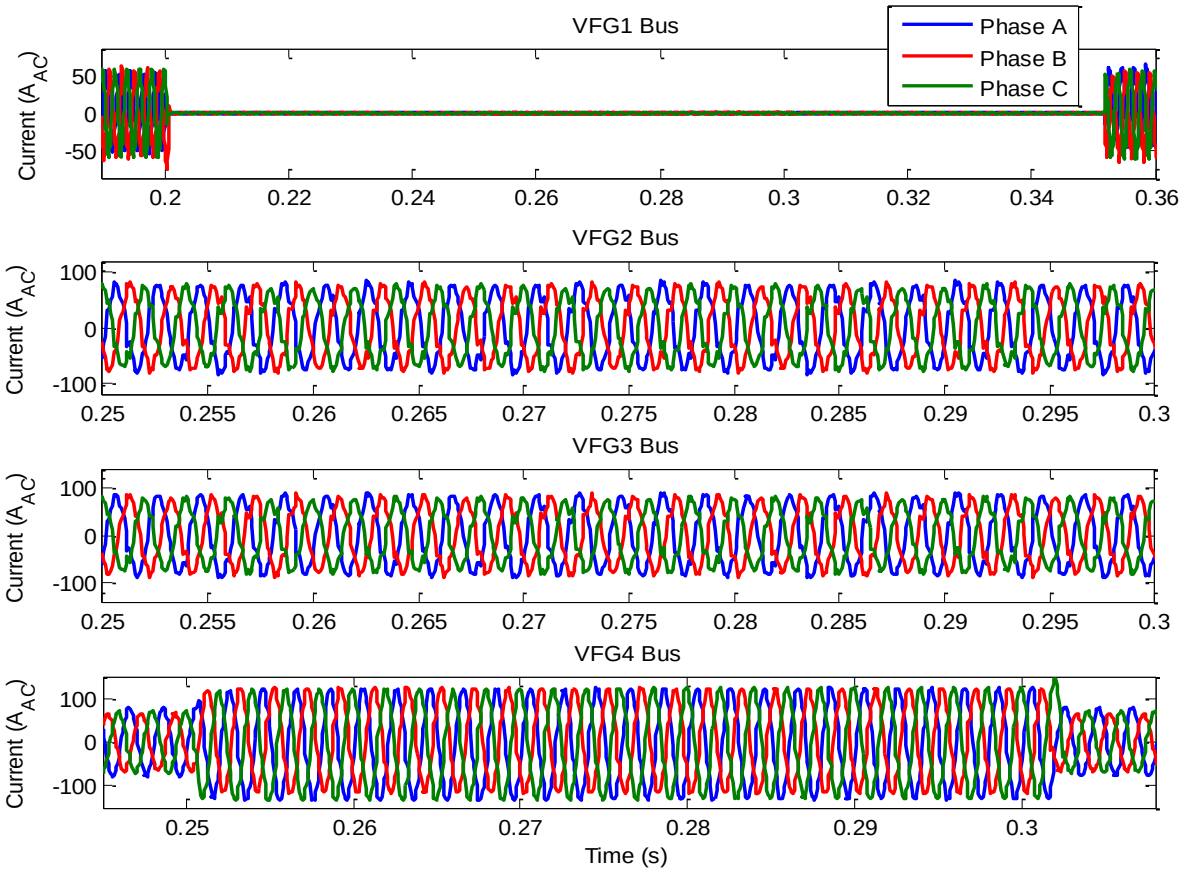

Figure 4.20. Zoom in to the current simulation results from VFG busses when VFG1 fails

[3] M. Dufour is the lead researcher in electric system simulation software for RT-LAB and he is one of the members of the jury of this thesis.

Figure 4.20 shows the DC ESS Bus and the BATT Bus achieve a constant near 28 VDC voltage when VFG1 and VFG2 fail at 200 ms and restore operation at 300, as in section 3.8. In addition, SSPCs switch within 2 ms, so that the DC ESS Bus and the BATT BUS voltage do not drop down to zero when VFG1 and VFG4 fail respectively. During the 50 ms delay, the DC ESS Bus reaches 24.59 VDC, while the BATT Bus reaches 25.53 VDC. In addition, there is a voltage ripple of 0.27 VDC while using SSN solver. Although, this ripple is within the requirements of [26].

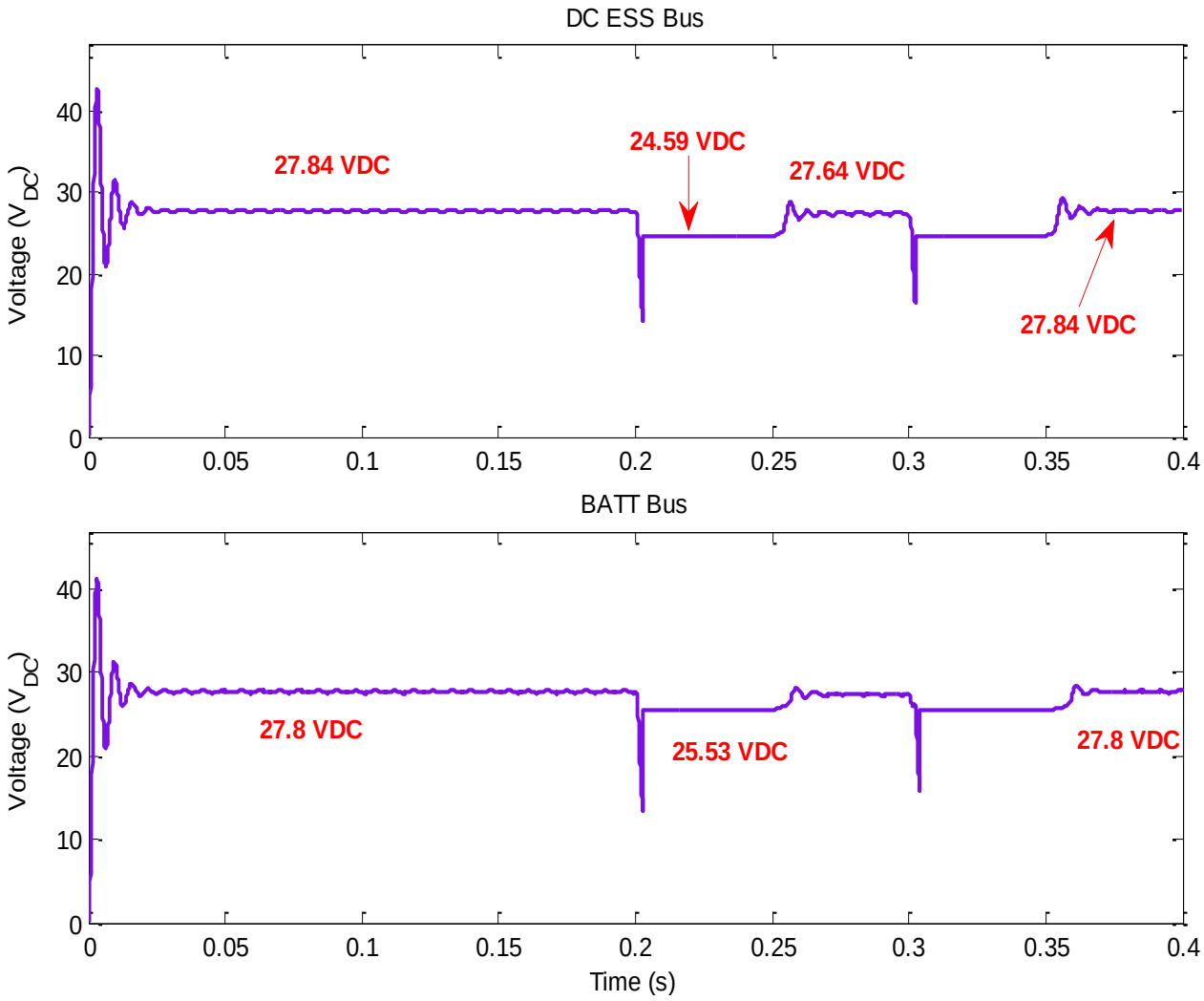

Figure 4.21. DC bus voltages results for DC ESS Bus and BATT Bus

It is important to mention that there can be another ways to decouple the model, as to regroup all the SS subsystems in one SS, or add the SS subsystems into the SM, but none of the solutions evaluated during this stage, showed a significant improvement while obtaining the results. For

that reason, the proposed real-time model in Figure 4.2 is the one used during simulations, since the way it is divided makes easier the transition from the off-line model to the real-time model. Moreover, the fact that each AC bus is a subsystem separated from the rest of the AC busses, makes it easier to output test signals in case of an HIL testing. These tests can be of great benefit while designing and integrating the electric system of the aircraft, since failures can be determined at an early stage of the aircraft's conception, helping significantly to reduce the test time and costs. In addition, HIL systems typically have the ability to automatically run through tests automatically by using a script, so that testing can be done without damaging equipment or endangering lives, and potentially damaging conditions can be detect and reported. Or even better, an electric abnormal behaviour inside the aircraft can be easily recreated and simulated with a specific protective or control device using HIL.

One of the applications for real-time simulation of the Global Express power system is that the appropriate protection settings can be determined before building the aircraft.

CONCLUSION

This research presented an initial attempt to model the Global Express aircraft electric power system in steady state and transient behaviours for both off-line and real-time simulations. The model was developed in Simulink and validated with EMTP-RV and available measurements. It was used to demonstrate the capability to study system performance under given operating conditions and potential benefits of conducting real-time simulations. In addition, the development of this research contributes to the study of various aircraft power system architectures and testing their performance within economical and reliability constraints.

Given the limitations in terms of system data found during the development of the presented research and given the necessity to create model blocks adequately representing the electrical characteristics of the actual aircraft, it was shown that the implementation achieved in this project, could be evaluated using the same tests founded in the literature, but using elements that better adjust to the reality of Global Express. This can be easily used in design and test stages of an aircraft.

Some important results are summarized for off-line simulations:

1. According to the literature, many simplifications and assumptions are generally made when simulating aircraft electric power system behaviour (often modeled as a single bus system). However, loads on more-electric aircrafts grow and diversify continuously and the ability of generators to deliver additional power will quickly become limited, so that transient performance analysis is becoming an important issue.
2. Even if DC loads are simulated as resistances and AC loads as RLC branches, efforts should be made to meet their real load behaviour, in order to take into account variable input voltages and temperature effects. They can affect both steady-state and transient performance behaviour. Component manufacturers should provide required information to ease aircraft certification process preventing over-design for certain cases and transient problems in others.
3. In terms of AC and DC cables, the latter correction must be carefully reviewed with respect to the current practices in aircraft design. More sophisticated models must be developed to account for higher frequency transients and for temperature and altitude

effects. In addition, the only reference when designing AC and DC cables dates from the early 50's, so that research on this topic must be conducted to account for new technological trends.

4. Logical controls must be validated within the detailed aircraft electric power system model, so that more sophisticated switch models can be used to investigate arcing problems causing a switch to stick during operation.

Some of the aspects listed above, are part of further research to be conducted in following projects.

Considering real-time simulations presented in this document:

1. SSN solver methodology is the most practical way to eliminate one of the principal constraints presented during the research, while converting off-line model to real-time. Although, there are some limitations in terms of memory related to the implementation of the solver within the aircraft electric power system, that must be checked to account for better time steps, since the model presents a large amount of three-phase switches.
2. A time step of 70 μs allows the Global Express power system to be simulated in real-time environment within the acceptable error percentages. This can results in the possibility to perform HIL simulations for control and protective device tests using the model developed in Simulink. The large amount of switches can create simulation performance constraints for repetitive operation cases or reduce memory capacity for real-time simulation using SSN solver methods.
3. Decreasing the time step of the real-time simulations, improving the amount of switches and performing HIL tests are part of the further research to be conducted in following projects.

Finally, the increased usage of electrical power in more-electric aircrafts increases the power demands on the electrical system, placing new constraints on its dynamic performance and on power quality. Any new concept or design must be extensively analyzed, tested, validated and certified before its implementation in an actual aircraft, so that research on simulation methods for aircraft power systems contributes to the creation of a model-based certification process.

REFERENCES

[1] S.J. Cutts, "A collaborative approach to the more electric aircraft", en *International Conference on Power Electronics, Machines and Drives*, Bath, United Kingdom, 2002, pp. 223-228.

[2] R. Newman, "The more electric engine concept", *Society of Automotive Engineers*, 2004.

[3] R.E.J. Quigley, "More Electric Aircraft", en *Conference and Exposition in Applied Power Electronics APEC'93*, San Diego, CA, USA, 1993, pp. 906-911.

[4] J. Chang y A. Wang, "New VF-ppower system architecture and evaluation for future aircraft", *IEEE Transactions on Aerospace and Electronic Systems*, vol. 42, no. 2, pp. 527-539, April 2006.

[5] K. Emadi y M. Ehsani, "Aircraft power systems: technology, state of the art, and future trends", *IEEE Aerospace and Electronic Systems Magazine*, vol. 15, no. 1, pp. 28-32, January 2000.

[6] A. Eid, H. El-Kishky, M. Abdel-Salam, y T. El-Mohandes, "Power quality investigation of VSCF aircraft electric power systems", en *42nd Southeastern Symposium on System Theory (SSST)*, Tyler, TX, USA, 2010, pp. 171 - 176.

[7] D. Izquierdo, R. Azcona, F. Del Cerro, C. Fernandez, y B. Delicado, "Electrical power distribution system (HV270DC), for application in more electric aircraft", en *2010 Twenty-Fifth Annual IEEE Conference and Exposition in Applied Power Electronics (APEC'10)*, Palm Springs, CA, USA, 2010, pp. 1300-1305.

[8] A. Emadi y M. Ehsani, "Multi-converter power electronic systems: definition and applications", en *IEEE 32nd Annual Power Electronics Specialists Conference, 2001 (PESC'01)*, Vancouver, BC, Canada, 2001, pp. 1230-1236.

[9] P.J. Normal, S.J. Galloway, y J.R. McDonald, "Simulating electrical faults within future

aircraft networks", *IEEE Transactions on Aerospace and Electronic Systems*, vol. 44, no. 1, pp. 99-110, January 2008.

[10] M. Sinnett. (2007, Avril) Boeing. [En línea]. http://www.boeing.com/commercial/aeromagazine/articles/qtr_4_07/article_02_1.html

[11] L. Faleiro. (2005, September) American Institute of Aeronautics and Astronautics. [En línea]. http://www.aiaa.org/aerospace/images/articleimages/pdf/AA_Sept05_FAL.pdf

[12] (2010) Frost and Sullivan. [En línea]. http://www.aerospace.frost.com

[13] M.J. Provost, "The more electric aero-engine: a general overview from an engine manufacturer", en *International Conference on Power Electronics, Machines and Drives*, Bath, United Kingdom, 2002, pp. 246-251.

[14] The MathWorks. (2011, June) MathWorks. [En línea]. http://www.mathworks.com/products/simulink/?BB=1

[15] J. Belanger, V. Lapointe, C. Dufur, y L. Schoen, "eMEGAsim: An open high-performance distributed real-time power grid simulator", en *Proceedings of the International Conference on Power Systems (ICPS)*, Bangalore, India, 2007.

[16] J. Mahseredjian, S. Dennetiere, L. Dube, B. Khodabakhchian, y L. Gerin-Lajoie, "On a new approach for the simulation of transients in power systems", *Electric Power Systems Research*, vol. 77, no. 11, pp. 1514-1520, September 2007.

[17] J.A. Weimer, "Electrical power technology for the more electric aircraft", en *AIAA/IEEE 12th Conference on Digital Avionics Systems*, Fort Worth, TX, USA, 1993, pp. 445-450.

[18] Aerospace Bombardier, "ATA 100 Breakdown", Bombardier, Montreal, QC, Canada, Training Manual 2003.

[19] Canadair, "Global Express / Global 5000 electrical load analysis report", Bombardier,

Montreal, QC, Canada, RAE-L700-103 REV G, 2002.

[20] D. o. Defense, "Military Specification: Analysis of Electric Load and Power Source Capacity", Department of Defense, Washington, USA, Military Specification MIL-E-7016, 1976.

[21] S.J. Exner, "Impedance data for 400-cycle aircraft distribution systems", AIEE Technical Paper, USA, Technical Paper 1952.

[22] R-T. Bouchard y G. Olivier, *Electrotechnique*, 2nd ed. Montreal, QC, Canada: Editions de l'Ecole Polytechnique de Montreal, 1999.

[23] K.W.E. Cheng, "Comparative study of AC/DC converters for more electric aircraft", en *Proceedings of the 1998 7th International Conference on Power Electronics and Variable Speed Drives*, London, United Kingdom, 1998, pp. 299-304.

[24] G. Gong, U. Drofenik, y J.W. Kolar, "12-pulse rectifier for more electric aircraft applications", en *IEEE International Conference on Industrial Technology*, vol. 2, Maribor, Slovenia, 2003, pp. 1096-1101.

[25] G. Gong et al., "Comparative evaluation of three-phase high-power-factor AC-DC converter concepts for application in future More Electric Aircraft", *IEEE Transactions on Industrial Electronics*, vol. 52, no. 3, pp. 727-737, June 2005.

[26] D. o. Defense, "Aircraft Electric Power Characteristics", Department of Defense, Washington, USA, Military Standard MIL-STD-704f, 2004.

[27] P. Venne, J-N. Paquin, y J. Belanger. (2010, October) The what, where and why of real-time simulation. Planet-RT, Opal-RT Technologies.

[28] Opal-RT Technologies Inc. (2011, June) eMEGAsim and eDRIVEsim Product Information & Simulation Application Examples. [En línea]. http://www.opal-rt.com/sites/defaut/files/technical_papers/

[29] C. Dufur, J. Mahseredjian, y J. Belanger, "A combined state-space nodal method for the simulation of power system transient", *IEEE Transactions on Power Delivery*, vol. 26, no. 2, pp. 928-935, April 2011.

[30] F. Tinney y W.S. Meyer, "Solution of Large Sparse Systems by Ordered Triangular Factorization", *IEEE Transactions on Automatic Control*, vol. 18, no. 4, pp. 333 - 346, August 1973.

ANNEXES

ANNEXE 1. AC Load Analysis Chart, Flight Phase G7 Cruise (500 Hz) [19]

	AC Bus 1					
	A-N		B-N		C-N	
DESCRIPTION	**WATTS**	**VAR**	**WATTS**	**VAR**	**WATTS**	**VAR**
ESS TRU 1 (A)	509	167	509	167	509	167
ELECTRO-HYDRAULIC PUMP #3B	0	0	0	0	0	0
REST OF THE CHARGES (PQ EQUIVALENT)	3513	1038	4054	312	3874	1764
TOTAL	**4022**	**1205**	**4563**	**479**	**4383**	**1931**
	AC Bus 2					
	A-N		**B-N**		**C-N**	
DESCRIPTION	**WATTS**	**VAR**	**WATTS**	**VAR**	**WATTS**	**VAR**
TRU 1	1504	494	1504	440	1504	440
ELECTRO-HYDRAULIC PUMP #2B	0	0	0	0	0	0
REST OF THE CHARGES (PQ EQUIVALENT)	3827	2093	4210	2147	4394	2147
TOTAL	**5331**	**2587**	**5714**	**2587**	**5898**	**2587**
	AC Bus 3					
	A-N		**B-N**		**C-N**	
DESCRIPTION	**WATTS**	**VAR**	**WATTS**	**VAR**	**WATTS**	**VAR**
TRU 3	1538	505	1538	505	1538	505
ELECTRO-HYDRAULIC PUMP #1B	0	0	0	0	0	0
REST OF THE CHARGES (PQ EQUIVALENT)	3983	1962	4875	1236	4875	2688
TOTAL	**5521**	**2467**	**6413**	**1741**	**6413**	**3193**
	AC Bus 4					
	A-N		**B-N**		**C-N**	
DESCRIPTION	**WATTS**	**VAR**	**WATTS**	**VAR**	**WATTS**	**VAR**
AC ESS BUS FEED	2184	186	1150	186	1435	186
ELECTRO-HYDRAULIC PUMP 3A	1580	1193	1580	1193	1580	1193
REST OF THE CHARGES (PQ EQUIVALENT)	2447	1018	2152	1018	2307	1018
TOTAL	**6211**	**2397**	**4882**	**2397**	**5322**	**2397**
	AC ESS Bus					
	A-N		**B-N**		**C-N**	
DESCRIPTION	**WATTS**	**VAR**	**WATTS**	**VAR**	**WATTS**	**VAR**
ESS TRU 2	565	186	565	186	565	186
REST OF THE CHARGES (PQ EQUIVALENT)	1619	0	585	0	870	0
TOTAL	**2184**	**186**	**1150**	**186**	**1435**	**186**